Computer Methods in Applied Mechanics and Engineering 452 (2026) 118695

Contents lists available at ScienceDirect

Comput. Methods Appl. Mech. Engrg.

journal homepage: www.elsevier.com/locate/cma

Error estimates and graded mesh refinement for isogeometric analysis in the vicinity of polar corners

Thomas Apel, Philipp Zilk *

Institute for Mathematics and Computer-Based Simulation, Universität der Bundeswehr München, Werner-Heisenberg-Weg 39, Neubiberg, 85577, Germany

ARTICLE INFO

2020 MSC:
65N30
65N25
65D07
65N50
35A21

Keywords:
Isogeometric analysis
Error estimates
Corner singularities
Local mesh refinement
Graded meshes
Polar parameterizations

ABSTRACT

Isogeometric analysis (IGA) combines exact geometric representations with higher-order accuracy for the numerical solution of partial differential equations. However, in geometrically complex settings – such as domains with corner singularities or non-standard parameterizations – these advantages may not be fully realized by standard IGA techniques. In particular, commonly used NURBS parameterizations can result in polar mappings, where one edge of the parametric domain is collapsed onto a single point, known as the polar point. Although widely used in computer-aided design, such configurations lack a full convergence theory. Additionally, reduced solution regularity near corners can significantly limit the performance of standard IGA, as higher-order convergence is no longer attainable.

In this work, both challenges are addressed by analyzing parameterizations in which the polar point coincides with a corner of the physical domain. To tackle the resulting singularity, a simple and effective local refinement strategy is proposed based on mesh grading toward the collapsed edge. This produces a locally refined mesh in the vicinity of the polar corner that accurately captures the singular behavior of the PDE solution.

To support this strategy, a numerical analysis tailored to polar domains with corners is developed. The framework includes the definition of polar function spaces on the parametric domain, a quasi-interpolant for polar splines, and the derivation of error estimates in weighted Sobolev norms. Optimal convergence is proven for smooth solutions under uniform refinement and for singular solutions using appropriately graded meshes. Numerical experiments on benchmark domains confirm the theoretical predictions and demonstrate the practical efficiency of the proposed method.

1. Introduction

1.1. Motivation

Isogeometric analysis (IGA), introduced in [1], combines Galerkin methods with computer-aided design (CAD) by employing spline-based shape functions such as B-splines and NURBS for both geometry representation and PDE solution approximation. This unified framework offers key advantages, including exact representations of curved geometries, efficient higher-order approximations, and enhanced smoothness of shape functions. However, standard Galerkin-based IGA faces substantial challenges on non-smooth

* Corresponding author.
E-mail addresses: thomas.apel@unibw.de (T. Apel), philipp.zilk@unibw.de (P. Zilk).

https://doi.org/10.1016/j.cma.2025.118695
Received 14 May 2025; Received in revised form 15 December 2025; Accepted 20 December 2025
Available online 6 January 2026

domains with geometric singularities such as corners. The reduced regularity of PDE solutions in the vicinity of singularities prevents higher-order convergence and significantly limits achievable accuracy. To overcome these limitations, various refinement strategies have been proposed in the literature, with adaptive algorithms being among the most popular. To this end, several advanced spline technologies have emerged, including T-splines, LR-splines, PHT-splines, and hierarchical approaches; a comprehensive overview is provided in [2]. While these methods enable localized refinement, they introduce additional complexity in both implementation and computation.

The reduced regularity associated with corner singularities is well understood and can often be characterized a priori, motivating simpler yet equally effective refinement schemes. It is well-known from classical finite element methods that these singularities can be efficiently handled through graded mesh refinement [3–7]. However, when grading tensor-product meshes on smoothly parameterized domains, the refinement inevitably propagates along the mapped edges of the parametric domain, resulting in a non-local refinement pattern, see, e.g., previous works on mesh grading in IGA [8,9].

The only scenario in which mapped graded tensor-product meshes achieve truly local refinement near a point singularity is when one edge of the parametric domain is collapsed into the corner. Such parameterizations closely resemble transformations from polar to Cartesian coordinates; consequently, these geometries are naturally referred to as *polar domains with corners*, the associated mappings as *polar parameterizations* and the considered corner as *polar corner*. By grading the parametric mesh toward the collapsed edge, refinement of the Bézier mesh can be effectively concentrated around the singularity, while maintaining the tensor-product structure of the mesh. As demonstrated numerically for the Laplace eigenvalue problem circular sectors in our recent work [10], this strategy leads to optimal approximation rates for singular solutions when suitable grading parameters are chosen. In the present paper, we extend this approach to more general corner domains and provide a comprehensive mathematical analysis.

Polar parameterizations emerge naturally within CAD applications, especially for rotationally symmetric domains. Examples include the modeling of cylindrical sector geometries arising in electromagnetics [11] and arterial geometries in biomechanics [12,13], and different applications in structural mechanics like the modelling of cylindrical continuum rods [14], vibration analysis of circular plates [12,15] or acoustic analysis of reactive mufflers [16]. Furthermore, polar parameterizations appear prominently in scaled boundary parameterizations within IGA [17], which have recently been extended to simulate plates and shells [18–20]. The widely known Pacman domain also serves as a singularly mapped benchmark for evaluating adaptive refinement strategies in IGA boundary element methods [21,22].

Nonetheless, polar mappings suffer from a lack of regularity, and standard isogeometric approximation spaces – defined as push-forwards of the corresponding parametric spaces – are not suitable [23,24]. The development of appropriate spline spaces for polar domains have become the subject of substantial recent interest [25,26]. Although polar parameterizations are extensively employed in practical engineering applications of IGA, their mathematical foundations, in particular, the availability of corresponding approximation estimates, still remain underdeveloped. A primary reason for this gap is the inherent singularity introduced at the polar point [23,24], which conflicts with the smoothness assumptions underlying classical IGA approximation theory [27,28]. Consequently, such singular configurations are typically excluded. To date, approximation properties in the presence of polar singularities have only been established for specialized cases, such as singularly parameterized triangular domains [29] and, more recently, within subdivision-based IGA frameworks [30].

The present work aims to bridge this gap by providing a detailed numerical analysis and deriving error estimates that account for the specific structure of polar parameterizations, thereby addressing the challenges associated with the presence of a polar point. Furthermore, we establish a theoretical foundation for the choice of the mesh grading parameter that is required to handle characteristic singularities of the PDE solution at the polar corner.

1.2. Main novelties and contributions

The main contributions of this work to the state of the art are as follows:

- **A numerical analysis framework tailored to polar parameterizations:** We develop a numerical analysis framework for isogeometric mappings that collapse one edge of the parametric domain onto a physical corner. This includes the definition of a quasi-interpolant for polar splines on the parametric square, the construction of a corresponding projection operator in the physical domain, and the introduction of a new class of polar function spaces. These spaces are built upon weighted Sobolev norms and are naturally suited for pull-backs of functions defined on polar domains with corners.
- **Error estimates for smooth solutions:** Within this framework, we derive error estimates in polar function spaces and transfer them to the physical domain. For a class of sufficiently smooth solutions, our analysis confirms optimal convergence rates that have been previously observed numerically for uniformly refined meshes mapped via a polar parameterization; see, for example, the recent study [30].
- **Error estimates for singular solutions:** We extend our analysis to functions exhibiting classical corner singularities at the polar point. These singularities are captured within appropriately defined weighted Sobolev spaces, enabling a systematic convergence analysis in the non-smooth setting.
- **A graded mesh refinement scheme toward the polar corner:** To approximate the singularity at the polar point, we introduce a boundary-fitted graded mesh refinement strategy based on a grading parameter. This approach effectively concentrates degrees of freedom near the polar corner and restores optimal approximation accuracy for non-smooth solutions.

- **Analysis of the optimal grading parameter:** By combining the known singular behavior of solutions with the structure of the polar function spaces, we derive explicit conditions on the grading parameter that ensure optimal convergence rates. This provides practical guidance for the construction of effective graded meshes.
- **Numerical implementation and illustrative examples:** We show how to integrate the proposed method into existing IGA codes with minimal effort. A series of benchmark Poisson problems on various polar domains with corners confirms the computational efficiency of the approach and validates the theoretical error estimates.

In particular, this paper contributes to several active research directions in the IGA community:

- **Alignment with CAD representations:** Rotationally symmetric geometries are naturally described in CAD using polar coordinates, as noted in the seminal IGA textbook [12]. Our analysis strengthens the mathematical foundation for incorporating such parameterizations within IGA. This addresses one of the original goals of IGA – seamless integration with CAD – and highlights a key advantage over classical FEM, which cannot exactly represent circular geometries.
- **Parameterization-sensitive error analysis:** Classical approximation theory in IGA assumes globally smooth parameterizations. In contrast, our framework explicitly accommodates one of the most common geometric singularities – the presence of a polar point [24,28,31]. Embedding the mapping properties directly into the analysis represents a first step toward parameterization-aware error estimates in IGA.
- **Simple local refinement methods for corner singularities:** Many local refinement methods in IGA rely on advanced spline technologies that require substantial implementation effort and additional libraries, see, e.g., [32]. In contrast, the graded mesh refinement proposed in this paper can be incorporated into existing IGA codes with minimal modifications, typically as a post-processing step of standard refinement routines. As such, it offers a practical and illustrative tool to study the impact of corner singularities and local refinement, making it particularly useful for both research and educational purposes.

1.3. Outline of the paper

The outline of this paper is as follows. Section 2 provides an overview of the mathematical foundations of IGA, which are subsequently applied in Section 3 to introduce polar parameterizations, the model problem under consideration and the proposed graded mesh refinement scheme. In particular, Section 3.4 states the key results of our work – namely error estimates in the vicinity of polar corners that establish optimal convergence rates for suitable mesh grading parameters. In Section 4, we construct a projector onto the space of polar splines and define polar function spaces on the parametric domain. These tools are then used in Section 5 to derive the necessary projection error estimates required for our convergence analysis. The theoretical results are confirmed through numerical experiments in Section 6. Finally, Section 7 summarizes the main findings and discusses potential extensions of this work.

In the sequel, the symbol C is used for a generic positive constant, which may be different at each occurrence. Moreover, for $a, b > 0$ we use the notation $a \sim b$ if there are positive constants C_1 and C_2 such that $C_1 b \le a \le C_2 b$. The mentioned constants are independent of the mesh parameter h and the function under consideration. Besides, we use standard multi-index notation. A multi-index is denoted by $\boldsymbol{\alpha} = (\alpha_1, \alpha_2) \in \mathbb{N}^2$, and we set $|\boldsymbol{\alpha}| := \alpha_1 + \alpha_2$. For two multi-indices $\boldsymbol{\alpha}, \boldsymbol{\gamma} \in \mathbb{N}^2$, the relations $\boldsymbol{\alpha} \ge \boldsymbol{\gamma}$ and $\boldsymbol{\alpha} \le \boldsymbol{\gamma}$ are understood componentwise.

2. Fundamentals of B-splines and NURBS

This section contains a brief overview of the fundamentals of B-Splines, NURBS and related quasi-interpolants, largely following the framework presented in the review paper [28]. For more details, the interested reader may consult the books [12,33,34].

2.1. Univariate B-splines and NURBS

First, we introduce the concept of B-splines and NURBS in the univariate case. Let $p \in \mathbb{N}_0$ and $n \in \mathbb{N}$. We call $\Xi := \{\xi_1, \xi_2, \dots, \xi_{n+p+1}\}$ a p-open knot vector if

$$\xi_1 = \xi_2 = \cdots = \xi_{p+1} < \xi_{p+2} \le \xi_{p+3} \le \cdots \le \xi_{n-1} \le \xi_n < \xi_{n+1} = \xi_{n+2} = \cdots = \xi_{n+p+1},$$

where $\xi_i \in \mathbb{R}$, $i = 1, \dots, n+p+1$, is called the i-th knot which is allowed to occur repeatedly. Without loss of generality, we assume that $\xi_1 = 0$ and $\xi_{n+p+1} = 1$. Further, we define the vector $Z = \{\zeta_1, \dots, \zeta_N\}$ of knots without repetitions, also called breakpoints, with

$$\Xi = \{\underbrace{\zeta_1, \dots, \zeta_1}_{m_1 \text{ times}}, \underbrace{\zeta_2, \dots, \zeta_2}_{m_2 \text{ times}}, \dots, \underbrace{\zeta_N, \dots, \zeta_N}_{m_N \text{ times}}\},$$

where $N \in \mathbb{N}$ is the total number of pairwise different knots and $m_j \in \mathbb{N}$ denotes the multiplicity of the breakpoint ζ_j such that $\sum_{j=1}^{N} m_j = n + p + 1$. For p-open knot vectors, $m_1 = m_N = p + 1$ always holds, and we assume $m_j \le p + 1$ for the internal knot multiplicities. The entries of Z define a mesh on the unit interval $[0, 1]$.

From the given knot vector, B-spline basis functions of degree p, denoted by

$$\widehat{B}_{i,p} : [0,1] \to \mathbb{R}, \quad \zeta \mapsto \widehat{B}_{i,p}(\zeta), \quad i = 1, 2, \dots, n,$$

can be constructed using the iterative scheme as explained, for instance, in [12, Section 2.1]. They build a basis of the space of splines on the subdivision Z, that is, piecewise polynomials of degree p with $p - m_j$ continuous derivatives at the internal breakpoints

ζ_j, $j = 2, \dots, N-1$, where $p - m_j = -1$ stands for a discontinuity at ζ_j. Besides other characteristics, the B-spline basis functions are non-negative and form a partition of unity. Finally, we denote by

$$S_p(\Xi) = \operatorname{span}\left\{ \widehat{B}_{i,p} : i = 1, 2, \dots, n \right\}$$

the univariate spline space spanned by the B-splines associated with the knot vector Ξ.

The support of each basis function is given by $\operatorname{supp}(\widehat{B}_{i,p}) = [\xi_i, \xi_{i+p+1}]$. For each interval $I_j = (\zeta_j, \zeta_{j+1})$, which can also be written as $I_j = (\xi_i, \xi_{i+1})$ for a unique i, we further define the support extension $\widetilde{I}_j$ by

$$\widetilde{I}_j = (\xi_{i-p}, \xi_{i+p+1}), \tag{2.1}$$

which represents the interior of the union of the supports of basis functions whose support intersects I_j, i.e.,

$$\overline{\widetilde{I}_j} = \bigcup_{\{k \,:\, \operatorname{supp}(\widehat{B}_{k,p}) \cap I_j \neq \emptyset\}} \operatorname{supp}(\widehat{B}_{k,p}) = [\xi_{i-p}, \xi_{i+p+1}].$$

Classical splines face restrictions in representing essential geometries like conic sections. To overcome this limitation, non-uniform rational B-splines (NURBS) are introduced, see [35] for more details. Therefore, the weight function

$$W(\zeta) = \sum_{l=1}^{n} w_l \, \widehat{B}_{l,p}(\zeta)$$

is determined by choosing positive constants $w_l > 0$, $l = 1, \dots, n$, which are called weights. The NURBS basis functions are defined by

$$\widehat{N}_{i,p}(\zeta) = \frac{w_i \widehat{B}_{i,p}(\zeta)}{\sum_{l=1}^{n} w_l \, \widehat{B}_{l,p}(\zeta)} = \frac{w_i \widehat{B}_{i,p}(\zeta)}{W(\zeta)}, \quad i = 1, \dots, n,$$

and we denote the corresponding NURBS space by

$$N_p(\Xi, W) = \operatorname{span}\left\{ \widehat{N}_{i,p} : i = 1, \dots, n \right\}.$$

Moreover, we say that $S_p(\Xi)$ and $N_p(\Xi, W)$ are refinements of given spline and NURBS spaces $S_{p^0}(\Xi^0)$ and $N_{p^0}(\Xi^0, W)$, if

$$S_{p^0}(\Xi^0) \subset S_p(\Xi) \quad \text{and} \quad N_{p^0}(\Xi^0, W) \subset N_p(\Xi, W), \tag{2.2}$$

respectively. B-splines and NURBS can be refined through knot insertion and degree elevation. In total, three refinement schemes can be constructed by combining the algorithms [1].

Next, we introduce a projection operator onto the space of univariate splines that is used in standard literature on isogeometric approximation theory [8,27,28]. We define

$$\Pi_{p,\Xi} : L^1([0,1]) \to S_p(\Xi), \quad \Pi_{p,\Xi}(v) := \sum_{i=1}^{n} \lambda_{i,p}(v) \, \widehat{B}_{i,p}, \tag{2.3}$$

where $\lambda_{j,p}$ are dual functionals with

$$\lambda_{i,p}(\widehat{B}_{k,p}) = \delta_{ik}, \tag{2.4}$$

and δ_{ik} is the Kronecker symbol. In general, $\Pi_{p,\Xi}$ is not an interpolation operator, but it is typically called a quasi-interpolant in the literature. The dual basis $\{\lambda_{i,p}\}_{i=1,\dots,n}$ can be chosen in multiple ways [36]. Here, we stick to the classical construction from [33, Section 4.6],

$$\lambda_{i,p}(v) = \int_{\xi_j}^{\xi_{j+p+1}} v(s) \, D^{p+1} \psi_i(s) \, \mathrm{d}s, \tag{2.5}$$

where $\psi_i(\zeta) = G_i(\zeta) \Psi_i(\zeta)$ with

$$\Psi_i(\zeta) = \frac{(\zeta - \xi_{i+1}) \cdots (\zeta - \xi_{i+p})}{p!} \tag{2.6}$$

and

$$G_i(\zeta) = g\left(\frac{2\zeta - \xi_i - \xi_{i+p+1}}{\xi_{i+p+1} - \xi_i} \right), \tag{2.7}$$

where g is the transition function described in [33, Theorem 4.37]. Note that the dual basis functionals (2.5) are well-defined for $v \in L^1([0,1])$, see [33, Theorem 4.41].

The presented quasi-interpolant is commonly adapted further to be interpolatory at the boundary $\widehat{\Gamma} = \{0, 1\}$, see [28],

$$\Pi^{\widehat{\Gamma}}_{p,\Xi} : C([0,1]) \to S_p(\Xi), \quad \Pi^{\widehat{\Gamma}}_{p,\Xi}(v) := \sum_{i=1}^{n} \lambda^{\widehat{\Gamma}}_{i,p}(v) \, \widehat{B}_{i,p} \quad \text{with} \tag{2.8}$$

$$\lambda^{\widehat{\Gamma}}_{1,p}(v) = v(0), \ \lambda^{\widehat{\Gamma}}_{n,p}(v) = v(1), \ \lambda^{\widehat{\Gamma}}_{i,p}(v) = \lambda_{i,p}(v), \quad i = 2, \dots, n-1.$$

Since we only consider open knot vectors, the first and last B-spline basis function are interpolatory, that is,

$$\lambda_{1,p}^{\widehat{\Gamma}}(B_{1,p}) = B_{1,p}(0) = 1 \quad \text{and} \quad \lambda_{n,p}^{\widehat{\Gamma}}(B_{n,p}) = B_{n,p}(1) = 1. \tag{2.9}$$

Moreover, we have

$$\lambda_{1,p}^{\widehat{\Gamma}}(B_{i,p}) = B_{i,p}(0) = 0 \quad \text{and} \quad \lambda_{n,p}^{\widehat{\Gamma}}(B_{i,p}) = B_{i,p}(1) = 0 \quad \text{for } i = 2, 3, \dots, n-1, \tag{2.10}$$

hence, the modified functionals $\lambda_{i,p}^{\widehat{\Gamma}}(v)$ also satisfy the dual functional property (2.4).

2.2. Bivariate B-splines and NURBS

Bivariate B-splines and NURBS are defined as tensor products of their univariate counterparts. Let $n_l \in \mathbb{N}$, the degrees $p_l \in \mathbb{N}$ and the p_l-open knot vectors $\Xi_l = \{\xi_{l,1}, \xi_{l,2} \dots, \xi_{l,n_l+p+1}\}$ be given for $l = 1, 2$. We define the polynomial degree vector $\boldsymbol{p} = (p_1, p_2)$ and the bivariate knot vector $\boldsymbol{\Xi} = (\Xi_1, \Xi_2)$. Further, let $N_l \in \mathbb{N}$ be the number of knots without repetition in the l-th direction such that the corresponding univariate knot vectors of breakpoints are given by $Z_l = \{\zeta_{l,1}, \zeta_{l,2} \dots, \zeta_{l,N_l}\}$ for $l = 1, 2$. They form a Cartesian grid in the parametric domain $\widehat{\Omega} = (0,1)^2$, which defines the parametric Bézier mesh $\widehat{\mathcal{M}}$,

$$\widehat{\mathcal{M}} := \Big\{ Q_{\boldsymbol{j}} \subset \widehat{\Omega} : Q_{\boldsymbol{j}} = Q_{(j_1,j_2)} = (\zeta_{1,j_1}, \zeta_{1,j_1+1}) \times (\zeta_{2,j_2}, \zeta_{2,j_2+1}), \boldsymbol{j} \in \boldsymbol{J} \Big\}, \tag{2.11}$$

where we introduce the set of multi-indices $\boldsymbol{J} = \{\boldsymbol{j} = (j_1, j_2) : 1 \le j_l \le N_l - 1, l = 1, 2\}$. The diameter of each element $Q_{\boldsymbol{j}} \in \widehat{\mathcal{M}}$ is denoted by $h_{Q_{\boldsymbol{j}}}$, and the global mesh size of $\widehat{\mathcal{M}}$ is defined as $h = \max\{h_{Q_{\boldsymbol{j}}} : Q_{\boldsymbol{j}} \in \widehat{\mathcal{M}}\}$. Moreover, we introduce the support extension of a Bézier element $Q_{\boldsymbol{j}} \in \widehat{\mathcal{M}}$ by

$$\widetilde{Q}_{\boldsymbol{j}} := \widetilde{I}_{1,j_1} \times \widetilde{I}_{2,j_2}, \tag{2.12}$$

where $\widetilde{I}_{l,j_l}$, $l = 1, 2$, are the univariate support extensions (2.1). Bivariate B-spline functions are then defined as

$$\widehat{B}_{\boldsymbol{i},\boldsymbol{p}} : [0,1]^2 \to \mathbb{R}, \quad \widehat{B}_{\boldsymbol{i},\boldsymbol{p}}(\boldsymbol{\zeta}) = \widehat{B}_{i_1,p_1}(\zeta_1)\, \widehat{B}_{i_2,p_2}(\zeta_2)$$

for $\boldsymbol{i} \in \boldsymbol{I} = \{\boldsymbol{i} = (i_1, i_2) : 1 \le i_l \le n_l, l = 1, 2\}$, and the spline space is given by

$$S_{\boldsymbol{p}}(\boldsymbol{\Xi}) = \operatorname{span}\Big\{ \widehat{B}_{\boldsymbol{i},\boldsymbol{p}} : \boldsymbol{i} \in \boldsymbol{I} \Big\}.$$

The corresponding bivariate NURBS basis functions read

$$\widehat{N}_{\boldsymbol{i},\boldsymbol{p}}(\boldsymbol{\zeta}) = \frac{w_{\boldsymbol{i}}\, \widehat{B}_{\boldsymbol{i},\boldsymbol{p}}(\boldsymbol{\zeta})}{W(\boldsymbol{\zeta})}$$

using the weight function

$$W(\boldsymbol{\zeta}) = \sum_{\boldsymbol{l} \in \boldsymbol{I}} w_{\boldsymbol{l}}\, \widehat{B}_{\boldsymbol{l},\boldsymbol{p}}(\boldsymbol{\zeta}), \tag{2.13}$$

where we choose weights $w_{\boldsymbol{l}} > 0$ for all $\boldsymbol{l} \in \boldsymbol{I}$. The space of NURBS on the parametric domain is finally denoted by

$$N_{\boldsymbol{p}}(\boldsymbol{\Xi}, W) = \operatorname{span}\Big\{ \widehat{N}_{\boldsymbol{i},\boldsymbol{p}} : \boldsymbol{i} \in \boldsymbol{I} \Big\}.$$

Refinements of bivariate spline and NURBS spaces can be obtained similar to (2.2) and the refining algorithms extend naturally to the bivariate setting.

NURBS parameterizations of planar geometries are defined as linear combinations of the tensor product functions introduced above,

$$\boldsymbol{F}(\boldsymbol{\zeta}) = \sum_{\boldsymbol{i} \in \boldsymbol{I}} \boldsymbol{c}_{\boldsymbol{i}}\, \widehat{N}_{\boldsymbol{i},\boldsymbol{p}}(\boldsymbol{\zeta}), \tag{2.14}$$

where each basis function is associated with a control point $\boldsymbol{c}_{\boldsymbol{i}} \in \mathbb{R}^2$, $\boldsymbol{i} \in \boldsymbol{I}$. The $\boldsymbol{F}$-image $\Omega = \boldsymbol{F}(\widehat{\Omega})$ of the parametric domain $\widehat{\Omega} = (0,1)^2$ is commonly referred to as the physical domain. Using this construction, exact parameterizations $\boldsymbol{F} : \widehat{\Omega} \to \Omega$ of various types of domains, including geometric primitives like conic sections, can be obtained [12,35,37,38].

To define a mesh in Ω, we consider the image under $\boldsymbol{F}$ of the partition given by the knot vectors without repetitions, i.e., each element $Q_{\boldsymbol{j}} \in \widehat{\mathcal{M}}$ of the parametric Bézier mesh (2.11) is mapped to an element $K_{\boldsymbol{j}} = \boldsymbol{F}(Q_{\boldsymbol{j}})$ in the physical domain. We set

$$\mathcal{M} := \big\{ K_{\boldsymbol{j}} \subset \Omega : K_{\boldsymbol{j}} = \boldsymbol{F}(Q_{\boldsymbol{j}}), \boldsymbol{j} \in \boldsymbol{J} \big\},$$

which is commonly known as the physical Bézier mesh, or simply Bézier mesh. The meshes for the coarsest knot vector $\boldsymbol{\Xi}^0 = (\Xi_1^0, \Xi_2^0)$ will be denoted by $\widehat{\mathcal{M}}_0$ and $\mathcal{M}_0$.

The univariate quasi-interpolant (2.8) can be generalized to the bivariate case by a tensor product construction [28],

$$\Pi_{\boldsymbol{p},\boldsymbol{\Xi}}(v) = \Big(\Pi_{p_1,\Xi_1} \otimes \Pi_{p_2,\Xi_2} \Big).$$

It can also be expressed in terms of a dual basis,

$$\Pi_{p,\Xi} : L^1([0,1]^2) \to S_p(\Xi), \quad \Pi_{p,\Xi}(v) = \sum_{i \in I} \lambda_{i,p}(v) \widehat{B}_{i,p}, \tag{2.15}$$

where the dual functionals are again given by tensor products [37, Chapter XVII],

$$\lambda_{i,p} = \lambda_{i_1,p_1} \otimes \lambda_{i_2,p_2}$$

and satisfy

$$\lambda_{i,p}(\widehat{B}_{k,p}) = \delta_{ik}. \tag{2.16}$$

Here, δ_{ik} stands for a multi-index Kronecker symbol, i.e.,

$$\delta_{ik} = \begin{cases} 1 & \text{if } i = (i_1, i_2) = (k_1, k_2) = k, \\ 0 & \text{else.} \end{cases}$$

This operator is typically modified further for the consideration of boundary conditions on the boundary $\widehat{\Gamma} = \partial\widehat{\Omega}$ of $\widehat{\Omega}$. Using the univariate construction (2.8), we define

$$\Pi^{\widehat{\Gamma}}_{p,\Xi} = \left(\Pi^{\widehat{\Gamma}}_{p_1,\Xi_1} \otimes \Pi^{\widehat{\Gamma}}_{p_2,\Xi_2} \right) : C([0,1]^2) \to S_p(\Xi). \tag{2.17}$$

Due to the properties (2.9) and (2.10), the modified projection satisfies a strong locality property on $\widehat{\Gamma}$. In more detail, $(\Pi^{\widehat{\Gamma}}_{p,\Xi} v)\big|_{\widehat{\Gamma}_i}$ only depends on $v\big|_{\widehat{\Gamma}_i}$ for every face $\widehat{\Gamma}_i$ of $\widehat{\Gamma}$. Moreover, we obtain a representation

$$\Pi^{\widehat{\Gamma}}_{p,\Xi}(v) = \sum_{i \in I} \lambda^{\widehat{\Gamma}}_{i,p}(v) \widehat{B}_{i,p} \tag{2.18}$$

with modified functionals $\lambda^{\widehat{\Gamma}}_{i,p} = \lambda^{\widehat{\Gamma}}_{i_1,p_1} \otimes \lambda^{\widehat{\Gamma}}_{i_2,p_2}$, $i \in I$, which also satisfy the dual functional property (2.16) since all considered knot vectors are open. Note that the notation $\widehat{\Gamma}$ is used both for $\widehat{\Gamma} = \{0,1\}$ in the univariate setting and $\widehat{\Gamma} = \partial\widehat{\Omega}$ in the tensor product configuration.

3. Main concepts and results

In this section, the main concepts and results of the paper are presented. First, we define polar parameterizations of domains with corners, introduce the model problem, and investigate regularity properties of the solutions. To address the corner singularity, we then explain the proposed graded mesh refinement scheme. Finally, in Section 3.4, the key results of our work are provided, including error estimates on graded polar meshes that establish optimal convergence rates for suitable grading parameters.

3.1. Polar parameterizations of domains with corners

Polar parameterizations in IGA have been extensively studied in multiple research works [23–26]. The terminology originates from the analogy with the classical transformation from polar to Cartesian coordinates. To establish notation and highlight essential properties, we introduce the following definition, which aligns closely with standard configurations in the literature.

Definition 3.1 (Polar parameterization, polar point, polar domain)**.** An isogeometric mapping $F : \widehat{\Omega} \to \Omega$ of the form (2.14), constructed as described in Section 2.2, is called a *polar parameterization* if it collapses the left edge of the parametric domain into a single point,

$$F(0, \zeta_2) = P = 0 \quad \text{for all } \zeta_2 \in [0,1], \tag{3.1}$$

where $P \in \mathbb{R}^2$ is termed the *polar point* and, without loss of generality, is always chosen as $P = 0$. The corresponding image $\Omega = F(\widehat{\Omega})$ is referred to as a *polar domain*.

Next, we specify the considered class of polar domains further with respect to the location of the polar point within the domain.

Definition 3.2 (Polar domain with corner, polar corner)**.** Let $\Omega \subset \mathbb{R}^2$ be a polar domain such that the polar point P lies on the boundary of the domain, i.e., $P \in \Gamma = \partial\Omega$. Then, P represents a vertex of the domain, and Ω is called a *polar domain with corner*. The corresponding interior angle at P is denoted by $\omega \in (0, 2\pi]$. In this context, P is also called the *polar corner* of the domain. Strictly speaking, the case $\omega = \pi$ does not constitute a corner in the geometric sense, but we still regard P as a corner of the parameterization for the purposes of the subsequent analysis.

Definition 3.2 is typically not required in the available literature on polar domains [23–26], and we point out the background of this choice in the following Remark.

Remark 3.3. The condition $\boldsymbol{P} \in \Gamma$ excludes parameterizations in which the polar point is located inside the domain. A well-known example of such an excluded scenario is the polar parameterization of a unit disk, which additionally requires prescribing periodic boundary conditions on the two boundary edges adjacent to the polar point. In most related publications, a periodicity condition is imposed explicitly [25,26]. Here, we instead require that the boundary of the parametric domain is mapped onto the boundary of the polar domain. The mathematical convergence analysis of the periodic case introduces additional challenges, which go beyond the scope of this paper. Nonetheless, the mathematical framework developed here may serve as a foundation for future investigations on polar domains without corners like the unit disk – in particular, since numerical results are very promising, see for instance [8, Remark 6.12].

In Fig. 1, we illustrate exemplary parameterizations of polar domains with corners, which will be discussed in more detail in Examples 3.6–3.8 at the end of this section. Beforehand, we explain how such isogeometric mappings can be constructed and point out some central properties. We denote the four boundary edges of the parametric domain by $\widehat{\Gamma}_i$, $i = 1, \dots, 4$, following the ordering proposed in [39], see also Fig. 1. The left edge of the parametric domain collapses as required in (3.1) if all the control points associated to $\widehat{\Gamma}_1$ are located at the polar point [23,24],

$$\boldsymbol{c}_{\boldsymbol{i}_\odot} = \boldsymbol{P} = \boldsymbol{0} \quad \text{for all } \boldsymbol{i}_\odot \in \boldsymbol{I}_\odot := \{\boldsymbol{i} = (i_1, i_2) \in \boldsymbol{I} : i_1 = 1\}, \tag{3.2}$$

where $\boldsymbol{I}_\odot \subset \boldsymbol{I}$ is called the polar index set and $\boldsymbol{I}$ is defined as in Section 2.2. In the following, we further demonstrate that the condition (3.5) on the Jacobian is fulfilled if the coarse linear knot vector

$$\Xi_1^0 = \{0, 0, 1, 1\}$$

is employed in the first parametric direction, as in Examples 3.6–3.8. Formula (2.14) and the partition of unity property of NURBS then yield that $\boldsymbol{F}$ is of the form

$$\boldsymbol{F}(\zeta_1, \zeta_2) = \sum_{i_2=1}^{n_2} \widehat{N}_{2,1}(\zeta_1) \widehat{N}_{i_2,p_2}(\zeta_2)\, \boldsymbol{c}_{(2,i_2)} = \zeta_1 \sum_{i_2=1}^{n_2} \widehat{N}_{i_2,p_2}(\zeta_2)\, \boldsymbol{c}_{(2,i_2)} = \zeta_1\, \boldsymbol{G}(\zeta_2)$$

with a function $\boldsymbol{G} = \big(G_1, G_2\big)^T : [0,1] \to \Gamma_2$ that only depends on ζ_2 and maps into the boundary part away from the polar point, $\Gamma_2 := \boldsymbol{F}(\widehat{\Gamma}_2) = \boldsymbol{G}([0,1]) \subset \partial\Omega$. The remaining parametric boundary edges are mapped onto the edges adjacent to the corner, $\Gamma_3 := \boldsymbol{F}(\widehat{\Gamma}_3)$, and $\Gamma_4 := \boldsymbol{F}(\widehat{\Gamma}_4)$. This motivates the following assumption which will be useful for the proofs in our paper.

Assumption 3.4. We assume that $\boldsymbol{F}$ is of the form

$$\boldsymbol{F}(\zeta_1, \zeta_2) = \zeta_1\, \boldsymbol{G}(\zeta_2) \tag{3.3}$$

with a function $\boldsymbol{G} = \big(G_1, G_2\big)^T : [0,1] \to \mathbb{R}^2$ such that

$$\big|\boldsymbol{G}(\zeta_2)\big| \sim 1.$$

Moreover, we assume that G_1 and G_2 have bounded derivatives at all points where $\boldsymbol{F}$ is differentiable with respect to the second component, and that

$$\big|\boldsymbol{G}(\zeta_2) \times \boldsymbol{G}'(\zeta_2)\big| = \Big|G_1(\zeta_2)\, G_2'(\zeta_2) - G_2(\zeta_2)\, G_1'(\zeta_2)\Big| \sim 1.$$

For completeness, we remind the reader that the isogeometric mapping $\boldsymbol{F}$ generally does not change during the refinement process. The Jacobian of a parameterization of the form (3.3) is given by

$$J_{\boldsymbol{F}}(\zeta_1, \zeta_2) = \begin{pmatrix} G_1(\zeta_2) & \zeta_1\, G_1'(\zeta_2) \\ G_2(\zeta_2) & \zeta_1\, G_2'(\zeta_2) \end{pmatrix} \tag{3.4}$$

at all points $\boldsymbol{\zeta} = (\zeta_1, \zeta_2) \in \widehat{\Omega}$ where $\boldsymbol{F}$ is differentiable with respect to ζ_2. Consequently, under Assumption 3.4, we obtain

$$\big|\det(J_{\boldsymbol{F}}(\zeta_1, \zeta_2))\big| = \Big|\zeta_1 \big(G_1(\zeta_2)\, G_2'(\zeta_2) - G_2(\zeta_2)\, G_1'(\zeta_2)\big)\Big| \sim \zeta_1. \tag{3.5}$$

The parameterization (3.3) contains a polar singularity in the sense that

$$\frac{\partial \boldsymbol{F}}{\partial \zeta_2}(0, \zeta_2) = (0,0)^T \quad \text{and} \quad \det(J_{\boldsymbol{F}}(0, \zeta_2)) = 0.$$

In this regard, the collapsing edge $\widehat{\Gamma}_1$ will sometimes also be called the singular edge. Furthermore, we set $\boldsymbol{\zeta}(\boldsymbol{x}) = (\zeta_1(\boldsymbol{x}), \zeta_2(\boldsymbol{x})) = \boldsymbol{F}^{-1}(\boldsymbol{x})$ for all $\boldsymbol{x} \neq \boldsymbol{0}$ and by the inverse function theorem, we have

$$J_{\boldsymbol{F}^{-1}}(\boldsymbol{x}) = J_{\boldsymbol{F}}^{-1}(\zeta_1(\boldsymbol{x}), \zeta_2(\boldsymbol{x})) = \frac{1}{\det(J_{\boldsymbol{F}}(\zeta_1(\boldsymbol{x}), \zeta_2(\boldsymbol{x})))} \begin{pmatrix} \zeta_1(\boldsymbol{x}) G_2'(\zeta_2(\boldsymbol{x})) & -\zeta_1(\boldsymbol{x}) G_1'(\zeta_2(\boldsymbol{x})) \\ -G_2(\zeta_2(\boldsymbol{x})) & G_1(\zeta_2(\boldsymbol{x})) \end{pmatrix}. \tag{3.6}$$

Due to Assumption 3.4 and (3.5), the determinant of the Jacobian of the inverse transformation is given by

$$\Big|\det\big(J_{\boldsymbol{F}^{-1}}(\boldsymbol{x})\big)\Big| \sim \frac{1}{\zeta_1(\boldsymbol{x})} \tag{3.7}$$

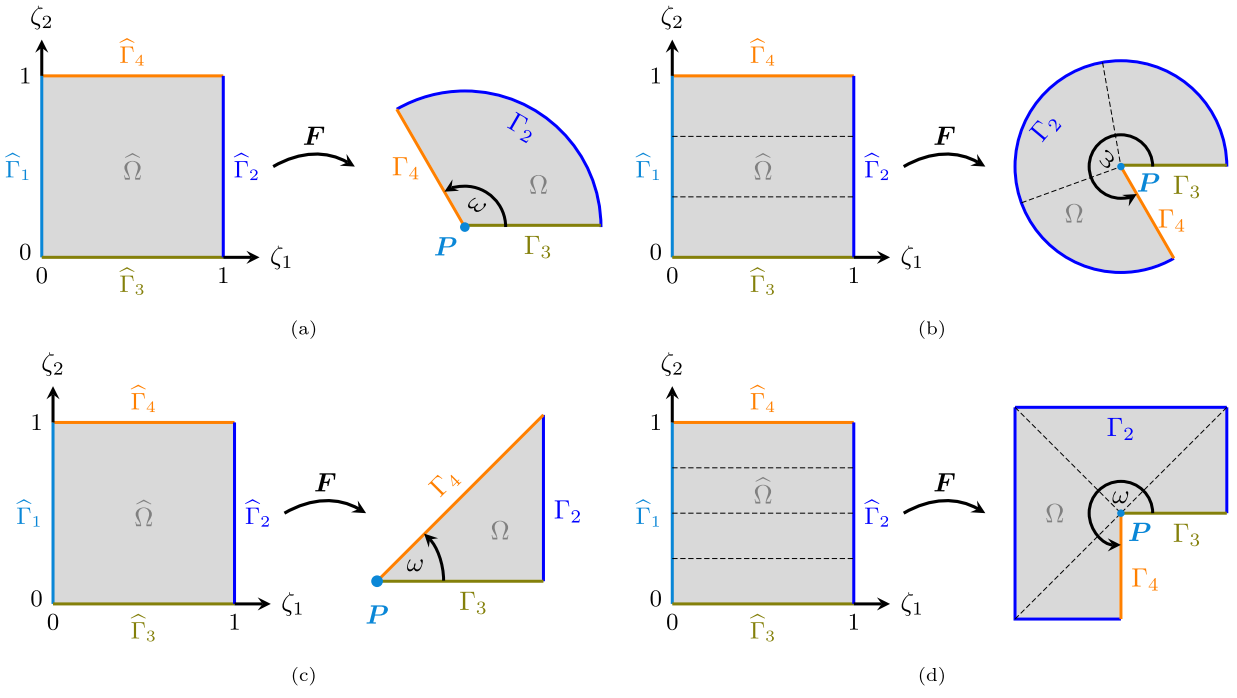

Fig. 1. Polar parameterizations of exemplary domains with corners and corresponding boundary notation. (a): Circular sector with angle $\omega = \frac{2}{3}\pi$ (b): Circular sector with angle $\omega = \frac{5}{3}\pi$, also known as Pacman domain. (c): Triangle. (d): L-shaped domain.

and blows up near the polar point. In this context, we further note another property. Let $r(\boldsymbol{x}) = |\boldsymbol{x}|$ be the distance of every point $\boldsymbol{x} \in \mathbb{R}^2$ to $\boldsymbol{0}$. Then, for all $\boldsymbol{x} \neq \boldsymbol{0}$, it follows from Assumption 3.4 that

$$r(\boldsymbol{x}) = r(\boldsymbol{F}(\boldsymbol{\zeta}(\boldsymbol{x}))) = r(\zeta_1(\boldsymbol{x})\,\boldsymbol{G}(\zeta_2(\boldsymbol{x}))) = \zeta_1(\boldsymbol{x})\big|\boldsymbol{G}(\zeta_2(\boldsymbol{x}))\big| \sim \zeta_1(\boldsymbol{x}), \tag{3.8}$$

while $r(\boldsymbol{0}) = 0$ trivially holds.

Lastly, we comment on the weight function (2.13) introduced in Section 2.2. Typically, as in the considered Examples 3.6–3.8, the weights associated with the same i_2-index are chosen identically,

$$w_{(1,i_2)} = w_{(2,i_2)} = \cdots = w_{(n_1,i_2)} \quad \text{for } i_2 = 1, 2, \ldots, n_2.$$

Using the partition of unity formed by univariate B-splines, it follows that the weight function has the form

$$W(\boldsymbol{\zeta}) = \sum_{\boldsymbol{i}\in\boldsymbol{I}} w_{\boldsymbol{i}}\,\widehat{B}_{\boldsymbol{i},\boldsymbol{p}}(\boldsymbol{\zeta}) = \sum_{i_1=1}^{n_1} \widehat{B}_{i_1,p_1}(\zeta_1) \sum_{i_2=1}^{n_2} w_{(1,i_2)}\,\widehat{B}_{i_2,p_2}(\zeta_2) = \sum_{i_2=1}^{n_2} w_{(1,i_2)}\,\widehat{B}_{i_2,p_2}(\zeta_2)$$

and thus depends only on ζ_2. This leads to the following assumption:

Assumption 3.5. The weight function (2.13) depends solely on ζ_2, that is, there exists a function $w : [0,1] \to \mathbb{R}$ such that

$$W(\boldsymbol{\zeta}) = w(\zeta_2) \quad \text{for all } \boldsymbol{\zeta} = (\zeta_1, \zeta_2) \in \widehat{\Omega}. \tag{3.9}$$

In the following, we investigate in more detail the polar domains with corners depicted in Fig. 1. Assumptions 3.4 and 3.5 hold for all considered parameterizations, confirming their practical relevance.

Example 3.6 (Circular sector)**.** Consider a circular sector Ω with interior angle $\omega \in (0, \pi)$ and starting angle $\varphi_0 \in [0, 2\pi)$. Without loss of generality, we assume the sector is centered at $\boldsymbol{P} = (0,0)$ and has radius 1, that is, $\Omega = \big\{(r\cos\varphi, r\sin\varphi) : 0 < r < 1, \varphi_0 < \varphi < \varphi_0 + \omega\big\}$. Such a sector can be parameterized using the knot vectors $\Xi_1^0 = \{0,0,1,1\}$ and $\Xi_2^0 = \{0,0,0,1,1,1\}$, along with the control points and weights provided in Table 1, see also [12,40]. An example that illustrates this parameterization for an interior angle of $\omega = \frac{2}{3}\pi$ is displayed in Fig. 1(a). The resulting isogeometric mapping is smooth throughout the interior of the domain, in more detail, it holds $\boldsymbol{F} \in \Big(C^2(\widehat{\Omega})\Big)^2$, see [8, p.10]. In contrast, a polar parameterization for a circular sector with angle $\omega \in (\pi, 2\pi]$ can be constructed by combining multiple small sectors. To this end, repeated knot values are inserted into the knot vector Ξ_2^0. For example, a circular sector of angle $\omega = \frac{5}{3}\pi$ can be composed of three smaller sectors, each having an angle of $\frac{5}{9}\pi$, using the knot vectors $\Xi_1^0 = \{0,0,1,1\}$ and $\Xi_2^0 = \Big\{0,0,0,\frac{1}{3},\frac{1}{3},\frac{2}{3},\frac{2}{3},1,1,1\Big\}$. The seven control points and corresponding weights are derived by combining those of the three smaller sectors as listed in Table 1, where repetitions are omitted. The resulting geometry mapping is visualized in Fig. 1(b). However,

Table 1
Definition of control points $\boldsymbol{c}_i$ and weights w_i, $\boldsymbol{i} \in \boldsymbol{I}$, for a polar parameterization of a circular sector with inner angle $\omega \in (0, \pi)$, starting angle $\varphi_0 \in [0, 2\pi)$ and radius 1.

$\boldsymbol{c}_{(i_1,i_2)}; w_{(i_1,i_2)}$	$i_2 = 1$	$i_2 = 2$	$i_2 = 3$
$i_1 = 1$	$(0,0)^T; 1$	$(0,0)^T; \cos(\frac{\omega}{2})$	$(0,0)^T; 1$
$i_1 = 2$	$(\cos(\varphi_0), \sin(\varphi_0))^T; 1$	$\left(\frac{\cos\left(\varphi_0+\frac{\omega}{2}\right)}{\cos\left(\frac{\omega}{2}\right)}, \frac{\sin\left(\varphi_0+\frac{\omega}{2}\right)}{\cos\left(\frac{\omega}{2}\right)}\right)^T; \cos\left(\frac{\omega}{2}\right)$	$(\cos(\varphi_0+\omega), \sin(\varphi_0+\omega))^T; 1$

Table 2
Definition of control points $\boldsymbol{c}_i$ and weights w_i, $\boldsymbol{i} \in \boldsymbol{I}$, for a polar parameterization of an L-shaped domain.

$\boldsymbol{c}_{(i_1,i_2)}; w_{(i_1,i_2)}$	$i_2 = 1$	$i_2 = 2$	$i_2 = 3$	$i_2 = 4$	$i_2 = 5$
$i_1 = 1$	$(0,0)^T; 1$	$(0,0)^T; 1$	$(0,0)^T; 1$	$(0,0)^T; 1$	$(0,0)^T; 1$
$i_1 = 2$	$(1,0)^T; 1$	$(1,1)^T; 1$	$(-1,1)^T; 1$	$(-1,-1)^T; 1$	$(0,-1)^T; 1$

inserting repeated knot values reduces the inter-element smoothness to C^0, thus yielding a parameterization $\boldsymbol{F} \in \left(C^0(\widehat{\Omega})\right)^2$. An explicit representation of such an isogeometric mapping, together with a detailed comparison to the classical transformation from polar to Cartesian coordinates is provided in [10] for the special case of a circular sector with angle $\omega = 2\pi$.

Example 3.7 (Triangle)**.** Another domain that can be represented by a polar parameterization is a triangle, using the knot vectors $\Xi_1^0 = \Xi_2^0 = [0, 0, 1, 1]$. For instance, choosing the control points as $\boldsymbol{c}_{(1,1)} = \boldsymbol{c}_{(1,2)} = (0, 0)$, $\boldsymbol{c}_{(2,1)} = (1, 0)$ and $\boldsymbol{c}_{(2,2)} = (0, 1)$ and weights $w_{\boldsymbol{i}} = 1$, $\boldsymbol{i} \in \boldsymbol{I}$, generates a triangular domain defined by the three distinct control points. In this construction, the polar singularity is located at the vertex $\boldsymbol{P} = (0, 0)$. Such triangular configurations have been extensively studied in previous works [29,41]. The resulting parameterization is given by

$$\boldsymbol{F} : \widehat{\Omega} \to \Omega, \quad (\zeta_1, \zeta_2) \mapsto (\zeta_1, \zeta_1\zeta_2),$$

which is smooth at all inner points of the domain, i.e., $\boldsymbol{F} \in \left(C^\infty(\widehat{\Omega})\right)^2$.

Example 3.8 (L-Shape)**.** More complex geometries can be constructed by combining multiple polar triangles. For instance, an L-shaped domain can be represented by connecting four polar triangles, each parameterized from a strip of the unit square via a polar mapping. Precisely, we can use the knot vectors $\Xi_1^0 = \{0, 0, 1, 1\}$ and $\Xi_2^0 = \left\{0, 0, \frac{1}{4}, \frac{1}{2}, \frac{3}{4}, 1, 1\right\}$ and the control points and weights listed in Table 2. The resulting isogeometric mapping is depicted in Fig. 1(d). Due to the repeated knot values in Ξ_2^0, the global mapping is only C^0-continuous, that is, $\boldsymbol{F} \in \left(C^0(\widehat{\Omega})\right)^2$.

Remark 3.9.

Lastly, we discuss limitations of the polar parameterizations considered in this work and compare them with alternative strategies available in the literature.

- Generally, the polar domains considered in this paper possess multiple corners, not only the polar corner. More specifically, at least two further corners usually occur at the intersections of the boundary edge Γ_2 with its adjacent edges Γ_3 and Γ_4, as illustrated in all examples shown in Fig. 1. Additional corners may also appear along the boundary segment Γ_2, as seen in the L-shaped domain discussed in Example 3.8. However, these corners do not correspond to polar points of the parameterization, and the approximation properties near such corners are well understood. In accordance with the focus of this paper, we therefore restrict our analysis to the local behavior near polar corners and do not further investigate the remaining ones.
- The continuity of the polar parameterizations depends strongly on the interior angle at the corner and leads to trade-offs determined by the chosen refinement strategy and the underlying geometry representation.
  - For corner angles $\omega < \pi$, the polar parameterization remains smooth throughout the interior of the domain, preserving all advantages of higher-order smooth spline spaces, see Examples 3.6 and 3.7.
  - For domains with interior angles $\omega > \pi$, repeated knot insertion is required, which reduces inter-element continuity, as demonstrated in Examples 3.6 and 3.8. This phenomenon can be explained via the geometric interpretation of NURBS parameterizations as projective transformations of piecewise quadratic curves and has been investigated in the literature, see, for instance, the discussion of circular arcs in the seminal IGA book [27, Section 2.2.1]. While C^0-continuity remains sufficient for second-order PDEs, higher smoothness can be achieved using more advanced parameterization techniques instead. These include multipatch constructions, unstructured spline methods such as splines on triangulations, D-patch constructions, subdivision-based discretizations, almost-C^1 schemes, and trimming; see for instance [25,26,30,42–44]. Given the range of available approaches, the list is not exhaustive. However, these methods typically require careful patch layout, interface compatibility, or specialized basis functions. In addition, trimming-based techniques may struggle with corner angles of 2π, as encountered in domains with cracks. In this work, we focus on the standard polar parameterization and intentionally keep the geometric complexity to a minimum in order to facilitate analysis and maintain compatibility with standard IGA frameworks.

- For the sake of simplicity, this work is confined to single-patch polar parameterizations. Extending the approach to multipatch configurations with potentially smooth coupling could overcome the continuity deficits and remains a topic for future research.

3.2. Model problem and regularity properties

In the following, we describe our main model problem and investigate reduced regularity properties of the resulting solutions, which lead to inaccurate approximation with standard methods. Let $\Omega \subset \mathbb{R}^2$ be a polar domain with corner, as introduced in Definition 3.2, and let $\partial\Omega = \Gamma = \Gamma_N \cup \Gamma_D$ be its boundary, where the Dirichlet and Neumann boundary are denoted by Γ_D and Γ_N, with $\Gamma_N \cap \Gamma_D = \emptyset$. We assume non-empty Dirichlet boundary, $\Gamma_D \neq \emptyset$, and require each boundary edge to be completely contained in either the Dirichlet or the Neumann boundary, i.e., $\Gamma_\gamma \subset \Gamma_D$ or $\Gamma_\gamma \subset \Gamma_N$ for $\gamma = 2, 3, 4$. Our model problem is the Poisson equation

$$\begin{aligned} -\Delta u &= f \quad \text{in } \Omega, \\ u &= 0 \quad \text{on } \Gamma_D, \\ \frac{\partial u}{\partial n} &= 0 \quad \text{on } \Gamma_N. \end{aligned} \tag{3.10}$$

For the sake of simplicity, we assume homogeneous boundary conditions. The numerical analysis of inhomogeneous boundary data adds further complexity which is not in the scope of this paper. The weak formulation of problem (3.10) reads: Find $u \in V_0$ such that

$$a(u, v) = b(v) \quad \forall v \in V_0, \tag{3.11}$$

where we define the spaces

$$V := H^1(\Omega) \quad \text{and} \quad V_0 := \{ v \in V : v = 0 \text{ on } \Gamma_D \} \tag{3.12}$$

and the bilinear and linear form

$$\begin{aligned} a &: V \times V \to \mathbb{R}, \quad a(u, v) := \int_\Omega \nabla u \cdot \nabla v \, \mathrm{d}\boldsymbol{x}, \\ b &: V \to \mathbb{R}, \quad b(v) := \int_\Omega f v \, \mathrm{d}\boldsymbol{x}. \end{aligned}$$

Since both forms are bounded and a is coercive on V_0, the variational problem (3.11) has a unique solution $u \in V_0$. Let further $V_{0h} \subset V_0$ be a subspace of finite dimension. The corresponding discrete problem reads: Find $u_h \in V_{0h}$ such that

$$a(u_h, v_h) = b(v_h) \quad \forall v_h \in V_{0h}, \tag{3.13}$$

which yields a unique discrete solution $u_h \in V_{0h}$.

The regularity of the solution u can be described conveniently using the concept of weighted Sobolev spaces, which we introduce in the following. For a given domain $\Omega \subset \mathbb{R}^2$, we denote the usual Sobolev spaces on Ω by $H^s(\Omega)$, $s \in \mathbb{N}_0$, with $L^2(\Omega) = H^0(\Omega)$. Moreover, let $\mathcal{D}'(\Omega)$ be the space of distributions on Ω.

Definition 3.10 (Weighted Sobolev spaces on the physical domain)**.** Let $\Omega \subset \mathbb{R}^2$ be a bounded domain and let $r = r(\boldsymbol{x}) = |\boldsymbol{x}| = \sqrt{x^2 + y^2}$ be the distance of every point $\boldsymbol{x} = (x, y) \in \Omega$ to $\mathbf{0}$. We define the weighted Sobolev spaces $H^s_\beta(\Omega)$ and $V^s_\beta(\Omega)$ for $s \in \mathbb{N}_0$ and $\beta \in \mathbb{R}$ by

$$H^s_\beta(\Omega) := \left\{ v \in \mathcal{D}'(\Omega) : \|v\|_{H^s_\beta(\Omega)} < \infty \right\} \quad \text{and} \quad V^s_\beta(\Omega) := \left\{ v \in \mathcal{D}'(\Omega) : \|v\|_{V^s_\beta(\Omega)} < \infty \right\},$$

respectively, where

$$\begin{aligned} \|v\|_{H^s_\beta(\Omega)} &:= \left(\sum_{|\boldsymbol{\alpha}| \le s} \left\| r^\beta D^{\boldsymbol{\alpha}} v \right\|^2_{L^2(\Omega)} \right)^{1/2} = \left(\sum_{|\boldsymbol{\alpha}| \le s} \int_\Omega \left| r(\boldsymbol{x})^\beta D^{\boldsymbol{\alpha}} v(\boldsymbol{x}) \right|^2 \mathrm{d}\boldsymbol{x} \right)^{1/2}, \\ \|v\|_{V^s_\beta(\Omega)} &:= \left(\sum_{|\boldsymbol{\alpha}| \le s} \left\| r^{\beta - s + |\boldsymbol{\alpha}|} D^{\boldsymbol{\alpha}} v \right\|^2_{L^2(\Omega)} \right)^{1/2} = \left(\sum_{|\boldsymbol{\alpha}| \le s} \int_\Omega \left| r(\boldsymbol{x})^{\beta - s + |\boldsymbol{\alpha}|} D^{\boldsymbol{\alpha}} v(\boldsymbol{x}) \right|^2 \mathrm{d}\boldsymbol{x} \right)^{1/2}. \end{aligned}$$

Corresponding seminorms are defined by

$$|v|_{H^s_\beta(\Omega)} := |v|_{V^s_\beta(\Omega)} := \left(\sum_{|\boldsymbol{\alpha}| = s} \left\| r^\beta D^{\boldsymbol{\alpha}} v \right\|^2_{L^2(\Omega)} \right)^{1/2}.$$

The Sobolev spaces on Ω without weight are denoted by $H^s(\Omega) = H^s_0(\Omega)$ and $V^s(\Omega) = V^s_0(\Omega)$ and we write $L^2_\beta(\Omega) = H^0_\beta(\Omega) = V^0_\beta(\Omega)$.

Such spaces have been studied both in the analytic setting [45–47] and in the context of finite element methods [3,6]. It is well-known that they form Hilbert spaces and corresponding embedding theorems have been derived. In particular, for all $s \in \mathbb{N}$ and $\beta \in \mathbb{R}$, the embedding

$$V^s_\beta(\Omega) \hookrightarrow H^s_\beta(\Omega). \tag{3.14}$$

follows directly.

In general, the solution u of the Poisson equation (3.10) has a singularity of type r^ν in the vicinity of the polar corner, where the singular exponent $\nu \in \mathbb{R}$ is defined by the boundary conditions and the corner angle ω. More precisely, it is $\nu = \frac{\pi}{\omega}$ for Dirichlet or Neumann boundary conditions on both edges adjacent to the corner and $\nu = \frac{\pi}{2\omega}$ for mixed boundary conditions at $r = 0$. In terms of weighted spaces, the regularity is characterized as follows. For Dirichlet and mixed boundary conditions at the corner, we have

$$u \in V^s_\beta(\Omega) \quad \text{for all } \beta \in \mathbb{R} \text{ with } s - 1 - \nu < \beta < s - 1 + \nu, \tag{3.15}$$

provided that the right-hand side satisfies $f \in V^{s-2}_\beta(\Omega)$ for $s \in \mathbb{N}, s \geq 2$. In addition, the a priori estimate

$$\|u\|_{V^s_\beta(\Omega)} \leq C \|f\|_{V^{s-2}_\beta(\Omega)} \tag{3.16}$$

holds [48, Chapter 2, Theorem 3.1]. For Neumann boundary conditions, additional restrictions are required due to the presence of constants in the solution. For instance, assuming that u vanishes at the polar corner restores the regularity results above at least for $s = 2$.

Remark 3.11. Consistent with the title and focus of this paper, we do not analyze solution regularity at the non-polar corners of the domain, see also Remark 3.9. At those vertices, we assume the solution is sufficiently smooth so as not to affect our local analysis around the polar corner.

3.3. Graded isogeometric mesh refinement for polar domains with corners

Next, we describe how isogeometric meshes can be refined in a graded way to tackle the corner singularities numerically. The idea of mesh grading toward corners is inspired by comparable approaches for finite elements [3–5,7]. Similar concepts have also been proposed in isogeometric literature [8,9], but only for smoothly parameterized domains, leading to non-local refinement along the mapped edges of a patch. In our recent work [10], we introduced the grading scheme for polar parameterizations of circular sectors, which will be generalized in the following. To simplify notation and without loss of generality, we assume that the coarse parametric Bézier mesh defined by the coarse knot vector $\boldsymbol{\Xi}^0 = (\Xi^0_1, \Xi^0_2)$ is uniform. That is, we have the coarse vectors of breakpoints

$$Z^0_l = \left\{ \zeta_{l,j_l} := (j_l - 1)h^0_l \,:\, 1 \leq j_l \leq N^0_l \right\}, \quad l = 1, 2,$$

with the uniform coarse mesh sizes $h^0_l = \frac{1}{N^0_l - 1}$ for some $N^0_l \in \mathbb{N}$. The construction extends analogously to non-uniform coarse meshes.

The central idea of our method is to modify the typical uniform refinement procedure for the coarse radial knot vector Ξ^0_1. In this way, we achieve a grading of the resulting Bézier mesh toward the corner of the polar domain. In more detail, let $\Xi^{\mathrm{u}}_1 = \{\xi^{\mathrm{u}}_{1,1}, \xi^{\mathrm{u}}_{1,2} \dots, \xi^{\mathrm{u}}_{1,n_1+p_1+1}\}$ be a uniform refinement of Ξ^0_1, obtained by standard knot insertion and degree elevation up to degree p_1, and let $Z^{\mathrm{u}}_1 = \{\zeta^{\mathrm{u}}_{1,j_1} := (j_1 - 1)h_1 \,:\, 1 \leq j_l \leq N_1\}$ be the corresponding uniform vector of knots without repetitions, where $h_1 = \frac{1}{N_1 - 1}$ for some $N_1 \in \mathbb{N}$ with $\frac{N_1 - 1}{N^0_1 - 1} \in \mathbb{N}$. We choose a *grading parameter* $\mu \in (0, 1]$ and define the graded knot vector Ξ_1 by taking all the entries of the uniform vector Ξ^{u}_1 to the power of $\frac{1}{\mu}$,

$$\Xi_1 = \left\{ \xi_{1,i_1} := (\xi^{\mathrm{u}}_{1,i_1})^{\frac{1}{\mu}} \,:\, 1 \leq i_1 \leq n_1 + p_1 + 1 \right\} = \left\{ (\xi^{\mathrm{u}}_{1,1})^{\frac{1}{\mu}}, (\xi^{\mathrm{u}}_{1,2})^{\frac{1}{\mu}}, \dots, (\xi^{\mathrm{u}}_{1,n_1+p_1+1})^{\frac{1}{\mu}} \right\}.$$

Hence, the corresponding graded vector of knots without repetitions is also given by taking all the entries of Z_1 to the power of $\frac{1}{\mu}$,

$$Z_1 = \left\{ \zeta_{1,j_1} := (\zeta^{\mathrm{u}}_{1,j_1})^{\frac{1}{\mu}} = \big((j_1 - 1)h_1\big)^{\frac{1}{\mu}} \,:\, 1 \leq j_1 \leq N_1 \right\}, \tag{3.17}$$

which we refer to as graded mesh refinement. Note that choosing $\mu = 1$ leads to standard uniform refinement, making the proposed scheme a generalization of classical refinement. In this sense, mesh grading may be interpreted as a post-processing of the uniform mesh. Throughout our paper, we work exclusively with graded refinement in the first parametric direction, allowing any $\mu \in (0, 1]$.

In ζ_2-direction, no adjustments are needed, and we employ a standard uniform refinement $\Xi_2 = \Xi^{\mathrm{u}}_2$ of Ξ^0_2 and its corresponding uniform vector of breakpoints

$$Z_2 = Z^{\mathrm{u}}_2 = \left\{ \zeta_{2,j_2} = \zeta^{\mathrm{u}}_{2,j_2} = (j_2 - 1)h_2 \,:\, 1 \leq j_2 \leq N_2 \right\}, \tag{3.18}$$

with $h_2 = \frac{1}{N_2 - 1}$ for $N_2 \in \mathbb{N}$ with $\frac{N_2 - 1}{N^0_2 - 1} \in \mathbb{N}$. Consequently, we obtain a graded parametric Bézier mesh

$$\widehat{\mathcal{M}}^\mu := \left\{ Q_{\boldsymbol{j}} \subset \hat{\Omega} \,:\, Q_{\boldsymbol{j}} = (\zeta_{1,j_1}, \zeta_{1,j_1+1}) \times (\zeta_{2,j_2}, \zeta_{2,j_2+1}) = \left((\zeta^{\mathrm{u}}_{1,j_1})^{\frac{1}{\mu}}, (\zeta^{\mathrm{u}}_{1,j_1+1})^{\frac{1}{\mu}} \right) \times \left(\zeta^{\mathrm{u}}_{2,j_2}, \zeta^{\mathrm{u}}_{2,j_2+1} \right), \boldsymbol{j} \in \boldsymbol{J} \right\},$$

which is locally refined towards the singular edge. The corresponding physical Bézier mesh

$$\mathcal{M}^\mu := \left\{ K_{\boldsymbol{j}} \subset \Omega \,:\, K_{\boldsymbol{j}} = \boldsymbol{F}(Q_{\boldsymbol{j}}), \boldsymbol{j} \in \boldsymbol{J} \right\}$$

is locally refined towards the polar corner of the domain. In Fig. 2(a) and (b), we illustrate the graded meshes exemplarily for a circular sector and an L-shaped domain.

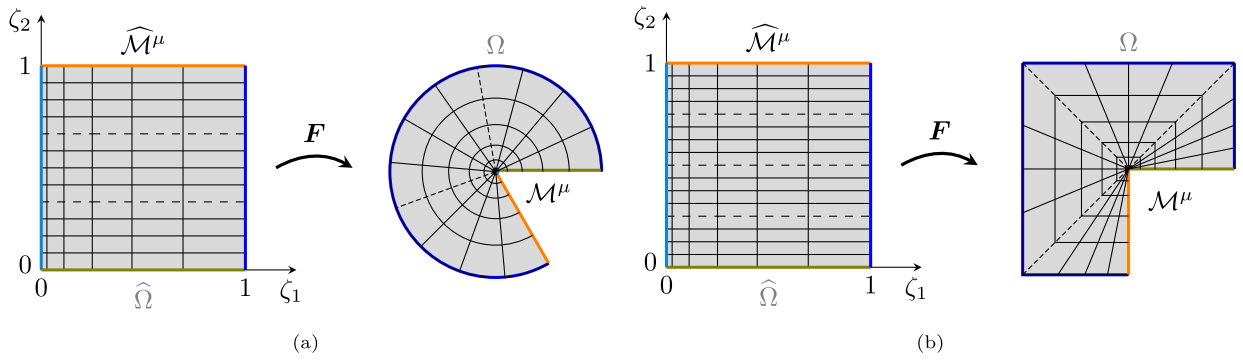

Fig. 2. Graded parametric and physical Bézier meshes. (a): Circular sector. (b): L-shaped domain.

Remark 3.12. Finally, we collect several observations on the proposed a priori grading scheme.

- Grading the mesh toward the polar corner enables resolution of the singularity through a better distribution of degrees of freedom, without increasing the total number compared to uniform refinement.
- Previous mesh grading strategies in IGA either restricted refinement to mapped edges of smoothly parameterized domains [8,9], or relied on trimming techniques that can fail when the corner angle equals 2π, see for instance [43]. In contrast, our approach enables mesh grading directly toward the polar point singularity and remains robust even for domains exhibiting cracks.
- Our analysis focuses on the local approximation behavior in the vicinity of the polar corner. This setting is particularly challenging due to the singularity of the isogeometric mapping. Therefore, the solution is assumed to be sufficiently smooth elsewhere, and the treatment of other corners is omitted; see also Remarks 3.9 and 3.11.
- Since corner singularities are local phenomena, the grading construction around the polar corner can be applied repeatedly to treat domains with multiple singularities, connected through a multipatch framework. An example is shown in Fig. 3(a), where several polar triangles are combined to form a U-shaped geometry. Alternatively, a discontinuous multipatch approach may be employed, as demonstrated in [43, Section 3.3]. For more general domains with one single corner singularity, scaled boundary parameterizations provide an effective alternative, as illustrated exemplarily in Fig. 3(b). A detailed investigation of these multipatch strategies lies beyond the scope of the present work.
- **A priori graded versus adaptive hierarchical refinement:** When the singular behavior at a corner is known or can be estimated a priori, graded refinement offers a conceptually simple and computationally efficient alternative to adaptive methods. In particular, it is sufficient to have a lower bound for the singular exponent ν, which is available for many PDE problems. Graded meshes achieve optimal convergence without requiring refinement indicators or major changes to solver infrastructure. Due to their simplicity, they enable highly accurate approximations on fine meshes, particularly when combined with higher-order basis functions. In this context, a priori mesh grading also provides a benchmark for the optimal convergence rates that adaptive methods based on a posteriori error estimators are expected to achieve. In contrast, fully adaptive methods offer significantly greater flexibility. The proposed grading approach cannot automatically detect and resolve unexpected singular behaviors – capabilities that adaptive hierarchical methods are specifically designed to address. Finally, we note that mesh grading preserves the global tensor-product structure of the underlying Bézier mesh. However, the resulting polar spline space (3.21) generally no longer possesses a tensor-product form, as can be seen from its basis representation (4.4), except for specific constellations of boundary conditions, see Remark 4.1. Conversely, hierarchical refinement breaks the global tensor-product structure but retains locally structured tensor-product meshes and spline spaces.

3.4. Main results

In this section, we state the main results of our paper, given by error estimates on polar domains with corners, which will then be proven in the subsequent sections. In particular, we establish optimal approximation rates on graded meshes with suitable grading parameters. Let Ω be a polar domain with corner and let $\widehat{V}_h = N_p(\Xi, W)$ be a standard NURBS space on $\widehat{\Omega}$, which has been obtained by graded refinement of the initial polar discretization, following an isoparametric approach. Throughout the remainder of the paper, we work under Assumptions 3.4 and 3.5. For simplicity, we further assume $h_1 \sim h_2$ for the mesh sizes in both parametric directions and set $h = \max\{h_1, h_2\}$. Moreover, $\boldsymbol{p} = (p_1, p_2)$ denotes the bivariate NURBS degree of the refined approximation space and $p = \min\{p_1, p_2\}$. The lack of regularity in the polar parameterization results in a variational crime when standard isogeometric approximation spaces

$$V_h = \left\{ f \circ \boldsymbol{F}^{-1} \,:\, f \in N_p(\Xi, W) \right\} = \operatorname{span}\left\{ N_{i,p}(\boldsymbol{x}) := \widehat{N}_{i,p} \circ \boldsymbol{F}^{-1}(\boldsymbol{x}) \,:\, i \in \boldsymbol{I} \right\} \tag{3.19}$$

are used since the basis functions associated to the control points collapsing in the polar point,

$$\left\{ N_{i_\odot,p} = \widehat{N}_{i_\odot,p} \circ \boldsymbol{F}^{-1} \,:\, i_\odot \in \boldsymbol{I}_\odot \right\}, \quad \text{with } \boldsymbol{I}_\odot \text{ from (3.2)}, \tag{3.20}$$

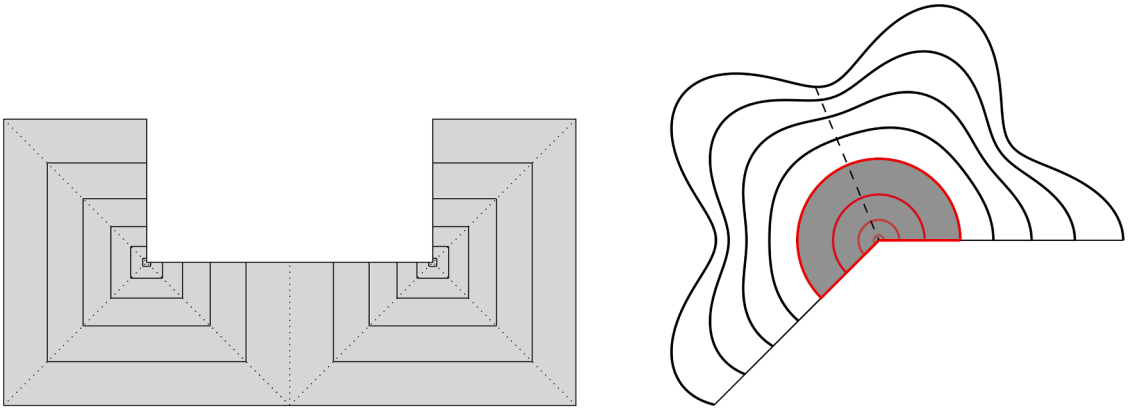

Fig. 3. Sketch of multipatch parameterizations for complex domains based on polar mappings. (a): U-shaped domain parameterized by eight polar triangles with graded meshes toward the two corners. (b): Scaled boundary parameterization of a segment of a flower-shaped domain, where a circular sector with a graded mesh is employed locally near the corner.

are not in $H^1(\Omega)$ and thus $V_h \not\subset V = H^1(\Omega)$, see [23,24]. Besides, the functions (3.20) are not well-defined at the polar point since the corresponding parametric functions are not constant on the singular edge $\widehat{\Gamma}_1$, which also implies that $V_h \not\subset C^0(\overline{\Omega})$. Instead, the modified polar approximation space

$$V_h^{\odot} := V_h \cap H^1(\Omega), \tag{3.21}$$

which was initially proposed in [23], see also [25], is employed. Note that the space also depends on the grading parameter μ and the polynomial degree $\boldsymbol{p}$, although this dependence is not indicated explicitly in the notation. It is well-known that (3.21) yields a space of NURBS that are C^0-continuous at the polar point $\boldsymbol{P}$. Advanced approaches have been proposed in the literature to generate higher continuity at the polar point [25,26]. Since our main focus lies on deriving error estimates for the second-order model problem (3.10), we only consider the simple construction (3.21), which satisfies the minimum regularity requirements for a standard Galerkin IGA approach [23,24,31] and keeps the complexity of the polar spline space as low as possible.

The main result of our paper is the optimal approximation power of the space $V_h^{\odot}$ with respect to the mesh parameter h for the approximation of possibly singular functions on Ω, provided that the grading parameter μ is chosen correctly. We formulate this in the following theorem.

Theorem 3.13. *Let $q \in \{0,1\}$ and $s \in \mathbb{N}$ with $2 \le s \le p+1$. Further, let $\nu \in \mathbb{R}$ such that $v \in V_\beta^s(\Omega)$ for all $\beta \in \mathbb{R}$ with $s-1-\nu < \beta < s-1$. If the mesh grading parameter $\mu \in (0,1]$ satisfies the condition*

$$\mu < \frac{\nu - q + 1}{s - q}, \tag{3.22}$$

then, for every $h > 0$, there is a NURBS function $v_h \in V_h^{\odot}$ on the corresponding graded mesh $\mathcal{M}^\mu$ such that

$$\|v - v_h\|_{H^q(\Omega)} \le C h^{s-q} \|v\|_{V_\beta^s(\Omega)}.$$

In particular, we derive a projection error estimate for sufficiently smooth functions on uniform meshes.

Corollary 3.14. *Let $q \in \{0,1\}$ and $s \in \mathbb{N}$ with $2 \le s \le p+1$. Moreover, let $\nu > s-1$ and $v \in V_\beta^s(\Omega)$ for all $\beta \in \mathbb{R}$ with $s-1-\nu < \beta < s-1$. Then, for every $h > 0$, there exists a NURBS function $v_h \in V_h^{\odot}$ on the corresponding uniform mesh $\mathcal{M}^1$ such that*

$$\|v - v_h\|_{H^q(\Omega)} \le C h^{s-q} \|v\|_{V^s(\Omega)}.$$

Proof. Since $\nu > s-1$ is equivalent to $\nu - q + 1 > s - q$, condition (3.22) is satisfied for $\mu = 1$, and the assertion follows directly from Theorem 3.13. □

Remark 3.15. In general, functions belonging to the standard Sobolev spaces $H^s(\Omega)$ do not satisfy the regularity assumptions of Corollary 3.14 for any s, since the definition of the weighted spaces $V_\beta^s(\Omega)$ involves stronger integrability conditions on lower-order derivatives, see Definition 3.10. Nevertheless, the numerical experiments indicate that uniform meshes still yield optimal approximation rates, see Example 6.1. Hence, the present result may not be sharp for functions with quadratically integrable derivatives, but it constitutes a first step toward a comprehensive analysis.

Since the approximation error in the H^1-norm decreases with the same order as the projection error, we can immediately deduce approximation error estimates for the model problem (3.10) by requiring the grading parameter to satisfy (3.22) for $q = 1$.

Corollary 3.16. *Let u be the solution of the variational model problem (3.11) such that the regularity property (3.15) is satisfied. Further, let $u_h \in V_h^{\odot}$ be the solution of the discrete weak problem (3.13), where the discretization is based on the graded mesh refinement scheme presented in Section 3.3 for NURBS degree $p = s - 1$. If the mesh grading parameter $\mu \in (0, 1]$ satisfies*

$$\mu < \frac{\nu}{p}, \tag{3.23}$$

we obtain optimal convergence with respect to the mesh size h in the energy norm and the L^2-norm,

$$\|u - u_h\|_{H^q(\Omega)} \le C h^{p+1-q} \|u\|_{V^s_\beta(\Omega)} \quad \text{for } q \in \{0, 1\}.$$

Proof. For $q = 1$, the assertion follows directly from Céa's lemma and Theorem 3.13. For $q = 0$, we apply a duality argument for weighted Sobolev spaces. Without loss of generality, let $\nu < 1$, since otherwise, we have the higher regularity $u \in H^2(\Omega)$ and a standard duality argument can be used. Now, let w be the solution of the dual problem

$$a(v, w) = (u - u_h, v) \quad \forall v \in H^1_0(\Omega), \tag{3.24}$$

where $(\cdot, \cdot)$ denotes the standard scalar product in $L^2(\Omega)$. For all $\varepsilon \in (0, 2\nu)$, we have $u - u_h \in V^0_{1-\nu+\varepsilon}(\Omega)$, and the regularity result (3.15) yields that $w \in V^2_{1-\nu+\varepsilon}(\Omega)$. Moreover, the a priori estimate (3.16) and the embedding $L^2(\Omega) = V^0_0(\Omega) \hookrightarrow V^0_{1-\nu+\varepsilon}(\Omega)$, which holds for all $\epsilon > 0$ and $\nu \le 1$, imply that

$$\|w\|_{V^2_{1-\nu+\varepsilon}(\Omega)} \le C \|u - u_h\|^2_{V^0_{1-\nu+\varepsilon}(\Omega)} \le C \|u - u_h\|^2_{L^2(\Omega)}. \tag{3.25}$$

By applying Eq. (3.24) and the Galerkin orthogonality, we further obtain

$$\|u - u_h\|^2_{L^2(\Omega)} = (u - u_h, u - u_h) = a(u - u_h, w) = a(u - u_h, w - w_h) \le \|u - u_h\|_{H^1(\Omega)} \|w - w_h\|_{H^1(\Omega)},$$

where $w_h \in V_h^{\odot}$ is the NURBS approximation of w from Theorem 3.13. Since the grading parameter satisfies $\mu < \frac{\nu}{p} \le \frac{\nu}{1}$, it follows with (3.24) and (3.25) that

$$\|u - u_h\|^2_{L^2(\Omega)} \le \left(C h^p \|u\|_{V^{p+1}_\beta(\Omega)} \right) \left(C h \|w\|_{V^2_{1-\nu+\varepsilon}(\Omega)} \right) \le C h^{p+1} \|u\|_{V^{p+1}_\beta(\Omega)} \|u - u_h\|^2_{L^2(\Omega)}.$$

Dividing by $\|u - u_h\|_{L^2(\Omega)}$ completes the proof. □

In particular, we obtain an approximation result for smooth solutions, corresponding to the projection error estimate in Corollary 3.14.

Corollary 3.17. *Let u be the solution of the variational model problem (3.11) such that the regularity property (3.15) is satisfied for $\nu > s - 1$. Further, let $u_h \in V_h^{\odot}$ be the solution of the discrete weak problem (3.13) on the corresponding uniform mesh $\mathcal{M}^1$ for NURBS degree $p = s - 1$. Then, it holds*

$$\|u - u_h\|_{H^q(\Omega)} \le C h^{p+1-q} \|u\|_{V^{p+1}(\Omega)} \quad \text{for } q \in \{0, 1\}.$$

Proof. Since $\nu > s - 1 = p$, condition (3.23) is satisfied for $\mu = 1$, and the assertion follows directly from Corollary 3.16. □

We finish this chapter with a remark on the explicit choice of grading parameter μ. Eq. (3.22) in Theorem 3.13 only states a necessary condition for optimal convergence, but for an actual computation it arises the question how to choose μ precisely. This has been discussed several times in the literature, see for instance [49]. Based on the numerical studies in [10], where the Laplace eigenfunctions of circular sectors, which possess comparable regularities as the solutions of our model problem (3.10), are approximated using different grading parameters, we choose

$$\mu = \min \left\{ 0.9 \cdot \frac{\nu}{p}, 1 \right\}. \tag{3.26}$$

3.5. Properties of graded meshes

In this section, we deduce essential properties of the constructed graded isogeometric meshes. The parametric and physical Bézier mesh both contain anisotropic elements [10]. Therefore, instead of using the seminal approximation framework described in [27], which is restricted to uniform meshes, we orientate ourselves on the anisotropic theory from [8,28]. To begin with, we show that graded parametric meshes satisfy a local quasi-uniformity assumption, see [28, Assumption 4.10]. In the following, we denote the edge lengths of each element $Q_j \in \widehat{\mathcal{M}}^\mu$ by h_{1,j_1} and h_{2,j_2}. We recall that h_1 and h_2 are the refinement parameters in each direction defined in Section 3.3, and $h = \max\{h_Q : Q \in \widehat{\mathcal{M}}^\mu\}$ is the global mesh size of $\mathcal{M}^\mu$.

Lemma 3.18. *The graded parametric Bézier mesh $\widehat{\mathcal{M}}^\mu$ is locally quasi-uniform for all $\mu \in (0, 1]$, i.e., there are constants $\theta_l \ge 1$, $l = 1, 2$, such that*

$$\theta_l^{-1} \le h_{l,j_l} / h_{l,j_l+1} \le \theta_l, \quad j_l = 1, 2, \dots, N_l - 2, \tag{3.27}$$

in particular, $\theta_1 = 2^{1/\mu} - 1$ and $\theta_2 = 1$.

Proof. In ζ_2-direction, the uniform vector of breakpoints (3.18) leads to a constant edge length,

$$h_{2,j_2} = \zeta_{2,j_2+1} - \zeta_{2,j_2} = (j_2\, h_2) - ((j_2-1)\, h_2) = h_2, \quad j_2 = 1, 2, \dots, N_2 - 1,$$

and thus condition (3.27) is fulfilled for $l = 2$ with $\theta_2 = 1$. In ζ_1-direction, the graded vector of knots without repetition (3.17) yields

$$h_{1,j_1} = \zeta_{1,j_1+1} - \zeta_{1,j_1} = \left(j_1^{1/\mu} - (j_1-1)^{1/\mu}\right) h_1^{1/\mu}, \quad j_1 = 1, \dots, N_1 - 1,$$

and we define

$$\Theta_1(j_1) := \frac{h_{1,j_1}}{h_{1,j_1+1}} = \frac{\left(j_1^{1/\mu} - (j_1-1)^{1/\mu}\right) h_1^{1/\mu}}{\left((j_1+1)^{1/\mu} - j_1^{1/\mu}\right) h_1^{1/\mu}} = \frac{j_1^{1/\mu} - (j_1-1)^{1/\mu}}{(j_1+1)^{1/\mu} - j_1^{1/\mu}}.$$

In Lemma C.1 of the Appendix, we show that the sequence $(\Theta_1(j_1))_{j_1=1}^{\infty}$ is monotonously increasing and satisfies $\lim_{j_1\to\infty} \Theta_1(j_1) = 1$. Furthermore, we have $\Theta_1(1) = \frac{1}{2^{1/\mu}-1} \in (0, 1]$, and we obtain the desired local quasi-uniformity property (3.27) for $l = 1$ with $\theta_1 = 2^{1/\mu} - 1$. □

Throughout this paper, we will refer to the parameter $\boldsymbol{\theta} = (\theta_1, \theta_2)$ in the sense of Lemma 3.18. In the following, we compute further quantities to describe the graded meshes in more detail. Due to property (3.27), it holds

$$h_{1,j_1} \le \theta_1 h_{1,j_1-1} \le \cdots \le \theta_1^{j_1-1} h_{1,1}.$$

Hence, for elements $Q_j \in \widehat{\mathcal{M}}^\mu$ that are located close to the singular edge, e.g., for $j_1 \le p_1 + 1$, we have

$$h_{1,j_1} \le C h_{1,1} = C h_1^{1/\mu}.$$

If $Q_j \in \widehat{\mathcal{M}}^\mu$ is not adjacent to the singular edge, e.g., $j_1 \ge 2$, the mean value theorem yields the existence of $x_0 \in ((j_1-1)h_1, j_1 h_1)$ such that

$$h_{1,j_1} = \zeta_{1,j_1+1} - \zeta_{1,j_1} = (j_1 h_1)^{\frac{1}{\mu}} - ((j_1-1)h_1)^{\frac{1}{\mu}} = \left(\frac{1}{\mu} - 1\right) h_1 (x_0)^{\frac{1}{\mu}-1}.$$

As the function $x \mapsto x^{1/\mu}$ is monotonously increasing, it follows by definition (3.17) and Lemma 3.18 that

$$h_{1,j_1} = C h_1 (x_0)^{\frac{1}{\mu}-1} \le C h_1 (j_1 h_1)^{\frac{1}{\mu}(1-\mu)} = C h_1 (\zeta_{1,j_1+1})^{1-\mu} \le C h_1 (\zeta_{1,j_1})^{1-\mu} \quad \text{for } j_1 \ge 2.$$

A similar way to prove this property is demonstrated in [50, page 143]. Furthermore, we denote the edge lengths of the support extension $\widetilde{Q}_j$ of $Q_j \in \widehat{\mathcal{M}}^\mu$ by $\widetilde{h}_{1,j_1}$ and $\widetilde{h}_{2,j_2}$. Due to the local quasi-uniformity of the mesh, we obtain similar relations,

$$\begin{aligned}
&\widetilde{h}_{1,j_1} \le C\, h_1^{1/\mu} && \text{for elements close to the singular edge, e.g., for } j_1 \le p_1 + 1,\\
&\widetilde{h}_{1,j_1} \le C\, h_1\, (\zeta_{1,j_1})^{1-\mu} && \text{for elements away from the singular edge, e.g., for } j_1 > p_1 + 1,\\
&\widetilde{h}_{2,j_2} \le C\, h_2 && \text{for all elements.}
\end{aligned} \tag{3.28}$$

For additional details, a more precise characterization of the support extensions is given in Section 5.1.

4. Function spaces and projectors for polar parameterizations

In this section, we describe suitable isogeometric approximation spaces on polar domains with corners and introduce a corresponding projector. Furthermore, we present the concept of polar Sobolev spaces on the parametric domain, which are defined as pull-backs of classical Sobolev spaces on the physical domain.

4.1. The polar approximation space and a suitable projection

We start by recalling polar spline and NURBS spaces, which have been studied extensively in isogeometric literature [23–26], and define a suitable projector into these spaces. A basis of the polar spline space (3.21) can be constructed by replacing all the basis functions (3.20) with a single function consisting of their sum [23,24],

$$N_{\odot,\boldsymbol{p}} := \sum_{i_\odot \in \boldsymbol{I}_\odot} N_{i_\odot,\boldsymbol{p}} = \sum_{i_2=1}^{n_2} N_{(1,i_2),\boldsymbol{p}}, \tag{4.1}$$

which satisfies $N_{\odot,\boldsymbol{p}} \in H^1(\Omega)$. In Fig. 4(a) and (b), we exemplarily display the excluded basis functions (3.20) and the modified basis function (4.1) for a coarse discretization of a circular sector with angle $\frac{5}{3}\pi$. The parametric B-spline and NURBS functions corresponding to the modified physical basis function (4.1) are given by

$$\begin{aligned}
&\widehat{B}_{\odot,\boldsymbol{p}} : [0,1]^2 \to \mathbb{R},\ \widehat{B}_{\odot,\boldsymbol{p}}(\boldsymbol{\zeta}) := \sum_{i_\odot \in \boldsymbol{I}_\odot} \widehat{B}_{i_\odot,\boldsymbol{p}}(\boldsymbol{\zeta}) \quad \text{and}\\
&\widehat{N}_{\odot,\boldsymbol{p}} : [0,1]^2 \to \mathbb{R},\ \widehat{N}_{\odot,\boldsymbol{p}}(\boldsymbol{\zeta}) := \sum_{i_\odot \in \boldsymbol{I}_\odot} \widehat{N}_{i_\odot,\boldsymbol{p}}(\boldsymbol{\zeta}),
\end{aligned} \tag{4.2}$$

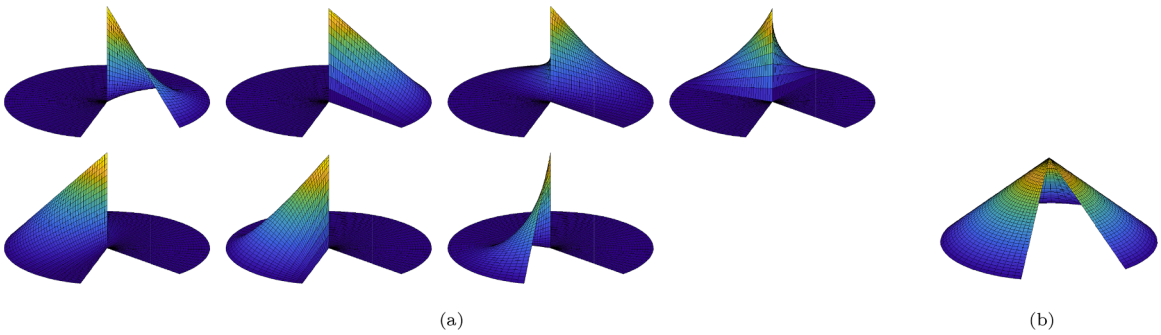

Fig. 4. Basis functions for a coarse discretization of a circular sector sector with angle $\omega = \frac{5}{3}\pi$. Some mesh lines that do not correspond to the coarse discretization are inserted for better visualization. (a) Standard singular basis functions (3.20). (b): Modified basis function (4.1).

respectively. In fact, due to the specific form (3.9) of the weight function required in Assumption 3.5, both functions reduce to the first univariate B-spline basis function in ζ_1-direction,

$$\widehat{B}_{\odot,\boldsymbol{p}}(\boldsymbol{\zeta}) = \sum_{i_2=1}^{n_2} \widehat{B}_{(1,i_2),\boldsymbol{p}}(\boldsymbol{\zeta}) = \widehat{B}_{1,p_1}(\zeta_1) \sum_{i_2=1}^{n_2} \widehat{B}_{i_2,p_2}(\zeta_2) = \widehat{B}_{1,p_1}(\zeta_1),$$

$$\widehat{N}_{\odot,\boldsymbol{p}}(\boldsymbol{\zeta}) = \frac{\sum_{i_2=1}^{n_2} w_{(1,i_2)} \widehat{B}_{(1,i_2),\boldsymbol{p}}(\boldsymbol{\zeta})}{W} = \frac{\widehat{B}_{1,p_1}(\zeta_1) \sum_{i_2=1}^{n_2} w_{(1,i_2)} \widehat{B}_{i_2,p_2}(\zeta_2)}{\sum_{i_2=1}^{n_2} w_{(1,i_2)} \widehat{B}_{i_2,p_2}(\zeta_2)} = \widehat{B}_{1,p_1}(\zeta_1).$$

Since univariate B-splines constructed from open knot vectors are interpolatory at the boundary, $\widehat{N}_{\odot,\boldsymbol{p}}$ is constant on $\widehat{\Gamma}_1$, with $\widehat{N}_{\odot,\boldsymbol{p}}(0,\cdot) = \widehat{B}_{1,p_1}(0) = 1$. Hence, the push-forward of $\widehat{N}_{\odot,\boldsymbol{p}}$ is well-defined and yields the modified NURBS basis function (4.1),

$$N_{\odot,\boldsymbol{p}} = \sum_{i_\odot \in \boldsymbol{I}_\odot} N_{i_\odot,\boldsymbol{p}} = \sum_{i_\odot \in \boldsymbol{I}_\odot} \widehat{N}_{i_\odot,\boldsymbol{p}} \circ \boldsymbol{F}^{-1} = \widehat{N}_{\odot,\boldsymbol{p}} \circ \boldsymbol{F}^{-1}. \tag{4.3}$$

Thus, we will write the basis of our approximation space throughout the paper as

$$V_h^\odot = \operatorname{span}\Big(\{N_{\odot,\boldsymbol{p}}\} \cup \Big\{ N_{\boldsymbol{i},\boldsymbol{p}} = \widehat{N}_{\boldsymbol{i},p_1} \circ \boldsymbol{F}^{-1} : \boldsymbol{i} \in \boldsymbol{I} \setminus \boldsymbol{I}_\odot \Big\} \Big), \tag{4.4}$$

noting that all basis functions are continuous in $\boldsymbol{P}$ with $N_{\odot,\boldsymbol{p}}(\boldsymbol{P}) = 1$ and $N_{\boldsymbol{i},\boldsymbol{p}}(\boldsymbol{P}) = 0$ for all $\boldsymbol{i} \in \boldsymbol{I} \setminus \boldsymbol{I}_\odot$.

Lastly, we define the space

$$V_{0h}^\odot = V_h^\odot \cap V_0 = \big\{ v \in V_h^\odot : v = 0 \text{ on } \Gamma_D \big\},$$

with V_0 from (3.12), which also takes homogeneous Dirichlet boundary conditions into account. Here, we highlight the following observation.

Remark 4.1. The structure of the modified approximation space with boundary conditions depends crucially on whether the polar corner is included in the homogeneous Dirichlet boundary. If this is the case, i.e., when Dirichlet or mixed boundary conditions are prescribed on the adjacent edges, the basis functions associated with the polar point are not active. Hence, the modified space with boundary conditions coincides with the standard space,

$$V_{0h}^\odot = V_h^\odot \cap V_0 = V_h \cap V_0 = V_{0h},$$

and the tensor-product structure is preserved. Only for Neumann boundary conditions at the corner is the modified space a proper subspace, $V_{0h}^\odot \subsetneq V_{0h}$.

In the next step, we define a projector onto the modified isogeometric approximation space $V_h^\odot$. In standard literature [8,27,28], a projection onto the usual approximation space V_h is constructed based on the multivariate quasi-interpolant for the parametric spline space (2.15), the parameterization $\boldsymbol{F}$ and the weight function W,

$$\Pi_{V_h} : L^1(\Omega) \to V_h, \quad \Pi_{V_h} v := \frac{\Pi_{\boldsymbol{p},\boldsymbol{\Xi}}(W(v \circ \boldsymbol{F}))}{W} \circ \boldsymbol{F}^{-1}. \tag{4.5}$$

However, the isogeometric mapping $\boldsymbol{F}$ is typically assumed to satisfy certain regularity properties, which are not fulfilled by polar parameterizations. In what follows, we propose a slightly modified projector that is adapted to the polar setting and maps into the subspace $V_h^\odot \subset V_h$.

The standard projection (4.5) is generally not well-defined at the polar point $\boldsymbol{P}$ due to the collapsing edge effect (3.1). This can be remedied by using a spline projector on the parametric domain that takes Dirichlet boundary conditions into account – in particular, on the singular edge $\widehat{\Gamma}_1$. For simplicity, we employ the modified quasi-interpolant (2.17), which is interpolatory at the complete

parametric boundary [8,28], and requires functions from $C([0,1]^2)$. We then define a projector onto the polar approximation space (3.21) by

$$\Pi_{V_h^\odot} : C(\overline{\Omega}) \to V_h^\odot, \quad \Pi_{V_h^\odot} v = \frac{\Pi^{\widehat{\Gamma}}_{p,\Xi}(W(v\circ \boldsymbol{F}))}{W} \circ \boldsymbol{F}^{-1}. \tag{4.6}$$

Due to the regularity property (3.15) of the considered PDE solution and the embeddings $V_\beta^s(\Omega) \hookrightarrow H_\beta^s(\Omega) \hookrightarrow H^{s-\beta}(\Omega) \hookrightarrow C(\overline{\Omega})$, which hold for $\beta < s-1$, see (3.14) and [51], it is justified to work with a projector that requires functions in $C(\overline{\Omega})$. The following Lemma establishes the expected properties of this projection.

Lemma 4.2. *The operator $\Pi_{V_h^\odot}$ is a well-defined projector onto $V_h^\odot$, that is, $\Pi_{V_h^\odot} v \in V_h^\odot$ for all $v \in C(\overline{\Omega})$ and $\Pi_{V_h^\odot} v = v$ for all $v \in V_h^\odot$. Moreover, we have $\Pi_{V_h^\odot} v \in V_{0h}^\odot$ for all $v \in C(\overline{\Omega})$ with $v = 0$ on Γ_D.*

Proof. Let $v \in C(\overline{\Omega})$ and $\widehat{v} = v \circ \boldsymbol{F}$. Then, $\widehat{v}$ is constant on $\widehat{\Gamma}_1$, and we set $c = v(\boldsymbol{P}) = \widehat{v}(0,\cdot)$. The first univariate dual functional defined in (2.8) satisfies

$$\lambda^{\widehat{\Gamma}}_{1,p_1}(W\widehat{v}(\cdot,\zeta_2)) = W\widehat{v}(0,\zeta_2) = c\, W(0,\zeta_2)$$

for all $\zeta_2 \in [0,1]$. Hence, the bivariate dual functionals corresponding to the collapsed edge reduce to

$$\lambda^{\widehat{\Gamma}}_{i_\odot,\boldsymbol{p}}(W\widehat{v}) = \left(\lambda^{\widehat{\Gamma}}_{1,p_1} \otimes \lambda^{\widehat{\Gamma}}_{i_2,p_2}\right)(W\widehat{v}) = \lambda^{\widehat{\Gamma}}_{i_2,p_2}(c\, W(0,\cdot)) = c\, \lambda^{\widehat{\Gamma}}_{i_2,p_2}(W(0,\cdot)). \tag{4.7}$$

Besides, most of the B-spline basis functions vanish on the collapsing edge $\widehat{\Gamma}_1$, the univariate quasi-interpolant $\Pi^{\widehat{\Gamma}}_{p_2,\Xi_2}$ defined in (2.8) is a projector onto $S_{p_2}(\Xi_2)$, and we have $W(0,\cdot) \in S_{p_2}(\Xi_2)$. Therefore, the modified bivariate quasi-interpolant (2.17), which is also given in the form (2.18), can be computed explicitly on the collapsed edge,

$$\begin{aligned}\left(\Pi^{\widehat{\Gamma}}_{p,\Xi}(W(v\circ\boldsymbol{F}))\right)(0,\cdot) &= \left(\Pi^{\widehat{\Gamma}}_{p,\Xi}(W\widehat{v})\right)(0,\cdot) = \sum_{i\in I} \lambda^{\widehat{\Gamma}}_{i,p}(W\widehat{v})\widehat{B}_{i,p}(0,\cdot) = \sum_{i_\odot \in I_\odot} \lambda^{\widehat{\Gamma}}_{i_\odot,p}(W\widehat{v})\widehat{B}_{i_\odot,p}(0,\cdot) \\ &= c\,\widehat{B}_{1,p_1}(0) \sum_{i_2=1}^{n_2} \lambda^{\widehat{\Gamma}}_{i_2,p_2}(W(0,\cdot))\widehat{B}_{i_2,p_2}(\cdot) = c\,\Pi^{\widehat{\Gamma}}_{p_2,\Xi_2}(W(0,\cdot)) = c\,W(0,\cdot).\end{aligned}$$

As a consequence, the projection $\Pi_{V_h^\odot} v$ is well-defined and continuous in $\boldsymbol{P}$, with $\left(\Pi_{V_h^\odot} v\right)(\boldsymbol{P}) = c$, and it holds $\Pi_{V_h^\odot} v \in H^1(\Omega)$, see [23,24]. By definition of the spaces (3.19) and (3.21), we further obtain $\Pi_{V_h^\odot} v \in V_h$ and also $\Pi_{V_h^\odot} v \in V_h^\odot$, and thus the operator (4.6) is well-defined.

Next, we show that $\Pi_{V_h^\odot}$ is indeed a projector. Therefore, let $v \in V_h^\odot$, that is, with (4.3) and (4.4),

$$v = c\, N_{\odot,p} + \sum_{i\in I\setminus I_\odot} \alpha_i N_{i,p} = c \sum_{i_\odot \in I_\odot} N_{i_\odot,p} + \sum_{i\in I\setminus I_\odot} \alpha_i N_{i,p},$$

where $c = v(\boldsymbol{P})$ and $\alpha_i \in \mathbb{R}, i \in \boldsymbol{I} \setminus \boldsymbol{I}_\odot$. Then, it is $v = \widehat{v}\circ\boldsymbol{F}^{-1}$ with

$$\widehat{v} = c\,\widehat{N}_{\odot,p} + \sum_{i\in I\setminus I_\odot} \alpha_i \widehat{N}_{i,p} = c \sum_{i_\odot \in I_\odot} \widehat{N}_{i_\odot,p} + \sum_{i\in I\setminus I_\odot} \alpha_i \widehat{N}_{i,p} \in N_p(\Xi),$$

see (4.2). Further, we have $\widehat{v} = \widehat{u}/W$ with

$$\widehat{u} = c \sum_{i\in I_\odot} w_{i_\odot} \widehat{B}_{i_\odot,p} + \sum_{i\in I\setminus I_\odot} \alpha_i w_i \widehat{B}_{i,p} \in S_p(\Xi).$$

Since $\Pi^{\widehat{\Gamma}}_{p,\Xi}$ is a projector onto $S_p(\Xi)$, it follows

$$\Pi_{V_h^\odot} v = \frac{\Pi^{\widehat{\Gamma}}_{p,\Xi}(W(v\circ\boldsymbol{F}))}{W} = \frac{\Pi^{\widehat{\Gamma}}_{p,\Xi}(W\widehat{v})}{W} = \frac{\Pi^{\widehat{\Gamma}}_{p,\Xi}(W\widehat{u}/W)}{W} = \frac{\Pi^{\widehat{\Gamma}}_{p,\Xi}(\widehat{u})}{W} = \frac{\widehat{u}}{W}\circ\boldsymbol{F}^{-1} = \widehat{v}\circ\boldsymbol{F}^{-1} = v$$

and the proof is complete. The result for the functions satisfying Dirichlet boundary conditions follows directly from the construction of the quasi-interpolant $\Pi^{\widehat{\Gamma}}_{p,\Xi}$. □

Remark 4.3. Note that all the constructions of Section 4.1 can be extended to a non-isoparametric approach by simply setting $W = 1$.

4.2. Polar Sobolev spaces on the parametric domain

In standard isogeometric approximation theory, error estimates are typically derived on the parametric domain and then transferred to the physical domain, where the Jacobian of the geometry mapping $\boldsymbol{F}$ and its inverse are assumed to be bounded [8,27,28]. This condition, however, is not satisfied by polar parameterizations, see Eqs. (3.5) and (3.7). Therefore, the corresponding transformations of derivatives and norms must be treated more carefully, as demonstrated in this section. Consequently, we introduce a novel class of Sobolev spaces on the parametric domain to characterize pull-backs of functions on polar domains with corners.

4.2.1. Polar transformation of derivatives

We start by analyzing the transformation between derivatives on the physical domain and their corresponding pull-back derivatives. To this end, we first introduce some notation. Let $\boldsymbol{\alpha} = (\alpha_1, \alpha_2) \in \mathbb{N}_0^2$ be a multi-index. We denote derivatives of functions $v : \Omega \to \mathbb{R}$ defined on the physical domain by

$$D^{\boldsymbol{\alpha}} v := \frac{\partial^{\alpha_1}}{\partial x^{\alpha_1}} \frac{\partial^{\alpha_2} v}{\partial y^{\alpha_2}} \quad \text{and} \quad \partial_x v = \frac{\partial v}{\partial x}, \, \partial_y v = \frac{\partial v}{\partial y}, \, \partial_{xx} v = \frac{\partial^2 v}{\partial x^2}, \, \dots .$$

In contrast, for a function $\widehat{v} : \widehat{\Omega} \to \mathbb{R}$ acting on the parametric domain, we write

$$\widehat{D}^{\boldsymbol{\alpha}} \widehat{v} := \frac{\partial^{\alpha_1}}{\partial \zeta_1^{\alpha_1}} \frac{\partial^{\alpha_2} \widehat{v}}{\partial \zeta_2^{\alpha_2}} \quad \text{and} \quad \widehat{\partial}_1 \widehat{v} = \frac{\partial \widehat{v}}{\partial \zeta_1}, \, \widehat{\partial}_2 \widehat{v} = \frac{\partial \widehat{v}}{\partial \zeta_2}, \, \widehat{\partial}_{11} \widehat{v} = \frac{\partial^2 \widehat{v}}{\partial \zeta_1^2}, \, \dots .$$

Moreover, following the framework in [8,28], we define the coordinate system naturally induced by $\boldsymbol{F}$, referred to as the $\boldsymbol{F}$-coordinate system, whose tangent base vectors $\boldsymbol{g}_1$ and $\boldsymbol{g}_2$ are given by

$$\boldsymbol{g}_i = \boldsymbol{g}_i(\boldsymbol{x}) = \frac{\partial \boldsymbol{F}}{\partial \zeta_i}(\boldsymbol{F}^{-1}(\boldsymbol{x})), \quad i = 1, 2.$$

As computed in (3.4), we have

$$\boldsymbol{g}_1(\boldsymbol{x}) = \begin{pmatrix} G_1'(\zeta_2(\boldsymbol{x})) \\ G_2'(\zeta_2(\boldsymbol{x})) \end{pmatrix} \quad \text{and} \quad \boldsymbol{g}_2(\boldsymbol{x}) = \begin{pmatrix} \zeta_1(\boldsymbol{x})\, G_1''(\zeta_2(\boldsymbol{x})) \\ \zeta_1(\boldsymbol{x})\, G_2''(\zeta_2(\boldsymbol{x})) \end{pmatrix}, \tag{4.8}$$

where we set $\boldsymbol{\zeta}(\boldsymbol{x}) = (\zeta_1(\boldsymbol{x}), \zeta_2(\boldsymbol{x})) = \boldsymbol{F}^{-1}(\boldsymbol{x})$ for all $\boldsymbol{x} \neq \boldsymbol{P}$. We also consider derivatives with respect to the $\boldsymbol{F}$-coordinates,

$$\frac{\partial v}{\partial \boldsymbol{g}_i}(\boldsymbol{x}) = \nabla v(\boldsymbol{x}) \cdot \boldsymbol{g}_i(\boldsymbol{x}) = \lim_{t \to 0} \frac{v(\boldsymbol{x} + t\boldsymbol{g}_i(\boldsymbol{x})) - v(\boldsymbol{x})}{t}, \quad i = 1, 2,$$

$$\frac{\partial^{\alpha_i} v}{\partial \boldsymbol{g}_i^{\alpha_i}} = \frac{\partial}{\partial \boldsymbol{g}_i} \left(\frac{\partial^{\alpha_i - 1} v}{\partial \boldsymbol{g}_i^{\alpha_i - 1}} \right) = \frac{\partial}{\partial \boldsymbol{g}_i} \left(\cdots \left(\frac{\partial}{\partial \boldsymbol{g}_i} \left(\frac{\partial v}{\partial \boldsymbol{g}_i} \right) \right) \right), \quad \alpha_i \in \mathbb{N}, i = 1, 2,$$

$$D_{\boldsymbol{F}}^{\boldsymbol{\alpha}} v = \frac{\partial^{\alpha_1}}{\partial \boldsymbol{g}_1^{\alpha_1}} \frac{\partial^{\alpha_2} v}{\partial \boldsymbol{g}_2^{\alpha_2}}, \quad \boldsymbol{\alpha} = (\alpha_1, \alpha_2) \in \mathbb{N}^2.$$

Now, let $\widehat{v} = v \circ \boldsymbol{F}$ be the pull-back of a sufficiently smooth function $v : \Omega \to \mathbb{R}$. As shown in [8, Proposition 5.1], we have

$$\mathrm{D}_{\boldsymbol{F}}^{\boldsymbol{\alpha}} v = (\widehat{D}^{\boldsymbol{\alpha}} \widehat{v}) \circ \boldsymbol{F}^{-1} = \left(\frac{\partial^{\alpha_1}}{\partial \zeta_1} \frac{\partial^{\alpha_2} \widehat{v}}{\partial \zeta_2} \right) \circ \boldsymbol{F}^{-1}, \tag{4.9}$$

i.e., in particular, $\mathrm{D}_{\boldsymbol{F}}^{(1,0)} v = \widehat{\partial}_1 \widehat{v} \circ \boldsymbol{F}^{-1}$ and $\mathrm{D}_{\boldsymbol{F}}^{(0,1)} v = \widehat{\partial}_2 \widehat{v} \circ \boldsymbol{F}^{-1}$. By inserting the polar tangent base vectors (4.8), we obtain the first directional derivatives at all points $\boldsymbol{x} \neq \boldsymbol{0}$ by

$$\mathrm{D}_{\boldsymbol{F}}^{(1,0)} v(\boldsymbol{x}) = G_1(\zeta_2(\boldsymbol{x}))\, \partial_x v(\boldsymbol{x}) + G_2(\zeta_2(\boldsymbol{x}))\, \partial_y v(\boldsymbol{x}), \tag{4.10}$$

$$\mathrm{D}_{\boldsymbol{F}}^{(0,1)} v(\boldsymbol{x}) = \zeta_1(\boldsymbol{x})\, G_1'(\zeta_2(\boldsymbol{x}))\, \partial_x v(\boldsymbol{x}) + \zeta_1(\boldsymbol{x})\, G_2'(\zeta_2(\boldsymbol{x}))\, \partial_y v(\boldsymbol{x}). \tag{4.11}$$

Vice versa, Eqs. (3.5), (3.6) and (4.9) yield

$$\partial_x v(\boldsymbol{x}) = G_2(\zeta_2(\boldsymbol{x}))\, \mathrm{D}_{\boldsymbol{F}}^{(1,0)} v(\boldsymbol{x}) - \frac{1}{\zeta_1(\boldsymbol{x})} G_2'(\zeta_2(\boldsymbol{x}))\, \mathrm{D}_{\boldsymbol{F}}^{(0,1)} v(\boldsymbol{x}), \tag{4.12}$$

$$\partial_y v(\boldsymbol{x}) = -G_1'(\zeta_2(\boldsymbol{x}))\, \mathrm{D}_{\boldsymbol{F}}^{(1,0)} v(\boldsymbol{x}) + \frac{1}{\zeta_1(\boldsymbol{x})} G_1(\zeta_2(\boldsymbol{x}))\, \mathrm{D}_{\boldsymbol{F}}^{(0,1)} v(\boldsymbol{x}). \tag{4.13}$$

In Lemmata A.1 and A.2 of the Appendix, we derive precise representations for the polar transformation of derivatives of arbitrary orders, thereby extending the formulas presented here.

4.2.2. Polar transformation of norms and polar Sobolev spaces

With that, we now consider the transformation of Sobolev norms on the physical domain to the parametric domain. To this end, we first define weighted function spaces on the parametric domain, which differ from the ones in Definition 3.10 in the sense that the distance of a point to the edge $\widehat{\Gamma}_1$, that is, the first coordinate ζ_1, is weighted and not the distance to $\boldsymbol{0}$. However, since those quantities correspond to each other, recall (3.8), this is a natural choice. That is, for $Q \subset \widehat{\Omega}$, we set

$$\widehat{H}_\beta^s(Q) := \left\{ \widehat{v} \in \mathcal{D}'(Q) : \|\widehat{v}\|_{\widehat{H}_\beta^s(Q)} < \infty \right\} \quad \text{and} \quad \widehat{V}_\beta^s(Q) := \left\{ \widehat{v} \in \mathcal{D}'(Q) : \|\widehat{v}\|_{\widehat{V}_\beta^s(Q)} < \infty \right\},$$

with the norms

$$\|\widehat{v}\|_{\widehat{H}_\beta^s(Q)}^2 := \sum_{|\boldsymbol{\alpha}| \le s} \left\| \zeta_1^\beta \widehat{D}^{\boldsymbol{\alpha}} \widehat{v} \right\|_{\widehat{L}^2(Q)}^2 := \sum_{|\boldsymbol{\alpha}| \le s} \int_Q \left| \zeta_1^\beta \widehat{D}^{\boldsymbol{\alpha}} \widehat{v}(\boldsymbol{\zeta}) \right|^2 \mathrm{d}\boldsymbol{\zeta},$$

$$\|\widehat{v}\|_{\widehat{V}_\beta^s(Q)}^2 := \sum_{|\boldsymbol{\alpha}| \le s} \left\| \zeta_1^{\beta - s + |\alpha|} \widehat{D}^{\boldsymbol{\alpha}} \widehat{v} \right\|_{\widehat{L}^2(Q)}^2 := \sum_{|\boldsymbol{\alpha}| \le s} \int_Q \left| \zeta_1^{\beta - s + |\alpha|} \widehat{D}^{\boldsymbol{\alpha}} \widehat{v}(\boldsymbol{\zeta}) \right|^2 \mathrm{d}\boldsymbol{\zeta}$$

and seminorms

$$|\hat{v}|^2_{\hat{H}^s_\beta(Q)} := |\hat{v}|^2_{\hat{V}^s_\beta(Q)} := \sum_{|\boldsymbol{\alpha}|=s} \left\| \zeta_1^\beta \hat{D}^{\boldsymbol{\alpha}} \hat{v} \right\|^2_{\hat{L}^2(Q)}.$$

The Sobolev spaces on Q without weight are denoted by $\hat{H}^s(Q) = \hat{H}^s_0(Q)$ and $\hat{V}^s(Q) = \hat{V}^s_0(Q)$ and we write $\hat{L}^2_\beta(Q) = \hat{H}^0_\beta(Q) = \hat{V}^0_\beta(Q)$ and $\hat{L}^2(Q) = \hat{H}^0(Q) = \hat{V}^0(Q)$. Similar to (3.14), for all $s \in \mathbb{N}$ and $\beta \in \mathbb{R}$, we have an embedding of the V-spaces into the H-spaces,

$$\hat{V}^s_\beta(Q) \hookrightarrow \hat{H}^s_\beta(Q). \tag{4.14}$$

In the following, let $K \in \mathcal{M}$ be an element of the Bézier mesh, $Q = \boldsymbol{F}^{-1}(K) \in \widehat{\mathcal{M}}$ its corresponding parametric element and let $\hat{v} = v \circ \boldsymbol{F}$ be the pull-back of a function $v : \Omega \to \mathbb{R}$. When working with smooth parameterizations as considered in [8,27,28], it can be shown that a function belongs to $H^s_\beta(K)$ if and only if its pull-back lies in $\hat{H}^s_\beta(Q)$. However, the same does not hold for pull-backs based on polar parameterizations. To demonstrate this, we first consider the pull-back of a function $v \in L^2(K)$. By a simple integral transformation, taking into account the Jacobian (3.5), we obtain the relation

$$\|v\|^2_{L^2(K)} = \int_Q |\hat{v}| |\det(J_{\boldsymbol{F}})| \, \mathrm{d}\boldsymbol{\zeta} \sim \int_Q |\hat{v}|^2 \zeta_1 \, \mathrm{d}\zeta_1 \, \mathrm{d}\zeta_2 = \|\hat{v}\|^2_{\hat{L}^2_{1/2}(Q)}, \tag{4.15}$$

that is, we have $v \in L^2(K)$ if and only if $\hat{v} \in \hat{L}^2_{1/2}(Q)$. In the next steps, we compute the transformation of Sobolev norms. By combining Eqs. (4.12), (4.13) and (4.9), the Jacobian determinant (3.5), a transformation of integrals and Assumption 3.4, we obtain

$$\begin{aligned} |v|^2_{V^1(K)} = |v|^2_{H^1(K)} &= \int_K |\partial_x v|^2 + \left|\partial_y v\right|^2 \mathrm{d}\boldsymbol{x} = \int_Q \left(\left(G_2 \, \hat{\partial}_1 \hat{v} - \frac{1}{\zeta_1} G_2' \, \hat{\partial}_2 \hat{v} \right)^2 + \left(-G_1' \, \hat{\partial}_1 \hat{v} + \frac{1}{\zeta_1} G_1 \, \hat{\partial}_2 \hat{v} \right)^2 \right) |\det(J_{\boldsymbol{F}})| \, \mathrm{d}\boldsymbol{\zeta} \\ &\le C \int_Q \left(\left(\hat{\partial}_1 \hat{v} \right)^2 + \left(\frac{1}{\zeta_1} \hat{\partial}_2 \hat{v} \right)^2 \right) \zeta_1 \, \mathrm{d}\boldsymbol{\zeta} = C \left(\left\| \hat{\partial}_1 \hat{v} \right\|^2_{\hat{L}^2_{1/2}(Q)} + \left\| \zeta_1^{-1} \hat{\partial}_2 \hat{v} \right\|^2_{\hat{L}^2_{1/2}(Q)} \right). \end{aligned}$$

By using (3.8) and again (3.5), it further follows

$$\left\| r^{-1} v \right\|^2_{L^2(K)} \sim \int_Q \left| \zeta_1^{-1} \hat{v} \right| \zeta_1 \, \mathrm{d}\boldsymbol{\zeta} = \left\| \zeta_1^{-1} \hat{v} \right\|^2_{\hat{L}^2_{1/2}(Q)}.$$

Thus, we have an estimate for the V^1-norm,

$$\|v\|^2_{V^1(K)} = \left\| r^{-1} v \right\|^2_{L^2(K)} + |v|^2_{V^1(K)} \le C \|\hat{v}\|^2_{\hat{V}^1_\odot(Q)}, \tag{4.16}$$

with $\|\hat{v}\|^2_{\hat{V}^1_\odot(Q)} := \left\| \zeta_1^{-1} \hat{v} \right\|_{\hat{L}^2_{1/2}(Q)} + \left\| \hat{\partial}_1 \hat{v} \right\|^2_{\hat{L}^2_{1/2}(Q)} + \left\| \zeta_1^{-1} \hat{\partial}_2 \hat{v} \right\|^2_{\hat{L}^2_{1/2}(Q)}$. In the other direction, it follows with relations (3.7), (3.8), (4.9), (4.10), and Assumption 3.4 that

$$\begin{aligned} \left\| \hat{\partial}_1 \hat{v} \right\|^2_{\hat{L}^2_{1/2}(Q)} &= \int_Q \left(\hat{\partial}_1 \hat{v} \right)^2 \zeta_1 \, \mathrm{d}\boldsymbol{\zeta} = \int_K \left(\hat{\partial}_1 \hat{v} \circ \boldsymbol{F}^{-1} \right)^2 \zeta_1(\boldsymbol{x}) |\det(J_{\boldsymbol{F}^{-1}})| \, \mathrm{d}\boldsymbol{x} \sim \int_K \left(\mathrm{D}^{(1,0)}_{\boldsymbol{F}} v \right)^2 \mathrm{d}\boldsymbol{x} \\ &= \int_K \left(G_1(\zeta_2(\boldsymbol{x})) \partial_x v + G_2(\zeta_2(\boldsymbol{x})) \partial_y v \right)^2 \mathrm{d}\boldsymbol{x} \le C \int_K |\partial_x v|^2 + \left|\partial_y v\right|^2 \mathrm{d}\boldsymbol{x} = C |v|^2_{V^1(K)}. \end{aligned}$$

By using similar arguments and (4.11), we compute

$$\begin{aligned} \left\| \zeta_1^{-1} \hat{\partial}_2 \hat{v} \right\|^2_{\hat{L}^2_{1/2}(Q)} &= \int_Q \left(\zeta_1^{-1} \hat{\partial}_2 \hat{v} \right)^2 \zeta_1 \, \mathrm{d}\boldsymbol{\zeta} \sim \int_K \left(\zeta_1^{-1}(\boldsymbol{x}) \, \mathrm{D}^{(0,1)}_{\boldsymbol{F}} v \right)^2 \mathrm{d}\boldsymbol{x} \\ &= \int_K \left(G_1'(\zeta_2(\boldsymbol{x})) \partial_x v + G_2'(\zeta_2(\boldsymbol{x})) \partial_y v \right)^2 \mathrm{d}\boldsymbol{x} \le C \int_K |\partial_x v|^2 + \left|\partial_y v\right|^2 \mathrm{d}\boldsymbol{x} = C |v|^2_{V^1(K)}. \end{aligned}$$

Hence, we have not only the one-way estimate (4.16), but the equivalence relation

$$\|v\|^2_{V^1(K)} \sim \|\hat{v}\|^2_{\hat{V}^1_\odot(Q)}. \tag{4.17}$$

To generalize this pattern, we introduce *weighted polar Sobolev spaces* of order $s \in \mathbb{N}_0$ with weight $\beta \in \mathbb{R}$ on any subset $Q \subset \hat{\Omega}$ of the parametric domain,

$$\hat{H}^s_{\odot,\beta}(Q) := \left\{ \hat{v} \in \mathcal{D}'(Q) : \|\hat{v}\|_{\hat{H}^s_{\odot,\beta}(Q)} < \infty \right\} \quad \text{and} \quad \hat{V}^s_{\odot,\beta}(Q) := \left\{ \hat{v} \in \mathcal{D}'(Q) : \|\hat{v}\|_{\hat{V}^s_{\odot,\beta}(Q)} < \infty \right\},$$

with the norms

$$\begin{aligned} \|\hat{v}\|^2_{\hat{H}^s_{\odot,\beta}(Q)} &:= \sum_{|\boldsymbol{\alpha}| \le s} \left\| \zeta_1^{\beta-\alpha_2} \hat{D}^{\boldsymbol{\alpha}} \hat{v} \right\|^2_{\hat{L}^2_{1/2}(Q)} = \sum_{|\boldsymbol{\alpha}| \le s} \int_Q \left| \zeta_1^{\beta-\alpha_2} \hat{D}^{\boldsymbol{\alpha}} \hat{v}(\boldsymbol{\zeta}) \right|^2 \zeta_1 \, \mathrm{d}\boldsymbol{\zeta}, \\ \|\hat{v}\|^2_{\hat{V}^s_{\odot,\beta}(Q)} &:= \sum_{|\boldsymbol{\alpha}| \le s} \left\| \zeta_1^{\beta-s+\alpha_1} \hat{D}^{\boldsymbol{\alpha}} \hat{v} \right\|^2_{\hat{L}^2_{1/2}(Q)} = \sum_{|\boldsymbol{\alpha}| \le s} \int_Q \left| \zeta_1^{\beta-s+\alpha_1} \hat{D}^{\boldsymbol{\alpha}} \hat{v}(\boldsymbol{\zeta}) \right|^2 \zeta_1 \, \mathrm{d}\boldsymbol{\zeta} \end{aligned}$$

and seminorms

$$|\hat{v}|^2_{\hat{H}^s_{\odot,\beta}(Q)} := |\hat{v}|^2_{\hat{V}^s_{\odot,\beta}(Q)} := \sum_{|\boldsymbol{\alpha}|=s} \left\| \zeta_1^{\beta-\alpha_2} \hat{D}^{\boldsymbol{\alpha}} \hat{v} \right\|^2_{\hat{L}^2_{1/2}(Q)}.$$

Polar Sobolev spaces without weight will be denoted by $\hat{H}^s_{\odot}(Q) = \hat{H}^s_{\odot,0}(Q)$ and $\hat{V}^s_{\odot}(Q) = \hat{V}^s_{\odot,0}(Q)$. Furthermore, it holds $\hat{H}^0_{\odot}(Q) = \hat{V}^0_{\odot}(Q) = \hat{L}^2_{1/2}(Q)$ and $\hat{H}^0_{\odot,\beta}(Q) = \hat{V}^0_{\odot,\beta}(Q) = \hat{L}^2_{1/2+\beta}(Q)$. We emphasize that the definition of the polar Sobolev spaces intrinsically includes the weight $\frac{1}{2}$, although this is not explicitly indicated in the notation.

A key property of the polar V-spaces is their natural correspondence to the standard V-spaces on the physical domain. Specifically, for all $s \in \mathbb{N}_0$, $\beta \in \mathbb{R}$ and $v \in V^s_\beta(K)$, the pull-back $\hat{v} = v \circ \boldsymbol{F}$ based on a polar parameterization satisfies

$$\|v\|_{V^s_\beta(K)} \sim \|\hat{v}\|_{\hat{V}^s_{\odot,\beta}(Q)}. \tag{4.18}$$

We verified this property for $\beta = 0$ and $s = 0, 1$ in (4.15) and (4.17). A technical proof valid for all $s \in \mathbb{N}$ and $\beta \in \mathbb{R}$ is provided in Lemma A.3 in the Appendix. Additionally, it is easy to see that

$$\|\hat{v}\|_{\hat{H}^s_{1/2+\beta}(Q)} \le C\|\hat{v}\|_{\hat{H}^s_{\odot,\beta}(Q)} \le C\|\hat{v}\|_{\hat{V}^s_{\odot,\beta}(Q)} \quad \text{for all } \hat{v} \in V^s_{\odot,\beta}(Q), \tag{4.19}$$

recall also (4.14), and thus the embeddings $\hat{V}^s_{\odot,\beta}(Q) \subset \hat{H}^s_{\odot,\beta}(Q) \subset \hat{H}^s_{1/2+\beta}(Q)$ hold.

4.2.3. *Bent polar Sobolev spaces*

In general, the Sobolev regularity of a pull-back function is affected not only by the polar singularity, but also by the reduced continuity of the isogeometric parameterization across element interfaces. In particular, polar parameterizations as defined in Section 3.1 are only C^0-continuous along coarse mesh lines if the associated knot values in the coarse knot vector Ξ^0_2 are repeated, see for instance Examples 3.6 and 3.8. Therefore, bent Sobolev spaces, as introduced in [27], must be taken into account.

Throughout this section, let $E \subset \Omega$ be a union of elements $K \in \mathcal{M}$ and let $\hat{E} = \boldsymbol{F}^{-1}(E) \subset \hat{\Omega}$ be the corresponding union of parametric elements. First, we note that some of the derivatives (4.9) with respect to the $\boldsymbol{F}$-coordinates may be in $L^2(K)$ for all $K \in E$, but not necessarily in $L^2(E)$. Therefore, we introduce the broken norms

$$\left\| \mathrm{D}^{\boldsymbol{\alpha}}_{\boldsymbol{F}} v \right\|^2_{\mathcal{L}^2(E)} = \sum_{K \in E} \left\| \mathrm{D}^{\boldsymbol{\alpha}}_{\boldsymbol{F}} v \right\|^2_{L^2(K)} \quad \text{and} \quad \left\| \mathrm{D}^{\boldsymbol{\alpha}}_{\boldsymbol{F}} v \right\|^2_{\mathcal{L}^2_\beta(E)} = \sum_{K \in E} \left\| \mathrm{D}^{\boldsymbol{\alpha}}_{\boldsymbol{F}} v \right\|^2_{L^2_\beta(K)},$$

which is useful for distributions that are not in $L^2_\beta(E)$, with $\beta \in \mathbb{R}$. This definition enables us to generalize the computations from Section 4.2.2 to unions of mesh elements. Even though we have the element-wise relation (4.18) for all $K \in E$, the pull-back $\hat{v} = v \circ \boldsymbol{F}$ of a function $v \in V^s_\beta(E)$ is not necessarily in $\hat{V}^s_{\odot,\beta}(\hat{E})$. For two adjacent parametric elements $Q_1, Q_2 \in \widehat{\mathcal{M}}$, let m_{Q_1,Q_2} denote the maximal order of continuous derivatives of $\boldsymbol{F}$ across their common edge $\partial Q_1 \cap \partial Q_2$. Then, we define *weighted bent Sobolev spaces* $\mathcal{X}^s_\beta(\hat{E}) = \mathcal{H}^s_\beta(\hat{E})$ and $\mathcal{X}^s_\beta(\hat{E}) = \mathcal{V}^s_\beta(\hat{E})$ of order $s \in \mathbb{N}$, $s \ge 1$ with weight $\beta > 0$ by

$$\mathcal{X}^s_\beta(\hat{E}) := \left\{ \hat{v} \in L^2(\hat{E}) : \left\{ \begin{array}{ll} \hat{v}_{|Q} \in \hat{X}^s_\beta(Q) & \text{for all } Q \in \hat{E} \text{ and} \\ \hat{\nabla}^q(\hat{v}_{|Q_1}) = \hat{\nabla}^q(\hat{v}_{|Q_2}) & \text{on } \partial Q_1 \cap \partial Q_2 \text{ for } q = 0, 1, \dots, \min\{m_{Q_1,Q_2}, s-1 \\ & \text{for all } Q_1, Q_2 \text{ with } \partial Q_1 \cap \partial Q_2 \neq \emptyset \end{array} \right\} \right\},$$

where we insert $\hat{X}^s_\beta(Q) = \hat{H}^s_\beta(Q)$ and $\hat{X}^s_\beta(Q) = \hat{V}^s_\beta(Q)$, respectively, and $\hat{\nabla}^q$ denotes the qth order partial derivative operator, with $\hat{\nabla}^0 v = v$. This definition yields well-defined Hilbert spaces endowed with the broken norm and seminorm

$$\|\hat{v}\|^2_{\mathcal{X}^s_\beta(\hat{E})} := \sum_{Q \in \hat{E}} \|\hat{v}\|^2_{\hat{X}^s_\beta(Q)}, \quad |\hat{v}|^2_{\mathcal{X}^s_\beta(\hat{E})} := \sum_{Q \in \hat{E}} |\hat{v}|^2_{\hat{X}^s_\beta(Q)}.$$

The standard bent Sobolev spaces without weight are denoted by $\mathcal{H}^s(\hat{E}) = \mathcal{H}^s_0(\hat{E})$ and $\mathcal{V}^s(\hat{E}) = \mathcal{V}^s_0(\hat{E})$.

In the next step, we combine the concepts of polar and bent function spaces and introduce *weighted bent polar Sobolev spaces* $\mathcal{X}^s_{\odot,\beta}(\hat{E}) = \mathcal{H}^s_{\odot,\beta}(\hat{E})$ and $\mathcal{X}^s_{\odot,\beta}(\hat{E}) = \mathcal{V}^s_{\odot,\beta}(\hat{E})$ of order $s \in \mathbb{N}$, $s \ge 1$ with weight $\beta > 0$,

$$\mathcal{X}^s_{\odot,\beta}(\hat{E}) := \left\{ \hat{v} \in L^2(\hat{E}) : \left\{ \begin{array}{ll} \hat{v}_{|Q} \in \hat{X}^s_{\odot,\beta}(Q) & \text{for all } Q \in \hat{E} \text{ and} \\ \hat{\nabla}^q(\hat{v}_{|Q_1}) = \hat{\nabla}^q(\hat{v}_{|Q_2}) & \text{on } \partial Q_1 \cap \partial Q_2 \text{ for } q = 0, 1, \dots, \min\{m_{Q_1,Q_2}, s-1 \\ & \text{for all } Q_1, Q_2 \text{ with } \partial Q_1 \cap \partial Q_2 \neq \emptyset \end{array} \right\} \right\},$$

where we insert $\hat{X}^s_{\odot,\beta}(Q) = \hat{H}^s_{\odot,\beta}(Q)$ and $\hat{X}^s_{\odot,\beta}(Q) = \hat{V}^s_{\odot,\beta}(Q)$, respectively, endowed with the broken norm and seminorm

$$\|\hat{v}\|^2_{\mathcal{X}^s_{\odot,\beta}(\hat{E})} := \sum_{Q \in \hat{E}} \|\hat{v}\|^2_{\hat{X}^s_{\odot,\beta}(Q)}, \quad |\hat{v}|^2_{\mathcal{X}^s_{\odot,\beta}(\hat{E})} := \sum_{Q \in \hat{E}} |\hat{v}|^2_{\hat{X}^s_{\odot,\beta}(Q)}.$$

Bent polar Sobolev spaces without weight are denoted by $\mathcal{H}^s_{\odot}(\hat{E}) = \mathcal{H}^s_{\odot,0}(\hat{E})$ and $\mathcal{V}^s_{\odot}(\hat{E}) = \mathcal{V}^s_{\odot,0}(\hat{E})$. From (4.18), we immediately obtain the characteristic relation

$$\|v\|_{V^s_\beta(E)} \sim \|\hat{v}\|_{\mathcal{V}^s_{\odot,\beta}(\hat{E})} \quad \text{for all } v \in V^s_\beta(E), \tag{4.20}$$

with $s \in \mathbb{N}_0$ and $\beta \in \mathbb{R}$, and Eq. (4.19) yields the estimate

$$\|\widehat{v}\|_{\mathcal{H}^s_{1/2+\beta}(\widehat{E})} \le C\|\widehat{v}\|_{\mathcal{H}^s_{\odot,\beta}(\widehat{E})} \le C\|\widehat{v}\|_{\mathcal{V}^s_{\odot,\beta}(\widehat{E})} \quad \text{for all } \widehat{v} \in \mathcal{V}^s_{\odot,\beta}(\widehat{E}). \tag{4.21}$$

Thus, the embeddings $\mathcal{V}^s_{\odot,\beta}(\widehat{E}) \subset \mathcal{H}^s_{\odot,\beta}(\widehat{E}) \subset \mathcal{H}^s_{1/2+\beta}(\widehat{E})$ hold.

In this context, suitable projectors $\Pi : \mathcal{X}^s_{\odot,\beta}(\widehat{\Omega}) \to S_{(s-1,s-1)}(\Xi)$ are required that map from weighted bent polar Sobolev spaces of order s into the spline spaces of degree $s-1$ and satisfy the crucial property

$$\widehat{v} - \Pi(\widehat{v}) \in \mathring{X}^s_{\odot,\beta}(\widehat{\Omega}) \quad \text{for all } \widehat{v} \in \mathcal{X}^s_{\odot,\beta}(\widehat{\Omega}). \tag{4.22}$$

The existence of such projectors can be shown by analogy to similar results from the literature [28].

4.2.4. Polar transformation of the projection error

Ultimately, we perform a transformation of the projection error, which will be needed to prove Theorem 3.13. Therefore, in addition to the computations above, the weight function has to be taken into account. For $q = 0$, we obtain

$$\begin{aligned}\left\|v - \Pi_{V_h^\odot} v\right\|^2_{L^2(K)} &= \int_K \left|v - \Pi_{V_h^\odot} v\right|^2 \mathrm{d}\boldsymbol{x} \sim \int_Q \left|v\circ\boldsymbol{F} - \Pi_{V_h^\odot} v\circ\boldsymbol{F}\right|^2 \zeta_1 \,\mathrm{d}\boldsymbol{\zeta} = \int_Q \left|\frac{W(v\circ\boldsymbol{F}) - \Pi^{\widehat{\Gamma}}_{p,\Xi}(W(v\circ\boldsymbol{F}))}{W}\right|^2 \zeta_1 \,\mathrm{d}\boldsymbol{\zeta} \\ &\le C\int_Q \left|W\widehat{v} - \Pi^{\widehat{\Gamma}}_{p,\Xi}(W\widehat{v})\right|^2 \zeta_1 \,\mathrm{d}\boldsymbol{\zeta} = C\left\|W\widehat{v} - \Pi^{\widehat{\Gamma}}_{p,\Xi}(W\widehat{v})\right\|^2_{\hat{L}^2_{1/2}(Q)},\end{aligned} \tag{4.23}$$

where we use the boundedness of W and its inverse W^{-1}, see [28], and set $\widehat{v} = v\circ\boldsymbol{F}$. For $q = 1$, we compute

$$\begin{aligned}\left|v - \Pi_{V_h^\odot} v\right|^2_{H^1(K)} &= \int_K \left|\partial_x\left(v - \Pi_{V_h^\odot} v\right)\right|^2 + \left|\partial_y\left(v - \Pi_{V_h^\odot} v\right)\right|^2 \mathrm{d}\boldsymbol{x} \\ &\sim \int_Q \left(\left|\widehat{\partial}_1\left(v\circ\boldsymbol{F} - \Pi_{V_h^\odot} v\circ\boldsymbol{F}\right)\right|^2 + \left|\frac{1}{\zeta_1}\widehat{\partial}_2\left(v\circ\boldsymbol{F} - \Pi_{V_h^\odot} v\circ\boldsymbol{F}\right)\right|^2\right)\zeta_1 \,\mathrm{d}\boldsymbol{\zeta} \\ &= \int_Q \left(\left|\widehat{\partial}_1\left(\frac{W\widehat{v} - \Pi^{\widehat{\Gamma}}_{p,\Xi}(W\widehat{v})}{W}\right)\right|^2 + \left|\frac{1}{\zeta_1}\widehat{\partial}_2\left(\frac{W\widehat{v} - \Pi^{\widehat{\Gamma}}_{p,\Xi}(W\widehat{v})}{W}\right)\right|^2\right)\zeta_1 \,\mathrm{d}\boldsymbol{\zeta} \\ &\le C\left(\left\|\widehat{\partial}_1\left(W\widehat{v} - \Pi^{\widehat{\Gamma}}_{p,\Xi}(W\widehat{v})\right)\right\|^2_{\hat{L}^2_{1/2}(Q)} + \left\|W\widehat{v} - \Pi^{\widehat{\Gamma}}_{p,\Xi}(W\widehat{v})\right\|^2_{\hat{L}^2_{1/2}(Q)}\right. \\ &\qquad \left. + \left\|\widehat{\partial}_2\left(W\widehat{v} - \Pi^{\widehat{\Gamma}}_{p,\Xi}(W\widehat{v})\right)\right\|^2_{\hat{L}^2_{-1/2}(Q)} + \left\|W\widehat{v} - \Pi^{\widehat{\Gamma}}_{p,\Xi}(W\widehat{v})\right\|^2_{\hat{L}^2_{-1/2}(Q)}\right),\end{aligned} \tag{4.24}$$

where we employ the Leibniz formula

$$\partial^{\boldsymbol{\alpha}}\left(\frac{g}{W}\right) = \sum_{\{\boldsymbol{\beta}:\boldsymbol{\beta}\le\boldsymbol{\alpha}\}} \binom{\boldsymbol{\alpha}}{\boldsymbol{\beta}} \left(\partial^{\boldsymbol{\beta}} g\right)\left(\partial^{\boldsymbol{\alpha}-\boldsymbol{\beta}} W^{-1}\right) \tag{4.25}$$

with $g = \widehat{v} - \Pi^{\widehat{\Gamma}}_{p,\Xi}\widehat{v}$ and Young's formula. Here, we remark again that the weight function W and its inverse W^{-1} as well as their derivatives are bounded [28]. Throughout the paper, the latter will be used multiple times, and the Leibniz formula will be applied in combination with the weight function without further explication.

Finally, let $E \subset \Omega$ be given by a union of elements $K \in \mathcal{M}$ and let $\widehat{E} = \boldsymbol{F}^{-1}(E) \subset \widehat{\Omega}$. Then, we have analogous results to (4.23) and (4.24), but with bent Sobolev spaces,

$$\left\|v - \Pi_{V_h^\odot} v\right\|^2_{L^2(E)} \le \left\|W\widehat{v} - \Pi^{\widehat{\Gamma}}_{p,\Xi}(W\widehat{v})\right\|^2_{\mathcal{L}^2_{1/2}(\widehat{E})}$$

and

$$\begin{aligned}\left|v - \Pi_{V_h^\odot} v\right|^2_{H^1(E)} &\le C\left(\left\|\widehat{\partial}_1\left(W\widehat{v} - \Pi^{\widehat{\Gamma}}_{p,\Xi}(W\widehat{v})\right)\right\|^2_{\mathcal{L}^2_{1/2}(\widehat{E})} + \left\|W\widehat{v} - \Pi^{\widehat{\Gamma}}_{p,\Xi}(W\widehat{v})\right\|^2_{\mathcal{L}^2_{1/2}(\widehat{E})}\right. \\ &\qquad \left. + \left\|\widehat{\partial}_2\left(W\widehat{v} - \Pi^{\widehat{\Gamma}}_{p,\Xi}(W\widehat{v})\right)\right\|^2_{\mathcal{L}^2_{-1/2}(\widehat{E})} + \left\|W\widehat{v} - \Pi^{\widehat{\Gamma}}_{p,\Xi}(W\widehat{v})\right\|^2_{\mathcal{L}^2_{-1/2}(\widehat{E})}\right).\end{aligned}$$

5. Proof of Theorem 3.13

In this section, we derive several error estimates for the proposed modified projector under graded h-refinement on polar domains with corners. These estimates are then combined to establish Theorem 3.13. The error is analyzed separately in the neighborhood of the polar point and in the remainder of the domain, which is not affected by the corner singularity.

5.1. Splitting of the polar domain

To begin, we explain in more detail how the model domain and the underlying meshes can be split suitably. Let $\widehat{\mathcal{M}}^\mu$ and $\mathcal{M}^\mu$ be graded parametric and physical meshes, respectively, resulting from the knot vectors Ξ_1 and Ξ_2 for some grading parameter $\mu \in (0,1]$ and polynomial degrees $\boldsymbol{p} = (p_1, p_2)$, recall Section 3.3. To describe a region surrounding the corner $\boldsymbol{P}$, we consider the physical Bézier elements $K_j = \boldsymbol{F}(Q_j) \in \mathcal{M}^\mu$ whose support extensions satisfy

$$\boldsymbol{P} \in \overline{\widetilde{K}_j} = \overline{\boldsymbol{F}(\widetilde{Q}_j)} = \boldsymbol{F}(\overline{\widetilde{Q}_j}),$$

that is, the closure of the support extension $\widetilde{K}_j$ contains the singularity. The corresponding parametric mesh elements Q_j are characterized by the condition

$$\Gamma_1 \cap \overline{\widetilde{Q}_j} = (\{0\} \times [0,1]) \cap \left(\overline{\widetilde{I}_{1,j_1}} \times \overline{\widetilde{I}_{2,j_2}}\right) = \left(\{0\} \cap \overline{\widetilde{I}_{1,j_1}}\right) \times \overline{\widetilde{I}_{2,j_2}} \neq \emptyset,$$

i.e., the singular edge Γ_1 touches the closure of the support extension $\widetilde{Q}_j$, which, by Eq. (2.12), is equivalent to $0 \in \overline{\widetilde{I}_{1,j_1}}$. The refined knot vector in ζ_1-direction can be expressed in terms of the breakpoints (3.17),

$$\Xi_1 = \{\xi_{1,1}, \xi_{1,2}, \dots, \xi_{1,n_1+p_1+1}\} = \{\underbrace{\zeta_{1,1}, \dots, \zeta_{1,1}}_{p_1+1 \text{ times}}, \zeta_{1,2}, \zeta_{1,3}, \dots, \zeta_{1,N_1-2}, \zeta_{1,N_1-1}, \underbrace{\zeta_{1,N_1}, \dots, \zeta_{1,N_1}}_{p_1+1 \text{ times}}\}. \tag{5.1}$$

Thus, it holds $n_1 + p_1 + 1 = N_1 + 2p_1$ and

$$I_{1,j_1} = \left(\zeta_{1,j_1}, \zeta_{1,j_1+1}\right) = \left(\xi_{1,j_1+p_1}, \xi_{1,j_1+p_1+1}\right), \quad j_1 = 1, 2, \dots, N_1 - 1.$$

With definition (2.1), we obtain

$$\widetilde{I}_{1,j_1} = \left(\xi_{1,j_1+p_1-p_1}, \xi_{1,j_1+p_1+p_1+1}\right) = \left(\xi_{1,j_1}, \xi_{1,j_1+2p_1+1}\right), \quad j_1 = 1, 2, \dots, N_1 - 1.$$

By construction (5.1), we further have $\xi_{1,j_1} = 0$ and hence, it is $0 \in \overline{\widetilde{I}_{1,j_1}}$ if and only if $j_1 \leq p_1 + 1$. Therefore, we divide the graded parametric and physical Bézier mesh $\widehat{\mathcal{M}}^\mu$ and $\mathcal{M}^\mu$ into two submeshes,

$$\widehat{\mathcal{M}}^\mu = \widehat{\mathcal{M}}^\mu_C \cup \widehat{\mathcal{M}}^\mu_R \quad \text{and} \quad \mathcal{M}^\mu = \mathcal{M}^\mu_C \cup \mathcal{M}^\mu_R,$$

respectively, with

$$\widehat{\mathcal{M}}^\mu_C := \{Q_j\}_{j_1 \in \{1,2,\dots,p_1+1\}, j_2 \in \{1,2,\dots,N_2\}}, \quad \widehat{\mathcal{M}}^\mu_R := \{Q_j\}_{j_1 \in \{p_1+2, p_1+3, \dots, N_1\}, j_2 \in \{1,2,\dots,N_2\}},$$
$$\mathcal{M}^\mu_C := \{K_j\}_{j_1 \in \{1,2,\dots,p_1+1\}, j_2 \in \{1,2,\dots,N_2\}}, \quad \mathcal{M}^\mu_R := \{K_j\}_{j_1 \in \{p_1+2, p_1+3, \dots, N_1\}, j_2 \in \{1,2,\dots,N_2\}}.$$

Induced by these partitions, we also divide the parametric domain into two subdomains,

$$\widehat{\Omega} = \widehat{\Omega}_C \cup \widehat{\Omega}_R, \text{ with } \widehat{\Omega}_C := (0, \zeta_{1,p_1+2}] \times (0,1) \text{ and } \widehat{\Omega}_R := [\zeta_{1,p_1+2}, 1) \times (0,1). \tag{5.2}$$

In this way, we obtain the desired partition of the physical domain,

$$\Omega = \Omega_C \cup \Omega_R,$$

into a small polar domain surrounding the corner,

$$\Omega_C := \boldsymbol{F}(\widehat{\Omega}_C) = \boldsymbol{G}(\widehat{\Omega}_C) = \left\{\zeta_1\, \boldsymbol{G}(\zeta_2) \in \mathbb{R}^2 : 0 < \zeta_1 \leq \zeta_{1,p_1+2}, 0 < \zeta_2 < 1\right\},$$

and the remaining ring-type domain

$$\Omega_R := \boldsymbol{F}(\widehat{\Omega}_R) = \left\{\zeta_1\, \boldsymbol{G}(\zeta_2) \in \mathbb{R}^2 : \zeta_{1,p_1+2} \leq \zeta_1 < 1, 0 < \zeta_2 < 1\right\},$$

where we used the representation of the polar parameterization $\boldsymbol{F}$ from Assumption 3.4. In Fig. 5, we provide an illustration of the partitioned domains and meshes for a circular sector and an L-shaped domain. Note that the splitting depends on the mesh size h_1 and the polynomial degree p_1 of the first univariate direction, which is not pointed out explicitly in the notation. Lastly, we define the overlapping domains consisting of the union of the support extensions of all elements in $\mathcal{M}^\mu_C$ and $\mathcal{M}^\mu_R$, respectively,

$$\widetilde{\widehat{\Omega}}_C := \bigcup_{Q_j \in \widehat{\mathcal{M}}^\mu_C} \widetilde{Q}_j, \quad \widetilde{\widehat{\Omega}}_R := \bigcup_{Q_j \in \widehat{\mathcal{M}}^\mu_R} \widetilde{Q}_j, \quad \widetilde{\Omega}_C := \bigcup_{K_j \in \mathcal{M}^\mu_C} \widetilde{K}_j, \quad \widetilde{\Omega}_R := \bigcup_{K_j \in \mathcal{M}^\mu_R} \widetilde{K}_j. \tag{5.3}$$

5.2. Projection error estimates

Next, we proceed with the projection error estimates for the two regions of the polar domain.

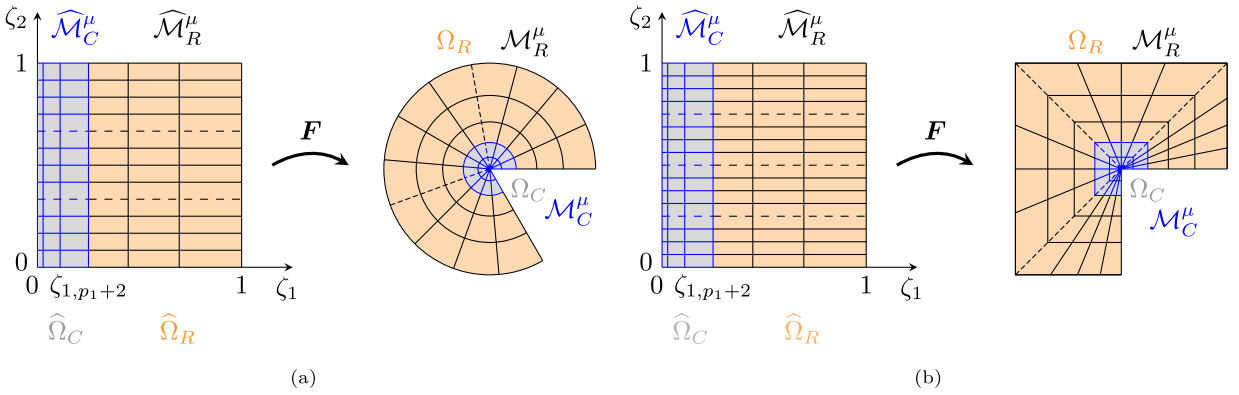

Fig. 5. Splitting of the parametric and physical domain and the corresponding meshes. (a): Circular sector (b): L-shaped domain.

5.2.1. Estimates on Ω_R

We begin by deriving estimates on Ω_R, where the distance to the singularity is strictly positive. In this setting, a similar strategy to that used in standard anisotropic approximation theory can be applied [8,28], in which element-wise estimates on the parametric domain are mapped to the physical domain via a change of variables. However, in contrast to the literature, the transformed quantities depend on the distance between each element and the singularity, and thus, by construction of Ω_R, also on the mesh size. The following element-wise error estimate on the parametric domain from the literature serves as the starting point for our analysis.

Lemma 5.1. *Let the integers $0 \le r_1 \le s_1 \le p_1 + 1$ and $0 \le r_2 \le s_2 \le p_2 + 1$. Then, there exists a constant C depending only on $\boldsymbol{p}, \theta$ such that for all elements $Q_j \in \widehat{\mathcal{M}}^\mu$, we have*

$$\left\| \widehat{D}^{(r_1,r_2)}(\widehat{v} - \Pi^{\widehat{\Gamma}}_{\boldsymbol{p},\boldsymbol{\Xi}}\widehat{v}) \right\|_{\widehat{L}^2(Q_j)} \le C \left(\widetilde{h}_{1,j_1}^{s_1-r_1} \left\| \widehat{D}^{(s_1,r_2)}\widehat{v} \right\|_{\mathcal{L}^2(\widetilde{Q}_j)} + \widetilde{h}_{2,j_2}^{s_2-r_2} \left\| \widehat{D}^{(r_1,s_2)}\widehat{v} \right\|_{\mathcal{L}^2(\widetilde{Q}_j)} \right)$$

for all functions $\widehat{v} : \widehat{\Omega} \to \mathbb{R}$ with $\widehat{D}^{(s_1,r_2)}\widehat{v}$, $\widehat{D}^{(r_1,s_2)}\widehat{v} \in \mathcal{L}^2(\widetilde{\Omega}_R)$, where $\widetilde{\Omega}_R$ is defined as in (5.3).

Proof. The result is proven in [8, Proposition 4.1] together with [8, Remark 4.2]. □

Based on Lemma 5.1, we can develop an estimate on the full ring-type domain part Ω_R. As in Section 3.4, we set $p = \min\{p_1, p_2\}$ from now on.

Theorem 5.2. *Let $q \in \{0, 1\}$ and $s \in \mathbb{N}$ with $2 \le s \le p + 1$. Further, let $v \in V_\beta^s(\widetilde{\Omega}_R)$ for all $\beta \in \mathbb{R}$ with $s - 1 - \nu < \beta < s - 1$, recall (3.15). If the mesh grading parameter satisfies condition (3.22), then there exists a constant C depending only on $p, \theta, \boldsymbol{F}, W$ such that*

$$\left| v - \Pi_{V_h^\odot} v \right|_{H^q(\Omega_R)} \le C h^{s-q} \|v\|_{V_\beta^s(\widetilde{\Omega}_R)},$$

with $\widetilde{\Omega}_R$ as defined in (5.3).

Proof. Let $K_j \in \mathcal{M}_R^\mu$ and $Q_j = \boldsymbol{F}^{-1}(K_j) \in \widehat{\mathcal{M}}_R^\mu$. By construction of the splitting from Section 5.1, the element K_j is not adjacent to the polar point, $\boldsymbol{P} \notin \overline{K_j}$, and thus the Jacobian of $\boldsymbol{F}$ is bounded on $\overline{Q_j}$. However, the bounds depend on the distance of K_j to the polar point, which is equivalent to the distance of Q_j to the singular edge $\widehat{\Gamma}_1$. In more detail, let $Q_j = (\zeta_{1,j_1}, \zeta_{1,j_1+1}) \times (\zeta_{2,j_2}, \zeta_{2,j_2+1}) \in \mathcal{M}_R^\mu$. Then, due to Eqs. (3.5), (3.7) and the local quasi-uniformity of the mesh, see Lemma 3.18, we have

$$\left|\det(J_{\boldsymbol{F}})\right| \sim \zeta_{1,j_1} \quad \text{and} \quad \left|\det(J_{\boldsymbol{F}^{-1}})\right| \sim \zeta_{1,j_1} \quad \text{in } \widetilde{Q}_j. \tag{5.4}$$

With (4.23), we thus obtain

$$\left\| v - \Pi^\odot_{V_h} v \right\|_{L^2(K_j)} \le C \left\| W\widehat{v} - \Pi^{\widehat{\Gamma}}_{\boldsymbol{p},\boldsymbol{\Xi}}(W\widehat{v}) \right\|_{\widehat{L}^2_{1/2}(Q_j)} \le C\zeta_{1,j_1}^{1/2} \left\| W\widehat{v} - \Pi^{\widehat{\Gamma}}_{\boldsymbol{p},\boldsymbol{\Xi}}(W\widehat{v}) \right\|_{\widehat{L}^2(Q_j)}$$

and with (4.24), it follows

$$\left| v - \Pi_{V_h} v \right|^2_{H^1(K_j)} \le C \left(\zeta_{1,j_1} \left\| \widehat{\partial}_1 \left(W\widehat{v} - \Pi^{\widehat{\Gamma}}_{\boldsymbol{p},\boldsymbol{\Xi}}(W\widehat{v}) \right) \right\|^2_{\widehat{L}^2(Q_j)} + \zeta_{1,j_1} \left\| W\widehat{v} - \Pi^{\widehat{\Gamma}}_{\boldsymbol{p},\boldsymbol{\Xi}}(W\widehat{v}) \right\|^2_{\widehat{L}^2(Q_j)} \right. \tag{5.5}$$

$$\left. + \zeta_{1,j_1}^{-1} \left\| \widehat{\partial}_2 \left(W\widehat{v} - \Pi^{\widehat{\Gamma}}_{\boldsymbol{p},\boldsymbol{\Xi}}(W\widehat{v}) \right) \right\|^2_{\widehat{L}^2(Q_j)} + \zeta_{1,j_1}^{-1} \left\| W\widehat{v} - \Pi^{\widehat{\Gamma}}_{\boldsymbol{p},\boldsymbol{\Xi}}(W\widehat{v}) \right\|^2_{\widehat{L}^2(Q_j)} \right). \tag{5.6}$$

First, we estimate the terms in line (5.5). Therefore, we use Lemma 5.1 with $s_1 = s$, $s_2 = s - q$, $r_1 = q$ and $r_2 = 0$ and apply the Leibniz formula (4.25), where we note that the weight function W and its inverse W^{-1} as well as their derivatives are bounded [28]. In more detail, we recall that the weight function has the form (3.9) and consequently, all derivatives $\widehat{D}^{\boldsymbol{\alpha}} W$ for $\boldsymbol{\alpha} \ge (1, 0)$ vanish.

It follows for $q \in \{0,1\}$ that

$$\begin{aligned}\left\|\widehat{\partial}_1^q\Big(W\widehat{v}-\Pi^{\widehat{\Gamma}}_{p,\Xi}(W\widehat{v})\Big)\right\|_{\widehat{L}^2(Q_j)} &\le C\left(\widetilde{h}_{1,j_1}^{s-q}\left\|\widehat{D}^{(s,0)}(W\widehat{v})\right\|_{\mathcal{L}^2(\widetilde{Q}_j)}+\widetilde{h}_{2,j_2}^{s-q}\left\|\widehat{D}^{(q,s-q)}(W\widehat{v})\right\|_{\mathcal{L}^2(\widetilde{Q}_j)}\right)\\ &\le C\left(\widetilde{h}_{1,j_1}^{s-q}\sum_{\substack{\boldsymbol{\alpha}\le(s,0)\\ \boldsymbol{\alpha}\ge(s,0)}}\left\|\widehat{D}^{\boldsymbol{\alpha}}\widehat{v}\right\|_{\mathcal{L}^2(\widetilde{Q}_j)}+\widetilde{h}_{2,j_2}^{s-q}\sum_{\substack{\boldsymbol{\alpha}\le(q,s-q)\\ \boldsymbol{\alpha}\ge(q,0)}}\left\|\widehat{D}^{\boldsymbol{\alpha}}\widehat{v}\right\|_{\mathcal{L}^2(\widetilde{Q}_j)}\right)\\ &= \left(\widetilde{h}_{1,j_1}^{s-q}\left\|\widehat{D}^{(s,0)}\widehat{v}\right\|_{\mathcal{L}^2(\widetilde{Q}_j)}+\widetilde{h}_{2,j_2}^{s-q}\sum_{\alpha_2=0}^{s-q}\left\|\widehat{D}^{(q,\alpha_2)}\widehat{v}\right\|_{\mathcal{L}^2(\widetilde{Q}_j)}\right).\end{aligned}$$

Now, we transfer these norms to the physical domain based on the ideas from Section 4.2.2. More precisely, we first perform an integral transformation and employ (4.9) as well as the bound (5.4) for the determinant of the inverse parameterization. Then, we bound the norms of the derivatives with respect to the $\boldsymbol{F}$-coordinates by the norms of the classical physical derivatives as shown in Lemma A.1. Such an argument will be used multiple times in the following and will be referred to as a change of variables. It follows

$$\begin{aligned}\zeta_{1,j_1}^{1/2}\left\|\widehat{\partial}_1^q\Big(W\widehat{v}-\Pi^{\widehat{\Gamma}}_{p,\Xi}(W\widehat{v})\Big)\right\|_{\widehat{L}^2(Q_j)} &\le C\left(\frac{\zeta_{1,j_1}}{\zeta_{1,j_1}}\right)^{1/2}\left(\widetilde{h}_{1,j_1}^{s-q}\left\|D_{\boldsymbol{F}}^{(s,0)}v\right\|_{\mathcal{L}^2(\widetilde{K}_j)}+\widetilde{h}_{2,j_2}^{s-q}\sum_{\alpha_2=0}^{s-q}\left\|D_{\boldsymbol{F}}^{(q,\alpha_2)}v\right\|_{\mathcal{L}^2(\widetilde{K}_j)}\right)\\ &\le C\left(\widetilde{h}_{1,j_1}^{s-q}\sum_{|\boldsymbol{\gamma}|\le s}\left\|D^{\boldsymbol{\gamma}}v\right\|_{\mathcal{L}^2(\widetilde{K}_j)}+\widetilde{h}_{2,j_2}^{s-q}\sum_{\alpha_2=0}^{s-q}\sum_{|\boldsymbol{\gamma}|\le q+\alpha_2}\left\|r^{\alpha_2}D^{\boldsymbol{\gamma}}v\right\|_{\mathcal{L}^2(\widetilde{K}_j)}\right)\\ &\le C\,h^{s-q}\left(\left(\zeta_{1,j_1}\right)^{(1-\mu)(s-q)}\sum_{|\boldsymbol{\gamma}|\le s}\left\|D^{\boldsymbol{\gamma}}v\right\|_{\mathcal{L}^2(\widetilde{K}_j)}+\sum_{\alpha_2=0}^{s-q}\sum_{|\boldsymbol{\gamma}|\le q+\alpha_2}\left\|r^{\alpha_2}D^{\boldsymbol{\gamma}}v\right\|_{\mathcal{L}^2(\widetilde{K}_j)}\right),\end{aligned}\tag{5.7}$$

where, in the last step, we inserted the mesh properties (3.28) with $h=\max\{h_1,h_2\}$. Due to the local quasi-uniformity of the mesh, recall Lemma 3.18, and relation (3.8), we further have

$$\zeta_{1,j_1}\sim\zeta_1(\boldsymbol{x})\sim r(\boldsymbol{x})\quad\text{for all }\boldsymbol{x}\in\widetilde{K}_j,\tag{5.8}$$

with $\boldsymbol{\zeta}(\boldsymbol{x})=(\zeta_1(\boldsymbol{x}),\zeta_2(\boldsymbol{x}))=\boldsymbol{F}^{-1}(\boldsymbol{x})\in\widetilde{Q}_j$. Moreover, we set $\beta=(1-\mu)(s-q)$. Then, as $\mu\in(0,1]$ satisfies condition (3.22), it holds

$$\beta\le s-q\quad\text{and}\quad\beta>\left(1-\frac{\nu-q+1}{s-q}\right)(s-q)=s-q-(\nu-q+1)=s-1-\nu.\tag{5.9}$$

By combining (5.7), (5.8) and (5.9), we obtain

$$\begin{aligned}\zeta_{1,j_1}^{1/2}\left\|\widehat{\partial}_1^q\Big(W\widehat{v}-\Pi^{\widehat{\Gamma}}_{p,\Xi}(W\widehat{v})\Big)\right\|_{\widehat{L}^2(Q_j)} &\le C\,h^{s-q}\left(\sum_{|\boldsymbol{\gamma}|\le s}\left\|r^{\beta}D^{\boldsymbol{\gamma}}v\right\|_{L^2(\widetilde{K}_j)}+\sum_{\alpha_2=0}^{s-q}\sum_{|\boldsymbol{\gamma}|\le q+\alpha_2}\left\|r^{\beta-(s-q)+\alpha_2}D^{\boldsymbol{\gamma}}v\right\|_{L^2(\widetilde{K}_j)}\right)\\ &\le C\,h^{s-q}\left(\sum_{|\boldsymbol{\gamma}|\le s}\left\|r^{\beta}D^{\boldsymbol{\gamma}}v\right\|_{L^2(\widetilde{K}_j)}+\sum_{\alpha_2=0}^{s-q}\sum_{|\boldsymbol{\gamma}|\le q+\alpha_2}\left\|r^{\beta-s+|\boldsymbol{\gamma}|}D^{\boldsymbol{\gamma}}v\right\|_{L^2(\widetilde{K}_j)}\right)\\ &\le C\,h^{s-q}\left(\sum_{|\boldsymbol{\gamma}|\le s}\left\|r^{\beta}D^{\boldsymbol{\gamma}}v\right\|_{L^2(\widetilde{K}_j)}+\sum_{|\boldsymbol{\gamma}|\le s}\left\|r^{\beta-s+|\boldsymbol{\gamma}|}D^{\boldsymbol{\gamma}}v\right\|_{L^2(\widetilde{K}_j)}\right)\\ &\le C\,h^{s-q}\left(\|v\|_{H^s_\beta(\widetilde{K}_j)}+\|v\|_{V^s_\beta(\widetilde{K}_j)}\right)\le C\,h^{s-q}\|v\|_{V^s_\beta(\widetilde{K}_j)}.\end{aligned}$$

Next, we estimate the first term in line (5.6) using Lemma 5.1 for $s_1=s-1$, $s_2=s$, $r_1=0$ and $r_2=1$ and the Leibniz formula (4.25),

$$\begin{aligned}\left\|\widehat{\partial}_2\Big(W\widehat{v}-\Pi^{\widehat{\Gamma}}_{p,\Xi}(W\widehat{v})\Big)\right\|_{\widehat{L}^2(Q)} &\le C\left(\widetilde{h}_{1,j_1}^{s-1}\left\|\widehat{D}^{(s-1,1)}(W\widehat{v})\right\|_{\mathcal{L}^2(\widetilde{Q}_j)}+\widetilde{h}_{2,j_2}^{s-1}\left\|\widehat{D}^{(0,s)}(W\widehat{v})\right\|_{\mathcal{L}^2(\widetilde{Q}_j)}\right)\\ &\le C\left(\widetilde{h}_{1,j_1}^{s-1}\sum_{\alpha_2=0}^{1}\left\|\widehat{D}^{(s-1,\alpha_2)}\widehat{v}\right\|_{\mathcal{L}^2(\widetilde{Q}_j)}+\widetilde{h}_{2,j_2}^{s-1}\sum_{\alpha_2=0}^{s}\left\|\widehat{D}^{(0,\alpha_2)}\widehat{v}\right\|_{\mathcal{L}^2(\widetilde{Q}_j)}\right).\end{aligned}$$

Then, we apply a change of variables and exploit the mesh properties (3.28) and (5.8),

$$\begin{aligned}\zeta_{1,j_1}^{-1/2}\left\|\widehat{\partial}_2\Big(W\widehat{v}-\Pi^{\widehat{\Gamma}}_{p,\Xi}(W\widehat{v})\Big)\right\|_{\widehat{L}^2(Q)} &\le C\,(\zeta_{1,j_1}\zeta_{1,j_1})^{-1/2}\left(\widetilde{h}_{1,j_1}^{s-1}\sum_{\alpha_2=0}^{1}\left\|D_{\boldsymbol{F}}^{(s-1,\alpha_2)}v\right\|_{\mathcal{L}^2(\widetilde{K}_j)}+\widetilde{h}_{2,j_2}^{s-1}\sum_{\alpha_2=0}^{s}\left\|D_{\boldsymbol{F}}^{(0,\alpha_2)}v\right\|_{\mathcal{L}^2(\widetilde{K}_j)}\right)\\ &\le C\,\zeta_{1,j_1}^{-1}\left(\widetilde{h}_{1,j_1}^{s-1}\sum_{\alpha_2=0}^{1}\sum_{|\boldsymbol{\gamma}|\le s-1+\alpha_2}\left\|r^{\alpha_2}D^{\boldsymbol{\gamma}}v\right\|_{\mathcal{L}^2(\widetilde{K}_j)}+\widetilde{h}_{2,j_2}^{s-1}\sum_{\alpha_2=0}^{s}\sum_{|\boldsymbol{\gamma}|\le\alpha_2}\left\|r^{\alpha_2}D^{\boldsymbol{\gamma}}v\right\|_{\mathcal{L}^2(\widetilde{K}_j)}\right)\\ &\le C\,h^{s-1}\left(\left(\zeta_{1,j_1}\right)^{(1-\mu)(s-1)}\sum_{\alpha_2=0}^{1}\sum_{|\boldsymbol{\gamma}|\le s+\alpha_2-1}\left\|r^{\alpha_2-1}D^{\boldsymbol{\gamma}}v\right\|_{L^2(\widetilde{K}_j)}+\sum_{\alpha_2=0}^{s}\sum_{|\boldsymbol{\gamma}|\le\alpha_2}\left\|r^{\alpha_2-1}D^{\boldsymbol{\gamma}}v\right\|_{L^2(\widetilde{K}_j)}\right).\end{aligned}$$

We set again $\beta = (1-\mu)(s-q)$ for $q = 1$ and recall that (5.9) is satisfied. It follows

$$\begin{aligned}
\zeta_{1,j_1}^{-1/2}\left\|\widehat{\partial}_2\left(W\widehat{v} - \Pi^{\widehat{\Gamma}}_{p,\Xi}(W\widehat{v})\right)\right\|_{\widehat{L}^2(Q)} &\le C\,h^{s-1}\left(\sum_{\alpha_2=0}^{1}\sum_{|\gamma|\le s+\alpha_2-1}\left\|r^{\beta+\alpha_2-1}D^\gamma v\right\|_{L^2(\widetilde{K}_j)} + \sum_{\alpha_2=0}^{s}\sum_{|\gamma|\le\alpha_2}\left\|r^{\beta-(s-1)+\alpha_2-1}D^\gamma v\right\|_{L^2(\widetilde{K}_j)}\right)\\
&\le C\,h^{s-1}\left(\sum_{\alpha_2=0}^{1}\sum_{|\gamma|\le s+\alpha_2-1}\left\|r^{\beta-s+|\gamma|}D^\gamma v\right\|_{L^2(\widetilde{K}_j)} + \sum_{\alpha_2=0}^{s}\sum_{|\gamma|\le\alpha_2}\left\|r^{\beta-s+|\gamma|}D^\gamma v\right\|_{L^2(\widetilde{K}_j)}\right)\\
&\le C\,h^{s-1}\sum_{|\gamma|\le s}\left\|r^{\beta-s+|\gamma|}D^\gamma v\right\|_{L^2(\widetilde{K}_j)} = C\,h^{s-1}\|v\|_{V^s_\beta(\widetilde{K}_j)}.
\end{aligned}$$

The second term in line (5.6) can be computed similarly,

$$\begin{aligned}
\zeta_{1,j_1}^{-1/2}\left\|\left(W\widehat{v} - \Pi^{\widehat{\Gamma}}_{p,\Xi}(W\widehat{v})\right)\right\|_{\widehat{L}^2(Q)} &\le C\left(\widetilde{h}^s_{1,j_1}\left\|\widehat{D}^{(s,0)}\widehat{v}\right\|_{\mathcal{L}^2(\widetilde{Q}_j)} + \widetilde{h}^s_{2,j_2}\sum_{\alpha_2=0}^{s}\left\|\widehat{D}^{(0,\alpha_2)}\widehat{v}\right\|_{\mathcal{L}^2(\widetilde{Q}_j)}\right)\\
&\le C\,\zeta_{1,j_1}^{-1}\left(\widetilde{h}^s_{1,j_1}\sum_{|\gamma|\le s}\|D^\gamma v\|_{\mathcal{L}^2(\widetilde{K}_j)} + \widetilde{h}^s_{2,j_2}\sum_{\alpha_2=0}^{s}\sum_{|\gamma|\le\alpha_2}\|r^{\alpha_2}D^\gamma v\|_{\mathcal{L}^2(\widetilde{K}_j)}\right)\\
&\le C\,h^{s-1}\left(\sum_{|\gamma|\le s}\left\|r^\beta D^\gamma v\right\|_{L^2(\widetilde{K}_j)} + \sum_{\alpha_2=0}^{s}\sum_{|\gamma|\le\alpha_2}\left\|r^{\beta-s+\alpha_2}D^\gamma v\right\|_{L^2(\widetilde{K}_j)}\right)\\
&\le C\,h^{s-1}\left(\|v\|_{H^s_\beta(\widetilde{K}_j)} + \sum_{\alpha_2=0}^{s}\sum_{|\gamma|\le\alpha_2}\left\|r^{\beta-s+|\gamma|}D^\gamma v\right\|_{L^2(\widetilde{K}_j)}\right) \le C\,h^{s-1}\|v\|_{V^s_\beta(\widetilde{K}_j)}.
\end{aligned}$$

Finally, we sum over all elements and remark that the overlap of support extensions depends only on the polynomial degree p and is thus bounded with respect to h. We obtain

$$\left|v - \Pi_{V_h}^{\odot} v\right|^2_{H^q(\Omega_R)} = \sum_{K\in\mathcal{M}^\mu_R}\left|v - \Pi^{\odot}_{V_h} v\right|^2_{H^q(K)} \le C\,h^{2(s-q)}\sum_{K\in\mathcal{M}^\mu_R}\|v\|^2_{V^s_\beta(\widetilde{K}_j)} \le Ch^{2(s-q)}\|v\|^2_{V^s_\beta(\widetilde{\Omega}_R)}$$

for $q \in \{0,1\}$ and the assertion follows. □

5.2.2. Estimates on Ω_C

Next, we analyze the projection error on the small polar domain Ω_C that is surrounding the polar point. Therefore, we adopt the proof strategy from [52], where a similar error estimate has been shown for interpolation with linear finite elements. The radial size of the corresponding parametric strip $\widehat{\Omega}_C$ will be denoted by $h_{1,\widehat{\Omega}_C} = \zeta_{1,p_1+2}$ such that $\widehat{\Omega}_C = \left(0, h_{1,\widehat{\Omega}_C}\right] \times (0,1)$, recall (5.2).

Theorem 5.3. *Let $q \in \{0,1\}$, $s \in \mathbb{N}$ with $2 \le s \le p+1$ and $v \in V^s(\widetilde{\Omega}_C)$. Then, there exists a positive constant C depending only on $p, \theta, \boldsymbol{F}, W$ such that*

$$\left|v - \Pi_{V_h}^{\odot} v\right|_{H^q(\Omega_C)} \le C h^{s-q}_{1,\widehat{\Omega}_C}\|v\|_{V^s(\widetilde{\Omega}_C)},$$

with $\widetilde{\Omega}_C$ as defined in (5.3).

Proof. Similar to the proof of Theorem 5.2, we transform the projection error to the polar coordinate system as illustrated in Section 4.2.4. For $q = 0$, we thus have

$$\left\|v - \Pi_{V_h}^{\odot} v\right\|^2_{L^2(\Omega_C)} \le C\left\|W\widehat{v} - \Pi^{\widehat{\Gamma}}_{p,\Xi}(W\widehat{v})\right\|^2_{\mathcal{L}^2_{1/2}(\widehat{\Omega}_C)},$$

and for $q = 1$, it follows

$$\begin{aligned}
\left|v - \Pi_{V_h}^{\odot} v\right|^2_{H^1(\Omega_C)} &\le C\left(\left\|\widehat{\partial}_1\left(W\widehat{v} - \Pi^{\widehat{\Gamma}}_{p,\Xi}(W\widehat{v})\right)\right\|^2_{\mathcal{L}^2_{1/2}(\widehat{\Omega}_C)} + \left\|W\widehat{v} - \Pi^{\widehat{\Gamma}}_{p,\Xi}(W\widehat{v})\right\|^2_{\mathcal{L}^2_{1/2}(\widehat{\Omega}_C)}\right. &(5.10)\\
&\left. + \left\|\widehat{\partial}_2\left(W\widehat{v} - \Pi^{\widehat{\Gamma}}_{p,\Xi}(W\widehat{v})\right)\right\|^2_{\mathcal{L}^2_{-1/2}(\widehat{\Omega}_C)} + \left\|W\widehat{v} - \Pi^{\widehat{\Gamma}}_{p,\Xi}(W\widehat{v})\right\|^2_{\mathcal{L}^2_{-1/2}(\widehat{\Omega}_C)}\right). &(5.11)
\end{aligned}$$

However, in contrast to Theorem 5.2, where the projection error on Ω_R is considered, the Jacobian of the inverse of the polar parameterization $\boldsymbol{F}$ is not bounded on Ω_C, see (3.7). In the following Lemmata 5.5–5.7, we will thus show that each of the weighted error terms is bounded by the bent polar Sobolev norm of v introduced in Section 4.2.3. With Eq. (4.21) and the transformation (4.20) back to the physical domain, we obtain the assertion,

$$\left|v - \Pi_{V_h}^{\odot} v\right|_{H^q(\Omega_C)} \le C h^{s-q}_{1,\widehat{\Omega}_C}\|\widehat{v}\|_{H^s_\odot\left(\widetilde{\widehat{\Omega}}_C\right)} \le C h^{s-q}_{1,\widehat{\Omega}_C}\|\widehat{v}\|_{\mathcal{V}^s_\odot\left(\widetilde{\widehat{\Omega}}_C\right)} \le C h^{s-q}_{1,\widehat{\Omega}_C}\|v\|_{V^s(\widetilde{\Omega}_C)},$$

where $\widetilde{\widehat{\Omega}}_C$ and $\widetilde{\Omega}_C$ are defined as in (5.3). □

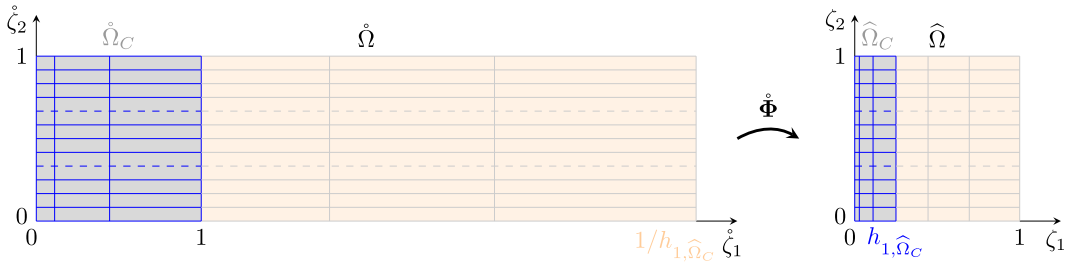

Fig. 6. Illustration of the scaling transformation $\mathring{\mathbf{\Phi}}$ with the reference domains $\mathring{\Omega}$ and $\mathring{\Omega}_C$ and the corresponding parametric domains $\widehat{\Omega}$ and $\widehat{\Omega}_C$.

An essential ingredient for the following estimates is the bijective scaling transformation between the parametric domain $\widehat{\Omega}$ and the reference domain $\mathring{\Omega} := (0, 1/h_{1,\widehat{\Omega}_C}) \times (0, 1)$, given by

$$\mathring{\mathbf{\Phi}} : \mathring{\Omega} \to \widehat{\Omega}, \quad \mathring{\mathbf{\Phi}}(\mathring{\zeta}_1, \mathring{\zeta}_2) = \begin{pmatrix} h_{1,\widehat{\Omega}_C} \mathring{\zeta}_1 \\ \mathring{\zeta}_2 \end{pmatrix} = \begin{pmatrix} \zeta_1 \\ \zeta_2 \end{pmatrix}. \tag{5.12}$$

In this way, the size of the reference domain corresponding to the parametric strip $\widehat{\Omega}_C$, namely

$$\mathring{\Omega}_C := \mathring{\mathbf{\Phi}}^{-1}\left(\widehat{\Omega}_C\right) = (0, 1)^2,$$

is independent of the global mesh size h, and a typical scaling argument can be applied. The transformation and reference domains are illustrated visually in Fig. 6. Any quantity that is transformed to the reference domain will be marked accordingly with a circle on top, e.g. $\mathring{v} = \widehat{v} \circ \mathring{\mathbf{\Phi}}$, and will be called the corresponding reference quantity or scaled quantity. Similarly, we denote the derivatives of a scaled function $\mathring{v} : \mathring{\Omega} \to \mathbb{R}$ by

$$\mathring{D}^{\boldsymbol{\alpha}} \mathring{v} := \frac{\partial^{\alpha_1}}{\partial \mathring{\zeta}_1^{\alpha_1}} \frac{\partial^{\alpha_2} \mathring{v}}{\partial \mathring{\zeta}_2^{\alpha_2}} \quad \text{and} \quad \mathring{\partial}_1 \mathring{v} = \frac{\partial \mathring{v}}{\partial \mathring{\zeta}_1}, \; \mathring{\partial}_2 \mathring{v} = \frac{\partial \widehat{v}}{\partial \mathring{\zeta}_2}, \; \mathring{\partial}_{11} \mathring{v} = \frac{\partial^2 \mathring{v}}{\partial \mathring{\zeta}_1^2}, \; \ldots.$$

Moreover, we define the reference domain of the extended parametric strip $\widetilde{\widehat{\Omega}}_C$, recall (5.3), by

$$\widetilde{\mathring{\Omega}}_C := \mathring{\mathbf{\Phi}}^{-1}\left(\widetilde{\widehat{\Omega}}_C\right) = \left(0, h_{1,\widetilde{\widehat{\Omega}}_C} \big/ h_{1,\widehat{\Omega}_C}\right) \times (0, 1),$$

which is displayed in the top row of Fig. 7. Its size is also independent of the mesh size, since the relation $h_{1,\widetilde{\widehat{\Omega}}_C}/h_{1,\widehat{\Omega}_C} \sim 1$ holds due to the local quasi-uniformity of the mesh, recall Lemma 3.18. Finally, we introduce the corresponding physical reference domains, which are obtained using the transformation

$$\breve{\mathbf{\Phi}} : \breve{\Omega} \to \Omega, \quad \breve{\mathbf{\Phi}}(\breve{x}, \breve{y}) = \begin{pmatrix} h_{1,\widehat{\Omega}_C} \breve{x} \\ h_{1,\widehat{\Omega}_C} \breve{y} \end{pmatrix} = \begin{pmatrix} x \\ y \end{pmatrix}, \tag{5.13}$$

with $\breve{\Omega} := \breve{\mathbf{\Phi}}^{-1}(\Omega)$, as illustrated in the bottom row of Fig. 7. Similarly to the parametric reference configuration, the sizes of $\breve{\Omega}_C := \breve{\mathbf{\Phi}}^{-1}(\Omega_C)$ and $\widetilde{\breve{\Omega}}_C := \breve{\mathbf{\Phi}}^{-1}\left(\widetilde{\Omega}_C\right)$ are independent of h. Any scaled quantity will be marked accordingly with a breve on top.

We start with a stability result for the scaled version of the quasi-interpolant defined in (2.17), which will be used more often in the remainder of this section.

Lemma 5.4. *Let either $\mathring{v} \in \widehat{H}^s_{1/2}\left(\widetilde{\mathring{\Omega}}_C\right)$ or $\mathring{v} \in \mathcal{H}^s_{1/2}\left(\widetilde{\mathring{\Omega}}_C\right)$ for $s \geq 2$. Then, it holds*

$$\left\| \mathring{\partial}_1^q \left(\mathring{\Pi}^{\widehat{\Gamma}}_{p,\Xi} \mathring{v} \right) \right\|^2_{\widehat{L}^2_{1/2}(\mathring{\Omega}_C)} \leq C \|\mathring{v}\|^2_{\widehat{H}^s_{1/2}\left(\widetilde{\mathring{\Omega}}_C\right)} \quad \text{or} \quad \left\| \mathring{\partial}_1^q \left(\mathring{\Pi}^{\widehat{\Gamma}}_{p,\Xi} \mathring{v} \right) \right\|^2_{L^2_{1/2}(\mathring{\Omega}_C)} \leq C \|\mathring{v}\|^2_{\mathcal{H}^s_{1/2}\left(\widetilde{\mathring{\Omega}}_C\right)},$$

respectively, for $q \in \{0, 1\}$.

Proof. Let $q \in \{0, 1\}$ and $\mathring{v} \in \widehat{H}^s_{1/2}\left(\widetilde{\mathring{\Omega}}_C\right)$. By using the representation (2.18) of $\mathring{\Pi}^{\widehat{\Gamma}}_{p,\Xi}$ and the stability property of the dual functionals [33, Theorem 4.41], we compute

$$\begin{aligned} \left\| \mathring{\partial}_1^q \left(\mathring{\Pi}^{\widehat{\Gamma}}_{p,\Xi} \mathring{v} \right) \right\|^2_{\widehat{L}^2_{1/2}(\mathring{\Omega}_C)} &= \int_{\mathring{\Omega}_C} \left| \mathring{\partial}_1^q \left(\sum_{i \in I} \mathring{\lambda}^{\widehat{\Gamma}}_{i,p}(\mathring{v}) \mathring{B}_{i,p} \right) \right|^2 \mathring{\zeta}_1 \, \mathrm{d}\mathring{\zeta}_1 \, \mathrm{d}\mathring{\zeta}_2 \leq \int_{\mathring{\Omega}_C} \left(\sum_{i \in I} \left| \mathring{\lambda}^{\widehat{\Gamma}}_{i,p}(\mathring{v}) \, \mathring{\partial}_1^q \mathring{B}_{i,p} \right| \right)^2 \mathring{\zeta}_1 \, \mathrm{d}\mathring{\zeta}_1 \, \mathrm{d}\mathring{\zeta}_2 \\ &\leq \int_{\mathring{\Omega}_C} \left(\sum_{i \in I} C \|\mathring{v}\|_{L^\infty\left(\widetilde{\mathring{\Omega}}_C\right)} \left| \mathring{\partial}_1^q \mathring{B}_{i,p} \right| \right)^2 \mathring{\zeta}_1 \, \mathrm{d}\mathring{\zeta}_1 \, \mathrm{d}\mathring{\zeta}_2 \leq C \|\mathring{v}\|^2_{C^0\left(\widetilde{\mathring{\Omega}}_C\right)} \int_{\mathring{\Omega}_C} \left(\sum_{i \in I} \left| \mathring{\partial}_1^q \mathring{B}_{i,p} \right| \right)^2 \mathring{\zeta}_1 \, \mathrm{d}\mathring{\zeta}_1 \, \mathrm{d}\mathring{\zeta}_2. \end{aligned}$$

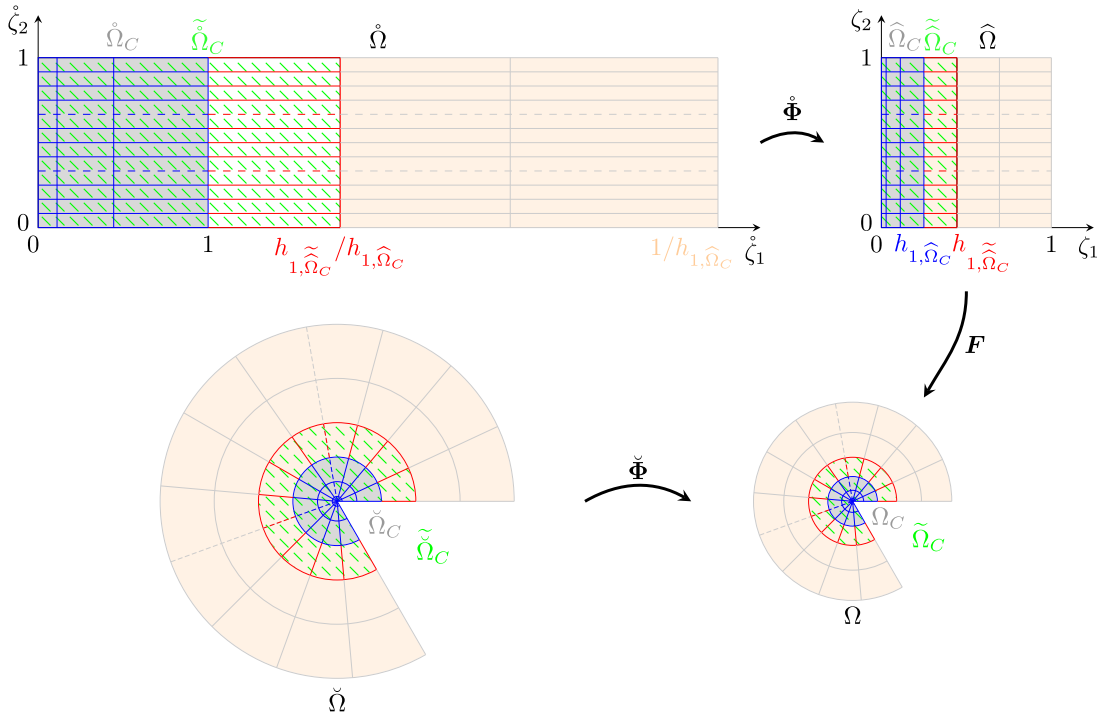

Fig. 7. First row: Illustration of the parametric scaling transformation (5.12), with the extended parametric strip $\widetilde{\widehat{\Omega}}_C$ and the corresponding reference domain $\widetilde{\mathring{\Omega}}_C$ being hatched in green. Second row: Illustration of the physical scaling transformation (5.13), with the extended small polar domain $\widetilde{\Omega}_C$ and the corresponding reference domain $\widetilde{\breve{\Omega}}_C$ being hatched in green. (For interpretation of the references to colour in this figure legend, the reader is referred to the web version of this article.)

The diameter of the reference domain $\mathring{\Omega}_C$ does not depend on the mesh size, and we have the embedding $\widehat{H}^s_{1/2}\big(\widetilde{\mathring{\Omega}}_C\big) \hookrightarrow C^0\Big(\overline{\widetilde{\mathring{\Omega}}_C}\Big)$, see [6, Theorem 4.7]. Hence, we obtain

$$\Big\|\mathring{\partial}_1^q\Big(\mathring{\Pi}^{\widehat{\Gamma}}_{p,\Xi}\mathring{v}\Big)\Big\|^2_{\widehat{L}^2_{1/2}(\mathring{\Omega}_C)} \le C\|\mathring{v}\|^2_{C^0\left(\overline{\widetilde{\mathring{\Omega}}_C}\right)} \int_{\mathring{\Omega}_C} 1\,\mathrm{d}\mathring{\zeta}_1\,\mathrm{d}\mathring{\zeta}_2 \le C\|\mathring{v}\|^2_{C^0\left(\overline{\widetilde{\mathring{\Omega}}_C}\right)} \le C\|\mathring{v}\|^2_{\widehat{H}^s_{1/2}\left(\widetilde{\mathring{\Omega}}_C\right)}.$$

To prove the assertion for bent Sobolev norms, we simply apply the estimate above on every mesh element and sum over all elements. □

Now, we estimate the two terms in line (5.10), that is, the projection error and its first parametric derivative in the $\mathcal{L}^2_{1/2}(\widehat{\Omega}_C)$-norm.

Lemma 5.5. *Let the assumptions of Theorem 5.3 hold. Then, for $q \in \{0,1\}$, it follows*

$$\Big\|\widehat{\partial}_1^q\Big(W\widehat{v} - \Pi^{\widehat{\Gamma}}_{p,\Xi}(W\widehat{v})\Big)\Big\|_{\mathcal{L}^2_{1/2}(\widehat{\Omega}_C)} \le C h^{s-q}_{1,\widehat{\Omega}_C} \|\widehat{v}\|_{\mathcal{H}^s_{\odot}\left(\widetilde{\widehat{\Omega}}_C\right)}.$$

Proof. First, we apply a typical scaling argument using the reference configuration introduced above and, to simplify notation, we set $\mathring{v} = \mathring{W}\mathring{v}$. We obtain

$$\begin{aligned}
\Big\|\widehat{\partial}_1^q\Big(W\widehat{v} - \Pi^{\widehat{\Gamma}}_{p,\Xi}(W\widehat{v})\Big)\Big\|_{\mathcal{L}^2_{1/2}(\widehat{\Omega}_C)} &= \left(\int_{\widehat{\Omega}_C} \Big(\widehat{\partial}_1^q\Big(W\widehat{v} - \Pi^{\widehat{\Gamma}}_{p,\Xi}(W\widehat{v})\Big)\Big)^2 \zeta_1\,\mathrm{d}\boldsymbol{\zeta}\right)^{1/2} \\
&= \left(\int_{\mathring{\Omega}_C} \left(\frac{\mathring{\partial}_1^q\Big(\mathring{W}\mathring{v} - \mathring{\Pi}^{\widehat{\Gamma}}_{p,\Xi}(\mathring{W}\mathring{v})\Big)}{h^q_{1,\widehat{\Omega}_C}}\right)^2 h_{1,\widehat{\Omega}_C}\,\mathring{\zeta}_1\,h_{1,\widehat{\Omega}_C}\,\mathrm{d}\mathring{\zeta}_1\,\mathrm{d}\mathring{\zeta}_2\right)^{1/2} \\
&= h^{1-q}_{1,\widehat{\Omega}_C} \Big\|\mathring{\partial}_1^q\Big(\mathring{v} - \mathring{\Pi}^{\widehat{\Gamma}}_{p,\Xi}\mathring{v}\Big)\Big\|_{\mathcal{L}^2_{1/2}(\mathring{\Omega}_C)}.
\end{aligned} \tag{5.14}$$

In the rest of the paper, such estimates will be used more often. The underlying steps will not be carried out in detail anymore, but we will refer to it as scaling argument.

Next, let $\mathcal{P}_{s-1}$ be the space of piecewise polynomials up to degree $s-1$ on $\mathring{\Omega}_C$ and $\mathring{\Pi}$ be the scaled projector from the bent Sobolev space to the spline space of degree $s-1$ that satisfies property (4.22). Due to Lemma 5.4, we have

$$\begin{aligned}\left\|\mathring{\partial}_1^q\left(\mathring{v}-\mathring{\Pi}\mathring{\Pi}^{\widehat{\Gamma}}_{\boldsymbol{p},\boldsymbol{\Xi}}\mathring{v}\right)\right\|_{\mathcal{L}^2_{1/2}(\mathring{\Omega}_C)} &= \inf_{\mathring{w}\in\mathcal{P}_{s-1}}\left\|\mathring{\partial}_1^q\left(\mathring{v}-\mathring{\Pi}(\mathring{v})-\mathring{w}-\mathring{\Pi}\mathring{\Pi}^{\widehat{\Gamma}}_{\boldsymbol{p},\boldsymbol{\Xi}}(\mathring{v}-\mathring{\Pi}(\mathring{v})-\mathring{w})\right)\right\|_{\mathcal{L}^2_{1/2}(\mathring{\Omega}_C)}\\ &\le \inf_{\mathring{w}\in\mathcal{P}_{s-1}}\left(\left\|\mathring{\partial}_1^q\left(\mathring{v}-\mathring{\Pi}(\mathring{v})-\mathring{w}\right)\right\|_{\mathcal{L}^2_{1/2}(\mathring{\Omega}_C)}+\left\|\mathring{\partial}_1^q\left(\mathring{\Pi}\mathring{\Pi}^{\widehat{\Gamma}}_{\boldsymbol{p},\boldsymbol{\Xi}}(\mathring{v}-\mathring{\Pi}(\mathring{v})-\mathring{w})\right)\right\|_{\mathcal{L}^2_{1/2}(\mathring{\Omega}_C)}\right)\\ &\le C\inf_{\mathring{w}\in\mathcal{P}_{s-1}}\left\|\mathring{v}-\mathring{\Pi}(\mathring{v})-\mathring{w}\right\|_{\mathcal{H}^s_{1/2}\left(\widetilde{\mathring{\Omega}}_C\right)} = \inf_{\mathring{w}\in\mathcal{P}_{s-1}}\left\|\mathring{v}-\mathring{\Pi}(\mathring{v})-\mathring{w}\right\|_{\widehat{H}^s_{1/2}\left(\widetilde{\mathring{\Omega}}_C\right)}.\end{aligned}$$

Then, we apply the weighted Deny-Lions-type argument [6, Theorem 4.6],

$$\inf_{\mathring{w}\in\mathcal{P}_{s-1}}\|\mathring{z}-\mathring{w}\|_{\widehat{H}^s_{1/2}\left(\widetilde{\mathring{\Omega}}_C\right)} \le C|\mathring{z}|_{\widehat{H}^s_{1/2}\left(\widetilde{\mathring{\Omega}}_C\right)} \tag{5.15}$$

for $\mathring{z}=\mathring{v}-\mathring{\Pi}(\mathring{v})\in\widehat{H}^s_{1/2}\left(\widetilde{\mathring{\Omega}}_C\right)$. Finally, we combine all the steps and use again the definition of $\mathring{\Pi}$, a scaling argument, the embedding (4.21) and the Leibniz formula (4.25) to compute

$$\begin{aligned}\left\|\widehat{\partial}_1^q\left(W\widehat{v}-\Pi^{\widehat{\Gamma}}_{\boldsymbol{p},\boldsymbol{\Xi}}(W\widehat{v})\right)\right\|_{\widehat{L}^2_{1/2}(\widehat{\Omega}_C)} &\le Ch^{1-q}_{1,\widehat{\Omega}_C}\inf_{\mathring{w}\in\mathcal{P}_{s-1}}\left\|\mathring{v}-\mathring{\Pi}(\mathring{v})-\mathring{w}\right\|_{\widehat{H}^s_{1/2}\left(\widetilde{\mathring{\Omega}}_C\right)} \le Ch^{1-q}_{1,\widehat{\Omega}_C}\left|\mathring{v}-\mathring{\Pi}(\mathring{v})\right|_{\widehat{H}^s_{1/2}\left(\widetilde{\mathring{\Omega}}_C\right)}\\ &= Ch^{1-q}_{1,\widehat{\Omega}_C}|\mathring{v}|_{\mathcal{H}^s_{1/2}\left(\widetilde{\mathring{\Omega}}_C\right)} \le Ch^{s-q}_{1,\widehat{\Omega}_C}|W\widehat{v}|_{\mathcal{H}^s_{1/2}\left(\widetilde{\mathring{\Omega}}_C\right)} \le Ch^{s-q}_{1,\widehat{\Omega}_C}\|\widehat{v}\|_{\mathcal{H}^s_{\circledcirc}\left(\widetilde{\mathring{\Omega}}_C\right)},\end{aligned}$$

and the demonstration is complete. □

In the proof of Lemma 5.5, the projector $\mathring{\Pi}$ that satisfies property (4.22) was only inserted for the interplay between bent Sobolev norms and their non-bent counterparts, recall Section 4.2.3. This adds a further technicality to the proof, which is not in the scope of this paper, and has already been investigated in detail in standard approximation literature [28]. For the sake of simplicity, we will not elaborate this argument anymore in the rest of our paper and, without loss of generality, we will assume that pull-backs of functions are sufficiently smooth across mesh lines. The generalization can always be done by inserting the projector $\mathring{\Pi}$ at the correct places, as shown in the demonstration of Lemma 5.5.

To continue the proof of Theorem 5.3, we estimate the first term in line (5.11) in the next lemma.

Lemma 5.6. *Let the assumptions of Theorem 5.3 hold. Then, it follows*

$$\left\|\widehat{\partial}_2\left(W\widehat{v}-\Pi^{\widehat{\Gamma}}_{\boldsymbol{p},\boldsymbol{\Xi}}(W\widehat{v})\right)\right\|_{\widehat{L}^2_{-1/2}(\widehat{\Omega}_C)} \le Ch^{s-1}_{1,\widehat{\Omega}_C}\|\widehat{v}\|_{\mathcal{H}^s_{\circledcirc}\left(\widetilde{\widehat{\Omega}}_C\right)}.$$

Proof. Let $c\in\mathbb{R}$ such that $\widehat{v}(0,\cdot)=v\circ\boldsymbol{F}(0,\cdot)=v(\boldsymbol{P})=c$. We define the auxiliary function $\widehat{v}_0=\widehat{v}-c\,\widehat{B}_{1,p_1}$, which satisfies $(W\widehat{v}_0)(0,\cdot)=(W\widehat{v})(0,\cdot)-cW\widehat{B}_{1,p_1}(0)=0$. Moreover, we have

$$\Pi^{\widehat{\Gamma}}_{\boldsymbol{p},\boldsymbol{\Xi}}(W\widehat{v}_0)=\Pi^{\widehat{\Gamma}}_{\boldsymbol{p},\boldsymbol{\Xi}}(W\widehat{v})-\Pi^{\widehat{\Gamma}}_{\boldsymbol{p},\boldsymbol{\Xi}}(cWB_{1,p_1})=\Pi^{\widehat{\Gamma}}_{\boldsymbol{p},\boldsymbol{\Xi}}(W\widehat{v})-cWB_{1,p_1}$$

and it follows $W\widehat{v}_0-\Pi^{\widehat{\Gamma}}_{\boldsymbol{p},\boldsymbol{\Xi}}(W\widehat{v}_0)=W\widehat{v}-\Pi^{\widehat{\Gamma}}_{\boldsymbol{p},\boldsymbol{\Xi}}(W\widehat{v})$ and $\Pi^{\widehat{\Gamma}}_{\boldsymbol{p},\boldsymbol{\Xi}}(W\widehat{v}_0)(0,\cdot)=0$. Using a scaling argument and the notation $\mathring{v}_0=\mathring{W}\mathring{v}_0$, we compute

$$\begin{aligned}\left\|\widehat{\partial}_2\left(W\widehat{v}-\Pi^{\widehat{\Gamma}}_{\boldsymbol{p},\boldsymbol{\Xi}}(W\widehat{v})\right)\right\|_{\widehat{L}^2_{-1/2}(\widehat{\Omega}_C)} &= \left\|\widehat{\partial}_2\left(W\widehat{v}_0-\Pi^{\widehat{\Gamma}}_{\boldsymbol{p},\boldsymbol{\Xi}}(W\widehat{v}_0)\right)\right\|_{\widehat{L}^2_{-1/2}(\widehat{\Omega}_C)}\\ &\le \left\|\widehat{\partial}_2(W\widehat{v}_0)\right\|_{\widehat{L}^2_{-1/2}(\widehat{\Omega}_C)}+\left\|\widehat{\partial}_2\left(\Pi^{\widehat{\Gamma}}_{\boldsymbol{p},\boldsymbol{\Xi}}(W\widehat{v}_0)\right)\right\|_{\widehat{L}^2_{-1/2}(\widehat{\Omega}_C)}\\ &\le \left\|\mathring{\partial}_2\mathring{v}_0\right\|_{\widehat{L}^2_{-1/2}(\mathring{\Omega}_C)}+\left\|\mathring{\partial}_2\left(\mathring{\Pi}\mathring{\Pi}^{\widehat{\Gamma}}_{\boldsymbol{p},\boldsymbol{\Xi}}\mathring{v}_0\right)\right\|_{\widehat{L}^2_{-1/2}(\mathring{\Omega}_C)},\end{aligned}$$

where all terms are well-defined despite the negative weight of the norms as the corresponding functions vanish for $\zeta_1=0$. In Lemma B.1, we show that the second derivative of our projector can be written as another projector, and in Lemma B.2, we estimate the corresponding norm. Hence, we obtain

$$\left\|\widehat{\partial}_2\left(W\widehat{v}-\Pi^{\widehat{\Gamma}}_{\boldsymbol{p},\boldsymbol{\Xi}}(W\widehat{v})\right)\right\|_{\widehat{L}^2_{-1/2}(\widehat{\Omega}_C)} \le C\left\|\mathring{\partial}_2\mathring{v}_0\right\|_{\widehat{L}^2_{-1/2}\left(\widetilde{\mathring{\Omega}}_C\right)} \le C\left\|\mathring{\partial}_2\mathring{v}_0\right\|_{\widehat{L}^2_{-1}\left(\widetilde{\mathring{\Omega}}_C\right)}.$$

It is shown in [6, Corollary 4.1] that, under the condition $\mathring{\partial}_2\mathring{v}_0(0,\cdot)=0$, the inequality

$$\left\|\mathring{\partial}_2\mathring{v}_0\right\|_{\widehat{L}^2_{-1}\left(\widetilde{\mathring{\Omega}}_C\right)} \le C\left|\mathring{\partial}_2\mathring{v}_0\right|_{\widehat{H}^1\left(\widetilde{\mathring{\Omega}}_C\right)}$$

holds. By a scaling argument, it follows

$$\begin{aligned}\left|\mathring{\partial}_2\mathring{v}_0\right|_{\hat{H}^1(\widetilde{\mathring{\Omega}}_C)} &\le C\left(\left\|\mathring{\partial}_{12}\mathring{v}_0\right\|_{\hat{L}^2(\widetilde{\mathring{\Omega}}_C)} + \left\|\mathring{\partial}_{22}\mathring{v}_0\right\|_{\hat{L}^2(\widetilde{\mathring{\Omega}}_C)}\right) \le C\left(\left\|\mathring{\partial}_{12}\mathring{v}_0\right\|_{\hat{L}^2_{-1/2}(\widetilde{\mathring{\Omega}}_C)} + \left\|\mathring{\partial}_{22}\mathring{v}_0\right\|_{\hat{L}^2_{-3/2}(\widetilde{\mathring{\Omega}}_C)}\right)\\ &\le Ch_{1,\hat{\Omega}_C}\left(\left\|\widehat{\partial}_{12}(W\widehat{v}_0)\right\|_{\hat{L}^2_{-1/2}(\widetilde{\widehat{\Omega}}_C)} + \left\|\widehat{\partial}_{22}(W\widehat{v}_0)\right\|_{\hat{L}^2_{-3/2}(\widetilde{\widehat{\Omega}}_C)}\right) \le Ch_{1,\hat{\Omega}_C}\|\widehat{v}\|_{\mathcal{H}^2_{\odot}(\widetilde{\widehat{\Omega}}_C)},\end{aligned}$$

which yields the assertion for $s = 2$. For higher regularity $s \ge 3$, the proof needs to be adapted. We rewrite the error in terms of the projector $\mathring{\Pi}^{\hat{\Gamma},\mathring{\partial}_2}_{\boldsymbol{p},\Xi}$ derived in Lemma B.1, and compute

$$\begin{aligned}\left\|\widehat{\partial}_2\left(W\widehat{v} - \Pi^{\hat{\Gamma}}_{\boldsymbol{p},\Xi}(W\widehat{v})\right)\right\|_{\hat{L}^2_{-1/2}(\widehat{\Omega}_C)} &= \left\|\mathring{\partial}_2\left(\mathring{v}_0 - \mathring{\Pi}^{\hat{\Gamma}}_{\boldsymbol{p},\Xi}\mathring{v}_0\right)\right\|_{\hat{L}^2_{-1/2}(\mathring{\Omega}_C)} = \left\|\mathring{\partial}_2\mathring{v}_0 - \mathring{\Pi}^{\hat{\Gamma},\mathring{\partial}_2}_{(p_1,p_2-1),\Xi}\left(\widehat{\partial}_2\mathring{v}_0\right)\right\|_{\hat{L}^2_{-1/2}(\mathring{\Omega}_C)}\\ &\le C\left\|\mathring{\partial}_2\mathring{v}_0 - \mathring{\Pi}^{\hat{\Gamma},\mathring{\partial}_2}_{(p_1,p_2-1),\Xi}\left(\widehat{\partial}_2\mathring{v}_0\right)\right\|_{\hat{L}^2_{-1}(\mathring{\Omega}_C)}\\ &\le C\left|\mathring{\partial}_2\mathring{v}_0 - \mathring{\Pi}^{\hat{\Gamma},\mathring{\partial}_2}_{(p_1,p_2-1),\Xi}\left(\widehat{\partial}_2\mathring{v}_0\right)\right|_{\hat{H}^1(\mathring{\Omega}_C)}\\ &= C\inf_{\mathring{w}\in\mathcal{P}_{s-2}}\left|\mathring{\partial}_2\mathring{v}_0 - \mathring{w} + \mathring{\Pi}^{\hat{\Gamma},\mathring{\partial}_2}_{(p_1,p_2-1),\Xi}\left(\widehat{\partial}_2\mathring{v}_0 - \mathring{w}\right)\right|_{\hat{H}^1(\mathring{\Omega}_C)}\\ &\le C\inf_{\mathring{w}\in\mathcal{P}_{s-2}}\left(\left|\mathring{\partial}_2\mathring{v}_0 - \mathring{w}\right|_{\hat{H}^1(\mathring{\Omega}_C)} + \left|\mathring{\Pi}^{\hat{\Gamma},\mathring{\partial}_2}_{(p_1,p_2-1),\Xi}\left(\widehat{\partial}_2\mathring{v}_0 - \mathring{w}\right)\right|_{\hat{H}^1(\mathring{\Omega}_C)}\right)\\ &\le C\inf_{\mathring{w}\in\mathcal{P}_{s-2}}\left\|\mathring{\partial}_2\mathring{v}_0 - \mathring{w}\right\|_{\hat{H}^1(\widetilde{\mathring{\Omega}}_C)}.\end{aligned} \tag{5.16}$$

In the last step, we used the H^1-stability of the new projector $\mathring{\Pi}^{\hat{\Gamma},\mathring{\partial}_2}_{\boldsymbol{p},\Xi}$ which can be shown as in [28]. Finally, by applying the embedding $\hat{H}^{s-1}_{1/2}(\mathring{\Omega}_C) \hookrightarrow \hat{H}^1(\mathring{\Omega}_C)$ from [6, Remark 4.1], the Deny-Lions type estimate (5.15), a scaling argument and the relation (4.21), we obtain

$$\begin{aligned}\left\|\widehat{\partial}_2\left(W\widehat{v} - \Pi^{\hat{\Gamma}}_{\boldsymbol{p},\Xi}(W\widehat{v})\right)\right\|_{\hat{L}^2_{-1/2}(\widehat{\Omega}_C)} &\le C\inf_{\mathring{w}\in\mathcal{P}_{s-2}}\left\|\mathring{\partial}_2\mathring{v}_0 - \mathring{w}\right\|_{\hat{H}^{s-1}_{1/2}(\widetilde{\mathring{\Omega}}_C)} \le C\left|\mathring{\partial}_2\mathring{v}_0\right|_{\hat{H}^{s-1}_{1/2}(\widetilde{\mathring{\Omega}}_C)} \le C|\mathring{v}_0|_{\hat{H}^s_{1/2}(\widetilde{\mathring{\Omega}}_C)}\\ &\le Ch^{s-1}_{1,\hat{\Omega}_C}|W\widehat{v}_0|_{\hat{H}^s_{1/2}(\widetilde{\widehat{\Omega}}_C)} \le Ch^{s-1}_{1,\hat{\Omega}_C}\|\widehat{v}\|_{\mathcal{H}^s_{1/2}(\widetilde{\widehat{\Omega}}_C)} \le Ch^{s-1}_{1,\hat{\Omega}_C}\|\widehat{v}\|_{\mathcal{H}^s_{\odot}(\widetilde{\widehat{\Omega}}_C)},\end{aligned}$$

and the assertion is established. □

Finally, we estimate the last term in line (5.11).

Lemma 5.7. *Let the assumptions of Theorem 5.3 hold. Then, it follows*

$$\left\|W\widehat{v} - \Pi^{\hat{\Gamma}}_{\boldsymbol{p},\Xi}(W\widehat{v})\right\|_{\hat{L}^2_{-1/2}(\widehat{\Omega}_C)} \le Ch^{s-1}_{1,\hat{\Omega}_C}\|\widehat{v}\|_{\mathcal{H}^s_{\odot}(\widetilde{\widehat{\Omega}}_C)}.$$

Proof. As in the proof of Lemma 5.6, we use again the auxiliary functions $\widehat{v}_0 = \widehat{v} - c\widehat{B}_{1,p_1}$ and set $\mathring{v}_0 = \mathring{W}\mathring{v}_0$. A scaling argument yields

$$\left\|W\widehat{v} - \Pi^{\hat{\Gamma}}_{\boldsymbol{p},\Xi}(W\widehat{v})\right\|_{\hat{L}^2_{-1/2}(\widehat{\Omega}_C)} = \left\|W\widehat{v}_0 - \Pi^{\hat{\Gamma}}_{\boldsymbol{p},\Xi}(W\widehat{v}_0)\right\|_{\hat{L}^2_{-1/2}(\widehat{\Omega}_C)} = \left\|\mathring{v}_0 - \mathring{\Pi}^{\hat{\Gamma}}_{\boldsymbol{p},\Xi}\mathring{v}_0\right\|_{\hat{L}^2_{-1/2}(\mathring{\Omega}_C)}.$$

Then, due to the H^1-stability of $\mathring{\Pi}^{\hat{\Gamma}}_{\boldsymbol{p},\Xi}$, we can show similar to (5.16) that

$$\left\|\mathring{v}_0 - \mathring{\Pi}^{\hat{\Gamma}}_{\boldsymbol{p},\Xi}\mathring{v}_0\right\|_{\hat{L}^2_{-1/2}(\mathring{\Omega}_C)} \le C\inf_{\mathring{w}\in\mathcal{P}_{s-1}}\left\|\mathring{v}_0 - \mathring{w}\right\|_{\hat{H}^1(\widetilde{\mathring{\Omega}}_C)}.$$

With the embedding $\hat{H}^s_{1/2}(\mathring{\Omega}_C) \hookrightarrow \hat{H}^1(\mathring{\Omega}_C)$ for $s \ge 2$, see [6, Remark 4.1], the Deny-Lions type estimate (5.15), another scaling argument and the relation (4.21), it follows

$$\left\|\mathring{v}_0 - \mathring{\Pi}^{\hat{\Gamma}}_{\boldsymbol{p},\Xi}\mathring{v}_0\right\|_{\hat{L}^2_{-1/2}(\mathring{\Omega}_C)} \le C\inf_{\mathring{w}\in\mathcal{P}_{s-1}}\left\|\mathring{v}_0 - \mathring{w}\right\|_{\hat{H}^s_{1/2}(\widetilde{\mathring{\Omega}}_C)} \le C|\mathring{v}_0|_{\hat{H}^s_{1/2}(\widetilde{\mathring{\Omega}}_C)} \le Ch^{s-1}_{1,\hat{\Omega}_C}|W\widehat{v}_0|_{\hat{H}^s_{1/2}(\widetilde{\widehat{\Omega}}_C)} \le Ch^{s-1}_{1,\hat{\Omega}_C}\|\widehat{v}\|_{\mathcal{H}^s_{\odot}(\widetilde{\widehat{\Omega}}_C)}$$

and the proof is complete. □

Recall that by proving Lemmata 5.5–5.7, the proof of Theorem 5.3 is complete. For now, we have assumed that $v \in V^s(\widetilde{\Omega}_C)$. However, as seen in Section 3.2, this is generally not the case for solutions of PDEs on polar domains with corners. Therefore, we show a corresponding result to Theorem 5.3 for functions with reduced regularity by moving to a weighted function space setting.

Theorem 5.8. *Let $q \in \{0,1\}$ and $s \in \mathbb{N}$ with $2 \le s \le p+1$. Further, let $v \in V^s_\beta(\widetilde{\Omega}_C)$ for all $\beta \in \mathbb{R}$ with $s-1-\nu < \beta < s-1$. Then, there is a positive constant C, depending only on p, θ, F, W, such that*

$$\left| v - \Pi^{\odot}_{V_h} v \right|_{H^q(\Omega_C)} \le C h^{s-q-\beta}_{1,\widehat{\Omega}_C} \|v\|_{V^s_\beta(\widetilde{\Omega}_C)},$$

with $\widetilde{\Omega}_C$ as defined in (5.3).

Proof. Just as in the proof of Theorem 5.3, we estimate the four error terms of the sum in (5.10) and (5.11). First, we adapt the stability result stated in Lemma 5.4, which is needed to estimate the first two terms. To this end, we use the embedding $H^s_\beta\left(\widetilde{\breve{\Omega}}_C\right) \hookrightarrow H^{s-\beta}\left(\widetilde{\breve{\Omega}}_C\right)$ from [51] on the physical scaled reference domain defined in (5.13), and combine it with the usual Sobolev embedding $H^{s-\beta}\left(\widetilde{\breve{\Omega}}_C\right) \hookrightarrow C^0\left(\overline{\widetilde{\breve{\Omega}}_C}\right)$ for $\beta < s-1$, see for instance [53]. Then, with the proof of Lemma 5.4, embedding (3.14) and transformation (4.18), we obtain

$$\left\| \mathring{\partial}^q_1 \left(\mathring{\Pi}^{\hat{\Gamma}}_{\boldsymbol{p},\boldsymbol{\Xi}} \mathring{v} \right) \right\|_{\hat{L}^2_{1/2}(\mathring{\widehat{\Omega}}_C)} \le C \|\mathring{v}\|_{C^0\left(\overline{\widetilde{\breve{\Omega}}_C}\right)} = C \|\breve{v}\|_{C^0\left(\overline{\widetilde{\breve{\Omega}}_C}\right)} \le C \|\breve{v}\|_{H^{s-\beta}\left(\widetilde{\breve{\Omega}}_C\right)} \le C \|\breve{v}\|_{H^s_\beta\left(\widetilde{\breve{\Omega}}_C\right)} \le C \|\breve{v}\|_{V^s_\beta\left(\widetilde{\breve{\Omega}}_C\right)} \le C \|\mathring{v}\|_{\hat{V}^s_{\odot,\beta}\left(\widetilde{\mathring{\Omega}}_C\right)}. \tag{5.17}$$

Moreover, we use transformation (4.18) and the embeddings $V^{s-\beta}\left(\widetilde{\breve{\Omega}}_C\right) \hookrightarrow V^1\left(\widetilde{\breve{\Omega}}_C\right)$ from [54, Lemma 2.29] and $V^s_\beta\left(\widetilde{\breve{\Omega}}_C\right) \hookrightarrow V^{s-\beta}\left(\widetilde{\breve{\Omega}}_C\right)$ from [51], where $s-\beta > 1$ is required, to show that

$$\|\mathring{v}\|_{\hat{V}^1_{\odot}\left(\widetilde{\mathring{\Omega}}_C\right)} \le C \|\breve{v}\|_{V^1\left(\widetilde{\breve{\Omega}}_C\right)} \le C \|\breve{v}\|_{V^{s-\beta}\left(\widetilde{\breve{\Omega}}_C\right)} \le C \|\breve{v}\|_{V^s_\beta\left(\widetilde{\breve{\Omega}}_C\right)} \le C \|\mathring{v}\|_{\hat{V}^s_{\odot,\beta}\left(\widetilde{\mathring{\Omega}}_C\right)}. \tag{5.18}$$

By the scaling argument (5.14) and the estimates (5.17), (4.19) and (5.18), it follows

$$\begin{aligned}
\left\| \hat{\partial}^q_1 \left(W \hat{v} - \Pi^{\hat{\Gamma}}_{\boldsymbol{p},\boldsymbol{\Xi}}(W\hat{v}) \right) \right\|_{\hat{L}^2_{1/2}(\hat{\Omega}_C)} &\le C h^{1-q}_{1,\widehat{\Omega}_C} \left\| \mathring{\partial}^q_1 \left(\mathring{v} - \mathring{\Pi}^{\hat{\Gamma}}_{\boldsymbol{p},\boldsymbol{\Xi}} \mathring{v} \right) \right\|_{\hat{L}^2_{1/2}(\mathring{\widehat{\Omega}}_C)} \\
&\le C h^{1-q}_{1,\widehat{\Omega}_C} \left(\|\mathring{v}\|_{\hat{H}^1_{1/2}(\mathring{\widehat{\Omega}}_C)} + \left\| \mathring{\partial}^q_1 \left(\mathring{\Pi}^{\hat{\Gamma}}_{\boldsymbol{p},\boldsymbol{\Xi}} \mathring{v} \right) \right\|_{\hat{L}^2_{1/2}(\mathring{\widehat{\Omega}}_C)} \right) \\
&\le C h^{1-q}_{1,\widehat{\Omega}_C} \left(\|\mathring{v}\|_{\hat{V}^1_{\odot}\left(\widetilde{\mathring{\Omega}}_C\right)} + \|\mathring{v}\|_{\hat{V}^s_{\odot,\beta}\left(\widetilde{\mathring{\Omega}}_C\right)} \right) \\
&\le C h^{1-q}_{1,\widehat{\Omega}_C} \|\mathring{v}\|_{\hat{V}^s_{\odot,\beta}\left(\widetilde{\mathring{\Omega}}_C\right)} \le C h^{s-q-\beta}_{1,\widehat{\Omega}_C} \|\hat{v}\|_{\mathcal{V}^s_{\odot,\beta}\left(\widetilde{\hat{\Omega}}_C\right)}.
\end{aligned}$$

Note that the V-spaces scale perfectly, which was exploited in the last line above in combination with the Leibniz formula (4.25). Next, we adapt the proof of Lemma 5.6. Let $\hat{v}_0$ be the auxiliary function defined there such that $\hat{v}_0(0,\cdot) = 0$ and let $\mathring{v}_0 = \mathring{W} \mathring{v}_0$ be the corresponding scaling, recall (5.12). By combining Lemmata B.1 and B.2, the definition of polar weighted Sobolev norms and (5.18), we obtain

$$\begin{aligned}
\left\| \hat{\partial}_2 \left(W \hat{v} - \Pi^{\hat{\Gamma}}_{\boldsymbol{p},\boldsymbol{\Xi}}(W\hat{v}) \right) \right\|_{\hat{L}^2_{-1/2}(\hat{\Omega}_C)} &= \left\| \mathring{\partial}_2 \left(\mathring{v}_0 - \mathring{\Pi}^{\hat{\Gamma}}_{\boldsymbol{p},\boldsymbol{\Xi}} \mathring{v}_0 \right) \right\|_{\hat{L}^2_{-1/2}(\mathring{\widehat{\Omega}}_C)} = \left\| \mathring{\partial}_2 \mathring{v}_0 - \mathring{\Pi}^{\hat{\Gamma},\mathring{\partial}_2}_{(p_1,p_2-1),\boldsymbol{\Xi}} (\hat{\partial}_2 \mathring{v}_0) \right\|_{\hat{L}^2_{-1/2}(\mathring{\widehat{\Omega}}_C)} \\
&\le C \left\| \mathring{\partial}_2 \mathring{v}_0 \right\|_{\hat{L}^2_{-1/2}\left(\widetilde{\mathring{\Omega}}_C\right)} \le C \|\mathring{v}_0\|_{\hat{V}^1_{\odot}\left(\widetilde{\mathring{\Omega}}_C\right)} \le C \|\mathring{v}_0\|_{\hat{V}^s_{\odot,\beta}\left(\widetilde{\mathring{\Omega}}_C\right)} \\
&\le C h^{s-1-\beta}_{1,\widehat{\Omega}_C} \|\hat{v}\|_{\mathcal{V}^s_{\odot,\beta}\left(\widetilde{\hat{\Omega}}_C\right)},
\end{aligned}$$

where, in the last step, we used again the perfect scaling of V-spaces.

Finally, the proof of Lemma 5.7 is modified analogously. Similar to Lemma B.2, stability of the projector $\mathring{\Pi}^{\hat{\Gamma}}_{\boldsymbol{p},\boldsymbol{\Xi}}$ in the $L^2_{-1/2}(\mathring{\widehat{\Omega}}_C)$-norm can be shown, and it follows

$$\left\| \mathring{v}_0 - \mathring{\Pi}^{\hat{\Gamma}}_{\boldsymbol{p},\boldsymbol{\Xi}} \mathring{v}_0 \right\|_{\hat{L}^2_{-1/2}(\mathring{\widehat{\Omega}}_C)} \le C \|\mathring{v}_0\|_{\hat{L}^2_{-1/2}\left(\widetilde{\mathring{\Omega}}_C\right)} \le C \|\mathring{v}_0\|_{\hat{V}^1_{\odot}\left(\widetilde{\mathring{\Omega}}_C\right)} \le C \|\mathring{v}_0\|_{\hat{V}^s_{\odot,\beta}\left(\widetilde{\mathring{\Omega}}_C\right)} \le C h^{s-1-\beta}_{1,\widehat{\Omega}_C} \|\hat{v}\|_{\mathcal{V}^s_{\odot,\beta}\left(\widetilde{\hat{\Omega}}_C\right)}.$$

Hence, we have estimated all four terms in (5.10) and (5.11). By the transformation (4.20) of the weighted polar Sobolev norms back to the physical domain, we obtain

$$\left| v - \Pi^{\odot}_{V_h} v \right|_{H^q(\Omega_C)} \le C h^{s-q-\beta}_{1,\widehat{\Omega}_C} \|\hat{v}\|_{\mathcal{V}^s_{\odot,\beta}\left(\widetilde{\hat{\Omega}}_C\right)} \le C h^{s-q-\beta}_{1,\widehat{\Omega}_C} \|v\|_{V^s_\beta(\widetilde{\Omega}_C)},$$

and the demonstration is complete. □

5.2.3. Estimates on the full domain Ω

Now, we are in the position to show an overall projection error estimate on polar domains with corners and prove optimal convergence for suitable grading parameters.

Theorem 5.9. *Let $q \in \{0,1\}$ and $s \in \mathbb{N}$ with $2 \le s \le p+1$. Further, let $v \in V_\beta^s(\Omega)$ for all $\beta \in \mathbb{R}$ with $s-1-\nu < \beta < s-1$. If the mesh grading parameter satisfies condition (3.22), we obtain optimal convergence of the projection with respect to the mesh size h,*

$$\left\| v - \Pi_{V_h^\odot} v \right\|_{H^q(\Omega)} \le C h^{s-q} \|v\|_{V_\beta^s(\Omega)}.$$

Proof. By the splitting of the model domain defined in Section 5.1, we obtain

$$\left\| v - \Pi_{V_h^\odot} v \right\|_{H^q(\Omega)}^2 = \left\| v - \Pi_{V_h^\odot} v \right\|_{H^q(\Omega_C)}^2 + \left\| v - \Pi_{V_h^\odot} v \right\|_{H^q(\Omega_R)}^2.$$

The second term has been estimated in Theorem 5.2. For the first term, we use Theorem 5.8 and the mesh properties (3.28), where $h_{1,\Omega_C} \sim \widetilde{h}_{1,j_1}$ holds by definition of Ω_C and Lemma 3.18. Besides, we set $\beta = (1-\mu)(s-q)$ such that (5.9) is satisfied. It follows

$$\left\| v - \Pi_{V_h^\odot} v \right\|_{H^q(\Omega_C)}^2 \le C h_{1,\Omega_C}^{2(s-q-\beta)} \|v\|_{V_\beta^s(\widetilde{\Omega}_C)} = C h_{1,\Omega_C}^{2(s-q)(1-1+\mu)} \|v\|_{V_\beta^s(\widetilde{\Omega}_C)} \le C h_1^{2(s-q)\mu/\mu} \|v\|_{V_\beta^s(\widetilde{\Omega}_C)} = C h_1^{2(s-q)} \|v\|_{V_\beta^s(\widetilde{\Omega}_C)}^2.$$

In total, for comparable refinement in both directions, that is, $h_1 \sim h_2$ and $h = \max\{h_1, h_2\}$, we have

$$\left\| v - \Pi_{V_h}^{\widehat{}} v \right\|_{H^q(\Omega)}^2 \le C h^{2(s-q)} \left(\|v\|_{V_\beta^s(\widetilde{\Omega}_C)}^2 + \|v\|_{V_\beta^s(\widetilde{\Omega}_R)}^2 \right) \le C h^{2(s-q)} \|v\|_{V_\beta^s(\Omega)}^2,$$

where we use that $\widetilde{\Omega}_C$ and $\widetilde{\Omega}_R$ have bounded intersection with respect to h, and the assertion is proven. □

The main results of our paper, in particular Theorem 3.13 and Corollary 3.16, follow immediately from Theorem 5.9. Additionally, in Corollaries 3.14 and 3.17, we have derived optimal convergence rates for the approximation of smooth functions on uniform meshes. Finally, for the sake of completeness, we point out the suboptimal convergence behavior when singular functions are approximated on uniform meshes.

Remark 5.10 (Approximation of singular solutions on uniform meshes)**.** The proof of Theorem 5.9 shows that, on uniform meshes, the convergence rate for the H^q-error of the projection is bounded by

$$s - q - \beta < s - q - (s - 1 - \nu) = \nu + 1 - q.$$

Hence, if $\nu + 1 < s$, the rate is suboptimal. The approximation error in the H^1-norm decreases with the same order as the projection error, namely $\nu - \varepsilon$ for some $\varepsilon > 0$. In contrast, in the L^2-norm, this is not the case: by using a duality argument, it can be proven that the order on uniform meshes is given by 2ν instead of $\nu + 1 - \varepsilon$.

6. Numerical results

In this section, we confirm our theoretical findings with numerical results. All experiments are carried out using the computing package GeoPDEs 3.0 [39,55]. The graded h-refinement method introduced in Section 3.3 can be implemented easily in GeoPDEs by adapting one line of the standard knot refining routine *kntrefine* provided in the package. The polar spline basis (4.4) is constructed by applying the extraction operator described in [25, Section 3.3.2] to the standard set of basis functions. If homogeneous Dirichlet boundary conditions are considered on one of the edges adjacent to the polar corner, this step can even be omitted, and the collapsing edge can be treated as a Dirichlet edge. Moreover, numerical studies have even shown that, from a computational point of view, it is possible to work with the standard singular basis functions (3.20), which is due to the use of quadrature rules, see for instance [56].

Throughout the examples, the maximum NURBS degree used is $p = 5$. Therefore, all integrals are computed using a Gauss-Legendre quadrature rule with 36 Gauss points per mesh element, where 6 quadrature nodes are employed in both univariate directions. Unless stated otherwise, for each degree p, we consider NURBS of maximal regularity $k = p - 1$ within the coarse mesh elements, recall Remark 3.9.

Example 6.1 (Smooth solution). In the first example, we solve the Poisson equation on a quarter of the unit disk. We impose homogeneous Dirichlet boundary conditions on the re-entrant edges and non-homogeneous Dirichlet conditions on the circular arc, derived from the exact solution

$$u : \Omega \to \mathbb{R}, \quad u(x,y) = \hat{u}(r,\varphi) = r^\nu \sin(\nu\varphi),$$

with $\nu = 2$. Here and in the following, the inverted breve accent is used to denote the considered function in polar coordinates, e.g., $\hat{u}(r,\varphi) = u(r\cos\varphi, r\sin\varphi) = u(x,y)$. Fig. 8(a) shows a numerical approximation of the solution computed on a uniform mesh with 16 subdivisions in each parametric direction. The double angle formula yields that the exact solution represents a polynomial in the physical domain,

$$u(x,y) = \hat{u}(r,\varphi) = r^2 \sin(2\varphi) = 2r^2 \sin\varphi\cos\varphi = 2xy.$$

Thus, the solution is smooth in the classical sense, with $u \in H^s(\Omega)$ for all $s \in \mathbb{N}$. In contrast, with respect to the V-spaces, we only have $u \in V_\beta^s(\Omega)$ for all $s \in \mathbb{N}$ and $\beta \in \mathbb{R}$ with $s - 1 - \nu < \beta < s - 1$, where $\nu = 2$. Consequently, in the sense of Corollary 3.17, where $\nu > s - 1$ is required, the integrability condition is limited to order $s \le 2$, see also Remark 3.15.

Fig. 8(b) and (c) show the approximation errors in the $H^1(\Omega)$- and $L^2(\Omega)$-norms plotted against the mesh size h, for NURBS of degree p on uniformly refined meshes corresponding to the grading parameter $\mu = 1$. As predicted by Corollary 3.17, we observe optimal

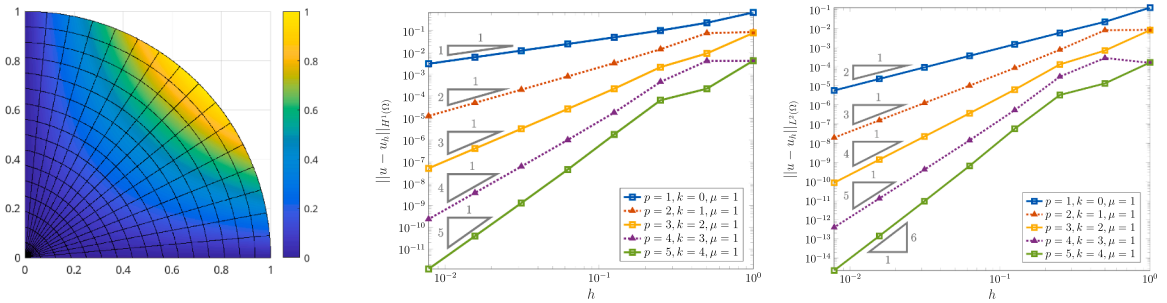

Fig. 8. Solving the Poisson equation on a quarter of the unit disk: (a): Plot of a numerical solution on a uniform mesh with 16 subdivisions for bicubic NURBS ($p = 3$). (b): $H^1(\Omega)$-error of the approximation. (c): $L^2(\Omega)$-error of the approximation.

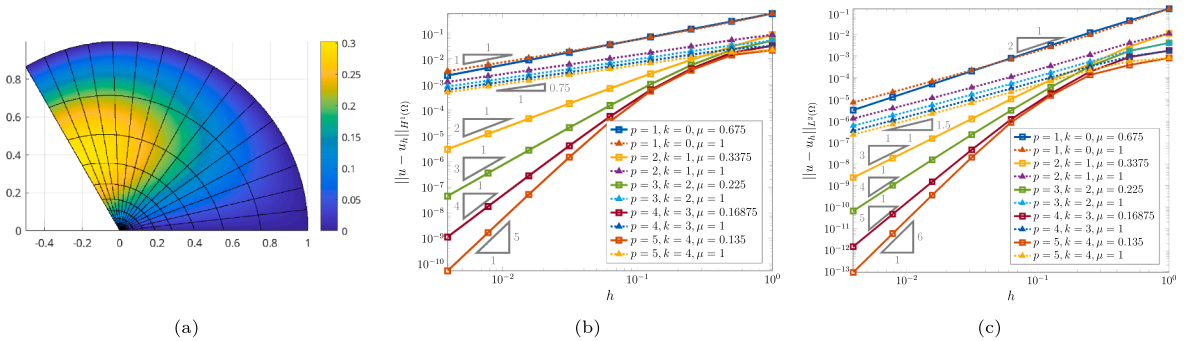

Fig. 9. Solving the Poisson equation on a circular sector with an inner angle of $\omega = \frac{2}{3}\pi$: (a): Plot of a numerical solution on a graded mesh with 16 subdivisions for bicubic NURBS. (b): $H^1(\Omega)$-error of the approximation. (c): $L^2(\Omega)$-error of the approximation.

convergence rates of order 1 in the $H^1(\Omega)$-norm and 2 in the $L^2(\Omega)$-norm for lowest-order NURBS. Higher order approximations also display optimal rates of order p in the $H^1(\Omega)$-norm and $p+1$ in the $L^2(\Omega)$-norm, but his behavior is not covered by the present theory and indicates that Corollary 3.17 is not sharp. In particular, higher order optimal approximation of polynomials in the physical domain remains to be shown. Despite the widespread use of this standard parameterization of a quarter disk – known to contain a polar singularity – corresponding error estimates have not been established up to now, as also noted in the recent work [30]. The discretization scheme examined here coincides exactly with the configuration analyzed in Section 5.1 (center-right column of Figure 8) of that paper. Although not yet complete, our results provide, at least in part, a mathematical explanation for the observed numerical convergence behavior.

Example 6.2 (Singular solution, mild corner angle). Next, we consider a circular sector with angle $\omega = \frac{2}{3}\pi$, see Example 3.6. As test problem, we consider the Poisson equation (3.10) with mixed homogeneous boundary conditions. With the right-hand side $f : \Omega \to \mathbb{R},\ f(x,y) = \hat{f}(r,\varphi) = -r^{\nu-1}\sin(\nu\varphi)(-2\nu-1)$, with $\nu = \frac{\pi}{2\omega} = \frac{3}{4}$, we obtain the solution

$$u : \Omega \to \mathbb{R}, \quad u(x,y) = \hat{u}(r,\varphi) = r^{\nu}\sin(\nu\varphi)(1-r).$$

Fig. 9(a) shows a numerical solution computed with bicubic NURBS on a graded mesh with 16 subdivisions in each parametric direction. As discussed in Section 3.2, the solution exhibits a singularity of type r^{ν} and satisfies the regularity property (3.15).

We plot the $H^1(\Omega)$- and $L^2(\Omega)$-errors of the approximations versus decreasing mesh size h in Fig. 9(b) and (c). For each NURBS degree p, we consider maximally smooth NURBS on both uniform and graded meshes, corresponding to grading parameters $\mu = 1$ and $\mu = 0.9\frac{\nu}{p}$, respectively, recall (3.26). As expected from Remark 5.10, the experimental convergence rates on uniform meshes are governed by the singularity and approach orders of ν and 2ν independent of the polynomial degree. In contrast, the use of graded meshes recovers optimal convergence rates of p and $p+1$ in the $H^1(\Omega)$- and $L^2(\Omega)$-norms, respectively, in full agreement with Corollary 3.16.

Example 6.3 (Singular solution, Quasi-Pacman domain). Now, we turn to a domain with a re-entrant corner of interior angle $\omega = \frac{3}{2}\pi$, parameterized by NURBS with knot vectors $\Xi_1 = \{0,0,1,1\}$ and $\Xi_2 = \Xi_1 = \{0,0,0,0,0,\frac{1}{2},\frac{1}{2},1,1,1,1,1\}$. The control points and weights, listed in Table 3, are chosen to resemble those of a circular sector composed of three $\frac{\pi}{2}$-sectors. The resulting geometry – referred to as the *Quasi-Pacman* domain – is a smoothly parameterized deformed circular sector.

Table 3
Definition of control points $\boldsymbol{c}_{\boldsymbol{i}}$, $\boldsymbol{i} \in \boldsymbol{I}$, for a polar parameterization of the Quasi-Pacman domain.

$\boldsymbol{c}_{(i_1,i_2)}; w_{(i_1,i_2)}$	$i_2 = 1$	$i_2 = 2$	$i_2 = 3$	$i_2 = 4$	$i_2 = 5$	$i_2 = 6$	$i_2 = 7$
$i_1 = 1$	$(0,0)^T; 1$	$(0,0)^T; \frac{1}{\sqrt{2}}$	$(0,0)^T; 1$	$(0,0)^T; \frac{1}{\sqrt{2}}$	$(0,0)^T; 1$	$(0,0)^T; \frac{1}{\sqrt{2}}$	$(0,0)^T; 1$
$i_1 = 2$	$(1,0)^T; 1$	$(1,1)^T; \frac{1}{\sqrt{2}}$	$(0,1)^T; 1$	$(-1,1)^T; \frac{1}{\sqrt{2}}$	$(-1,0)^T; 1$	$(-1,-1)^T; \frac{1}{\sqrt{2}}$	$(0,-1)^T; 1$

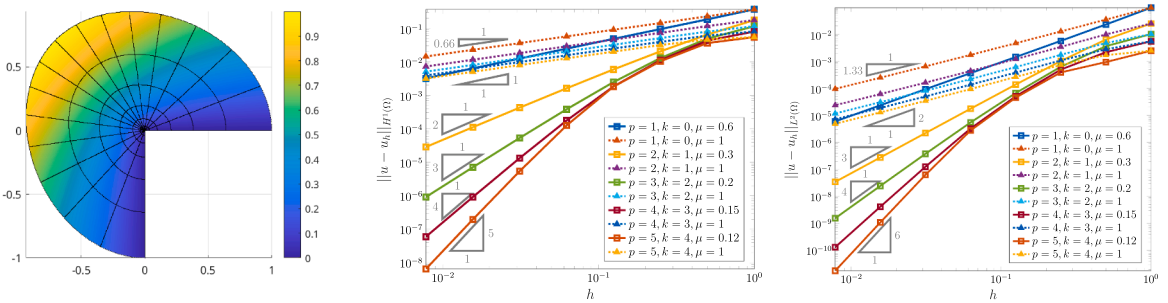

Fig. 10. Solving the Poisson equation on the Quasi-Pacman domain: (a): Plot of a numerical solution on a graded mesh for biquadratic NURBS. (b): $H^1(\Omega)$-error of the approximation. (c): $L^2(\Omega)$-error of the approximation.

We solve the Poisson equation with homogeneous Dirichlet boundary conditions on the re-entrant edges and inhomogeneous Dirichlet conditions on the arc. The data is derived from the exact solution

$$u : \Omega \to \mathbb{R}, \quad u(x, y) = \hat{u}(r, \varphi) = r^{\nu} \sin(\nu\varphi),$$

with $\nu = \frac{2}{3}$, for which (3.15) holds, consistent with our theory. In Fig. 10, we illustrate an exemplary numerical solution as well as the approximation errors for both uniform and graded meshes. As in the preceding experiment, we observe that graded meshes recover optimal convergence rates, which are not achieved by uniform meshes, as predicted by Corollary 3.16 and Remark 5.10.

Example 6.4 (Pacman domain). We proceed by solving our model problem (3.10) on the Pacman domain, which is defined as a circular sector with angle $\omega = \frac{5}{3}\pi$, see Example 3.6. In contrast to the previous tests, the resulting parameterization only satisfies the global continuity $\boldsymbol{F} \in (C^0(\widehat{\Omega}))^2$. We consider homogeneous Dirichlet boundary conditions on the circular edge and homogeneous Neumann boundary conditions on the re-entrant edges. With the right-hand side $f : \Omega \to \mathbb{R}$, $f(x, y) = \hat{f}(r, \varphi) = -r^{\nu-1} \cos(\nu\varphi)(-2\nu - 1)$, with $\nu = \frac{\pi}{\omega} = \frac{3}{5}$, we obtain the solution

$$u : \Omega \to \mathbb{R}, \quad u(x, y) = \hat{u}(r, \varphi) = r^{\nu} \cos(\nu\varphi)(1 - r),$$

which has the required regularity (3.15). Note that this is not always the case when Neumann boundary conditions are considered at the corner, however, in the present setting, the solution has the required properties by construction. In Fig. 11(a), we illustrate a numerical approximation with cubic NURBS on a graded mesh, obtained after subdividing each of the coarse mesh elements shown in Fig. 1(b) four times in radial direction and one time in angular direction. Note that the function and the corresponding mesh lines are visualized in the style of a surface plot.

The $H^1(\Omega)$- and $L^2(\Omega)$-errors are plotted for decreasing mesh size h in Fig. 11(b) and (c), using both uniform and graded meshes. Again, graded meshes recover optimal rates, as expected from the approximation error estimate in Corollary 3.16.

Finally, we investigate the impact of the C^0-lines at the interfaces of the coarse mesh elements. Compared with the Quasi-Pacman domain from the previous example, which is based on a global C^2- parameterization and deals with a similar singularity, we observe no loss in convergence. Moreover, in Fig. 12, we display the errors for C^0- and C^{p-1}-smooth NURBS, where higher continuity is only present within the coarse elements. The results clearly show that increased smoothness – although not global – leads to significantly smaller error constants per degree of freedom, both in the energy and L^2-norm. Since the space of C^0-splines on the parametric domain coincides with the classical finite element space, this demonstrates an advantage of our method over classical FEM, in addition to the benefit of exact representation of circular geometries.

Example 6.5 (L-shaped domain, comparison with adaptive hierarchical refinement).

Finally, we solve the Poisson equation on the L-shaped domain, parameterized as explained in Example 3.8. We compare the results of our mesh grading approach with the adaptive hierarchical refinement available in GeoPDEs [32], where the domain is represented by two trapezoidal patches connected with C^0-coupling.

Case 1: Mild singularity. We first consider an example from the literature, see [57, Section 5, Example 1], namely the approximation of the function

$$u : \Omega \to \mathbb{R}, \quad u(x, y) = \hat{u}(r, \varphi) = r^{\nu} \sin(\nu\varphi)$$

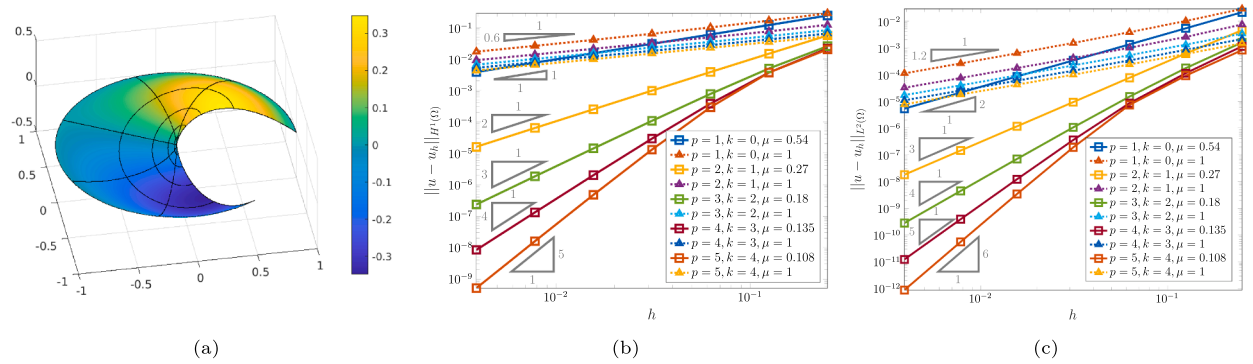

Fig. 11. Solving the Poisson equation on the Pacman domain: (a): Surface plot of an approximation on a graded mesh for bicubic NURBS. (b): $H^1(\Omega)$-error of the approximation. (c): $L^2(\Omega)$-error of the approximation.

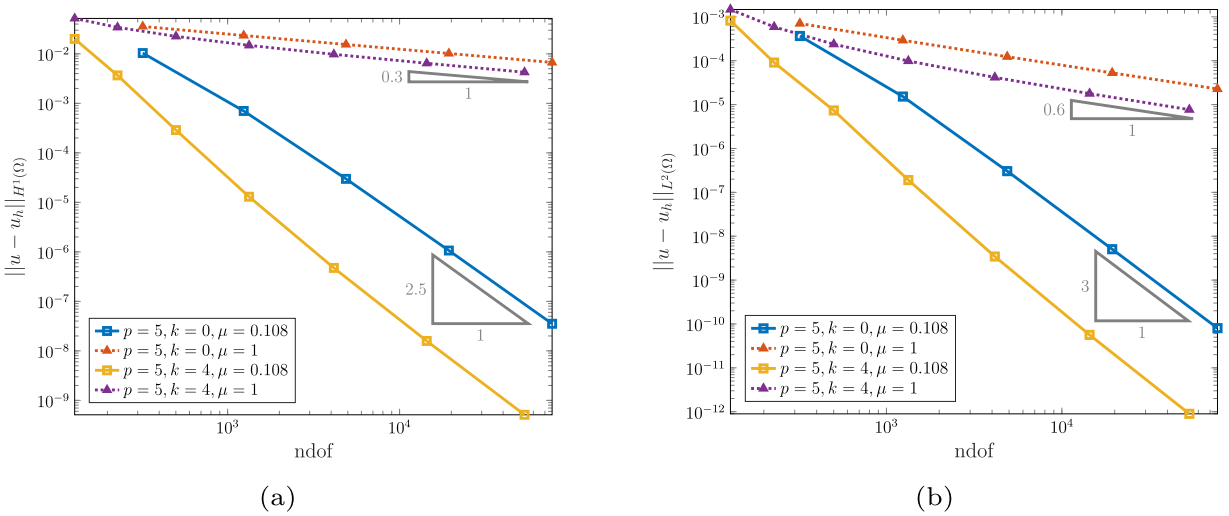

Fig. 12. Solving the Poisson equation on the Pacman domain with smoothness $k = 0$ and $k = p - 1$: (a): $H^1(\Omega)$-error of the approximation. (b): $L^2(\Omega)$-error of the approximation.

with the mild singular exponent $\nu = \frac{4}{3}$. Similar to the mentioned paper, the adaptive simulation starts from a coarse 4×4 mesh on each patch with Dörfler's parameter equal to 0.9 for the marking of the elements. A numerical solution on a graded mesh and the $H^1(\Omega)$- and $L^2(\Omega)$-errors for both methods versus the number of degrees of freedom are shown in Fig. 13, where we note that $h^{-2} \sim \text{ndof}$ holds. Both approaches achieve the expected convergence rates of $\frac{p}{2}$ in $H^1(\Omega)$ and $\frac{p+1}{2}$ in $L^2(\Omega)$, with the adaptive method slightly more accurate per degree of freedom. However, memory limitations in the hierarchical GeoPDEs implementation prevent computations with very large numbers of degrees of freedom, whereas fine graded meshes are easily generated in our approach. Although this is not a strict performance comparison – GeoPDEs may not be optimized for hierarchical splines – it illustrates the simplicity and efficiency of our mesh grading scheme.

Case 2: Strong singularity and mixed boundary conditions. As a second test case, we consider mixed boundary conditions at the re-entrant corner and homogeneous Dirichlet conditions elsewhere, i.e., we have the strong singular exponent $\nu = \frac{1}{3}$. The right-hand side is chosen as

$$f : \Omega \to \mathbb{R}, \quad f(x, y) = \hat{f}(r, \varphi) = r^{\nu}\big((4 + 4\nu - 2r^2 - \nu r^2)\sin(\nu\varphi) + \nu r^2 \sin(\varphi(\nu - 4))\big),$$

which yields the manufactured solution

$$u : \Omega \to \mathbb{R}, \quad u(x, y) = \hat{u}(r, \varphi) = r^{\nu}\sin(\nu\varphi)(1 - r^2 + r^4\cos^2(\varphi)\sin^2(\varphi)).$$

The identity $(1 - x)(1 + x)(1 - y)(1 + y) = 1 - r^2 + r^4\cos^2\varphi\sin^2\varphi$ ensures that $u = 0$ on Γ_2. As discussed in Section 3.2, the solution satisfies $u \in V^s_\beta(\Omega)$ for all $(s, \beta) \in \mathbb{N} \times \mathbb{R}$ with $s - 1 - \nu < \beta < s - 1 + \nu$. A surface plot of the exact solution is shown in Fig. 14(a), where some mesh lines are inserted for visualization purposes.

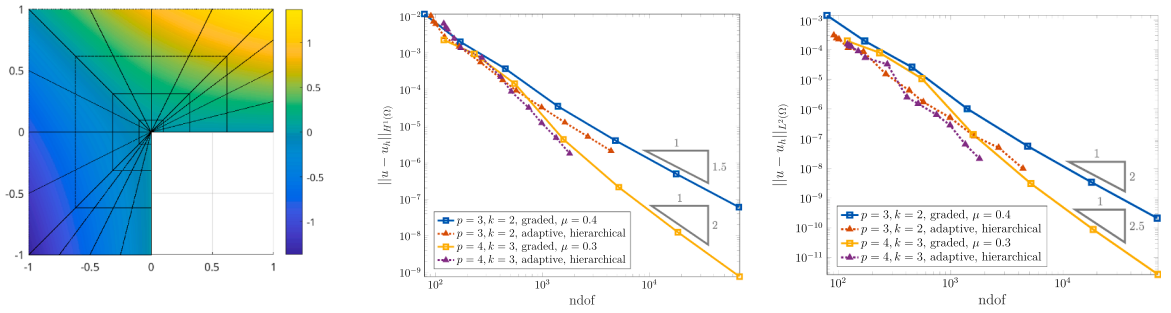

Fig. 13. Solving the Poisson equation with a weak singular exponent on the L-shaped domain with graded and adaptive hierarchical refinement: (a): Plot of the numerical solution on a graded mesh for biquadratic NURBS. (b): $H^1(\Omega)$-error of the approximation. (c): $L^2(\Omega)$-error of the approximation.

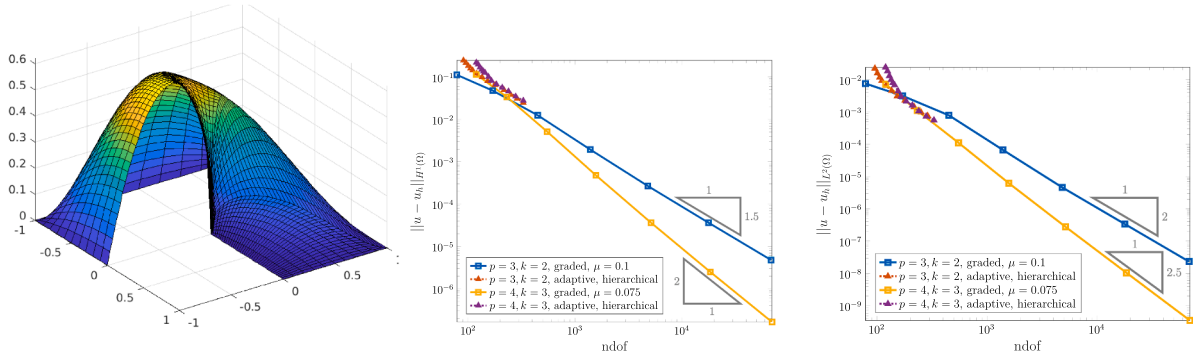

Fig. 14. Solving the Poisson equation with a strong singular exponent on the L-shaped domain with graded and adaptive hierarchical refinement: (a): Plot of the exact solution, where some mesh lines are inserted for visualization purposes. (b): $H^1(\Omega)$-error of the approximation. (c): $L^2(\Omega)$-error of the approximation.

Fig. 14(b) and (c) report the $H^1(\Omega)$- and $L^2(\Omega)$-errors versus the number of degrees of freedom for both methods. In this case, adaptive hierarchical refinement struggles to reproduce the optimal convergence rates achieved by graded meshes. In addition, our method allows straightforward computations on very fine meshes, yielding very small absolute errors, which were not attainable with the adaptive refinement.

Example 6.6 (Transverse vibrations of a circular drum with crack). The Laplace eigenvalue problem on circular sectors, for which exact solutions are known, has been studied in detail in our recent work [10]. The numerical results in Section 5.1 of this paper, where both smooth and singular eigenfunctions are approximated with uniform and graded refinement, respectively, serve as a further verification of our theory. Corollary 3.16 can be extended in a standard way to the setting of eigenvalue problems. In particular, we also obtain optimal results for a corner angle of $\omega = 2\pi$, that is, a unit disk with crack.

7. Conclusion & outlook

In this paper, we analyzed the approximation properties of splines in the vicinity of polar corners. To address the lack of regularity in classical polar parameterizations – beyond the scope of standard isogeometric approximation theory – we introduced polar Sobolev spaces on the parametric domain, derived corresponding error estimates, and transformed these results back to the polar domain. We proved optimal convergence rates for smooth solutions on uniform meshes and for singular solutions on meshes graded toward the polar point, under suitable conditions on the grading parameter. This establishes a mesh grading approach in IGA that, unlike previous methods, enables local refinement toward point singularities and offers a simple, efficient alternative to adaptive methods. Finally, we demonstrated that the proposed grading scheme is straightforward to implement and yields excellent numerical performance.

Our work serves as a foundation for further research in various directions. First, it remains to be shown whether a result comparable to Theorem 3.13 also holds for weighted H-spaces as introduced in Definition 3.10. Such an extension would cover the polynomial case considered in Example 6.1 and the general Neumann case discussed at the end of Section 3.2. Second, the approach may be extended to polar domains without corner, such as the unit disk, which arise in many practical applications, e.g., in mathematical

biology [58]. Besides, generalizations to other model problems and equations, as well as the treatment of inhomogeneous Dirichlet boundary conditions at the polar corner, deserve further investigation. In this context, for higher-order PDEs such as the biharmonic equation, an extension of our approach to C^k-smooth polar splines with $k \geq 1$ [25,26] is required. In the same spirit, a promising direction for future research is the use of Tchebycheffian splines in defining the polar parameterization [59–61], which may provide a remedy for the limitation of existing C^0-lines in the domain representation highlighted in Remark 3.9. Moreover, the proposed graded refinement can be combined with a hierarchical scheme to avoid anisotropic elements near the corner [10, Section 5.4]. The corresponding error estimates remain to be established and are of particular interest, as non-graded meshes on hierarchical scaled boundary parameterizations yield suboptimal convergence [30, Section 5.1]. Finally, extensions to more complex geometries and multipatch formulations should also be explored.

Declaration of generative AI and AI-assisted technologies in the writing process

During the preparation of this work, the authors used ChatGPT and DeepL Write to fix writing errors and to improve the readability and language in some parts of the manuscript. After using these tools, the authors reviewed and edited the content and take full responsibility for the content of the published article.

CRediT authorship contribution statement

Thomas Apel: Writing – review & editing, Validation, Supervision, Resources, Methodology, Investigation, Formal analysis, Conceptualization; **Philipp Zilk:** Writing – review & editing, Writing – original draft, Visualization, Validation, Software, Methodology, Investigation, Formal analysis, Data curation, Conceptualization.

Data availability

No data was used for the research described in the article.

Declaration of competing interest

The authors declare that they have no known competing financial interests or personal relationships that could have appeared to influence the work reported in this paper.

Acknowledgment

The authors thank Johannes Pfefferer and Max Winkler for sharing their expertise on the concepts of mesh grading for finite elements and weighted Sobolev spaces. Further, the authors express their gratitude to Giancarlo Sangalli and Thomas Takacs for motivating scientific discussions, which helped to place the results of this paper within the existing literature on isogeometric approximation theory, and to Rafael Vázquez for providing an open-source software package for IGA and for his prompt assistance with any related questions. In this context, we also thank Michele Torre for his help related to the hierarchical refinement package. Finally, we thank Yannick Grüters for the construction of the Quasi-Pacman domain and the anonymous referees for their comments which led to a great improvement of the paper.

Appendix A. Polar transformation of higher order derivatives and Sobolev norms

In the first appendix, we provide polar transformation formulas for higher order derivatives. These are used to prove the identity (4.18), which justifies the introduction of polar Sobolev spaces on the parametric domain. To begin, we show how the derivatives with respect to the $\boldsymbol{F}$-coordinate system, as defined in Section 4.2.1, can be represented in terms of standard physical derivatives. Throughout all the section, $\boldsymbol{F}$-derivatives are considered only at all points where $\boldsymbol{F}$ is sufficiently smooth, i.e., not on mesh lines corresponding to repeated knot values nor at the polar point.

Lemma A.1. *For each multi-index $\boldsymbol{\alpha}$, there exist bounded functions $G_{\boldsymbol{\gamma}} : [0,1] \to \mathbb{R}$ for $1 \leq |\boldsymbol{\gamma}| \leq |\boldsymbol{\alpha}|$ such that*

$$D_{\boldsymbol{F}}^{\boldsymbol{\alpha}} v = \sum_{1 \leq |\boldsymbol{\gamma}| \leq |\boldsymbol{\alpha}|} \zeta_1^{-\alpha_1 + |\boldsymbol{\gamma}|} G_{\boldsymbol{\gamma}} D^{\boldsymbol{\gamma}} v, \tag{A.1}$$

where we write $\boldsymbol{\zeta} = (\zeta_1, \zeta_2) = (\zeta_1(\boldsymbol{x}), \zeta_2(\boldsymbol{x})) = \boldsymbol{F}^{-1}(\boldsymbol{x})$ and $G_{\boldsymbol{\gamma}} = G_{\boldsymbol{\gamma}}(\zeta_2(\boldsymbol{x}))$ for all $\boldsymbol{x} \neq \boldsymbol{0}$.

Proof. We prove the assertion by induction over $|\boldsymbol{\alpha}|$. For $|\boldsymbol{\alpha}| = 1$, the result follows from identities (4.10) and (4.11), which serve as the induction base. We now demonstrate the induction step. Assume that the identity (A.1) holds for all multi-indices $\boldsymbol{\alpha}$ with $|\boldsymbol{\alpha}| = s \in \mathbb{N}$. From now on, $G_{\boldsymbol{\gamma}}$ denotes generic bounded coefficient functions depending only on ζ_2, and their precise form may change from line to line. By using (4.10), the product rule, the fact that $G_{\boldsymbol{\gamma}}$ only depends on ζ_2 and an index shift, we compute

$$D_{\boldsymbol{F}}^{(\alpha_1+1,\alpha_2)} v = D_{\boldsymbol{F}}^{(1,0)} \left(D_{\boldsymbol{F}}^{\boldsymbol{\alpha}} v \right) = D_{\boldsymbol{F}}^{(1,0)} \left(\sum_{1 \leq |\boldsymbol{\gamma}| \leq |\boldsymbol{\alpha}|} \zeta_1^{-\alpha_1 + |\boldsymbol{\gamma}|} G_{\boldsymbol{\gamma}} D^{\boldsymbol{\gamma}} v \right)$$

$$
\begin{aligned}
&= \sum_{1\le|\gamma|\le|\alpha|} \Big[D_F^{(1,0)}\Big(\zeta_1^{-\alpha_1+|\gamma|}\Big) G_\gamma D^\gamma v + \zeta_1^{-\alpha_1+|\gamma|} G_\gamma D_F^{(1,0)}\big(D^\gamma v\big)\Big] \\
&= \sum_{1\le|\gamma|\le|\alpha|} \Big[(-\alpha_1+|\gamma|)\zeta_1^{-(\alpha_1+1)+|\gamma|} G_\gamma D^\gamma v + \zeta_1^{-\alpha_1+|\gamma|} G_\gamma \big(G_1\,\partial_x(D^\gamma v) + G_2\,\partial_y(D^\gamma v)\big)\Big] \\
&= \sum_{1\le|\gamma|\le|\alpha|} (-\alpha_1+|\gamma|)\zeta_1^{-(\alpha_1+1)+|\gamma|} G_\gamma D^\gamma v + \sum_{1\le|\gamma'|\le|\alpha|+1} \zeta_1^{-(\alpha_1+1)+|\gamma'|} G_{\gamma'} D^{\gamma'} v \\
&= \sum_{1\le|\gamma|\le|\alpha|+1} \zeta_1^{-(\alpha_1+1)+|\gamma|} G_\gamma D^\gamma v.
\end{aligned}
$$

Similarly, we obtain with (4.11) that

$$
\begin{aligned}
D_F^{(\alpha_1,\alpha_2+1)} v &= D_F^{(0,1)}\big(D_F^\alpha v\big) = D_F^{(0,1)}\Bigg(\sum_{1\le|\gamma|\le|\alpha|} \zeta_1^{-\alpha_1+|\gamma|} G_\gamma D^\gamma v\Bigg) = \sum_{1\le|\gamma|\le|\alpha|} \zeta_1^{-\alpha_1+|\gamma|} D_F^{(0,1)}\big(G_\gamma D^\gamma v\big) \\
&= \sum_{1\le|\gamma|\le|\alpha|} \zeta_1^{-\alpha_1+|\gamma|}\Big(G'_\gamma D^\gamma v + G_\gamma\big(\zeta_1 G'_1 \partial_x(D^\gamma v) + \zeta_1 G'_2 \partial_y(D^\gamma v)\big)\Big) = \sum_{1\le|\gamma|\le|\alpha|+1} \zeta_1^{-\alpha_1+|\gamma|} G_\gamma D^\gamma v.
\end{aligned}
$$

Thus, Eq. (A.1) holds for all α' with $|\alpha'| = s+1$, completing the induction. □

Now we show the converse direction, i.e., how standard physical derivatives can be expressed through directional derivatives.

Lemma A.2. *For each multi-index α, there exist bounded functions $G_\gamma : [0,1] \to \mathbb{R}$ for $1 \le |\gamma| \le |\alpha|$ such that*

$$
D^\alpha v = \sum_{1\le|\gamma|\le|\alpha|} \zeta_1^{-|\alpha|+\gamma_1} G_\gamma D_F^\gamma v, \tag{A.2}
$$

where we write $\zeta = (\zeta_1,\zeta_2) = (\zeta_1(x),\zeta_2(x)) = F^{-1}(x)$ and $G_\gamma = G_\gamma(\zeta_2(x))$ for all $x \ne 0$.

Proof. We proceed by induction on $|\alpha|$, in analogy to the proof of Lemma A.1. For $|\alpha| = 1$, the statement follows from (4.12) and (4.13). Assume that the formula (A.2) holds for all multi-indices α with $|\alpha| = s \in \mathbb{N}$ and let again G_γ denote generic bounded coefficient functions depending only on ζ_2. Then, we find from (4.12) that

$$
\begin{aligned}
\partial_x\zeta_1 &= G_2\,\mathrm{D}_F^{(1,0)}\zeta_1 - \zeta_1^{-1} G'_2\,\mathrm{D}_F^{(0,1)}\zeta_1 = G_2, \\
\partial_x(G_\gamma) &= G_2\,\mathrm{D}_F^{(1,0)} G_\gamma - \zeta_1^{-1} G'_2\,\mathrm{D}_F^{(0,1)} G_\gamma = -\zeta_1^{-1} G'_2 G'_\gamma,
\end{aligned}
$$

and thus

$$
\begin{aligned}
D^{(\alpha_1+1,\alpha_2)} v &= D^{(1,0)}\big(D^\alpha v\big) = \partial_x\Bigg(\sum_{1\le|\gamma|\le|\alpha|} \zeta_1^{-|\alpha|+\gamma_1} G_\gamma D_F^\gamma v\Bigg) \\
&= \sum_{1\le|\gamma|\le|\alpha|} \Big[\partial_x\Big(\zeta_1^{-|\alpha|+\gamma_1}\Big) G_\gamma D_F^\gamma v + \zeta_1^{-|\alpha|+\gamma_1}\partial_x\big(G_\gamma D_F^\gamma v\big)\Big] \\
&= \sum_{1\le|\gamma|\le|\alpha|} (-|\alpha|+\gamma_1)\zeta_1^{-(|\alpha|+1)+\gamma_1}\partial_x\zeta_1\, G_\gamma D_F^\gamma v + \sum_{1\le|\gamma|\le|\alpha|} \zeta_1^{-|\alpha|+\gamma_1}\Big(\partial_x(G_\gamma) D_F^\gamma v + G_\gamma\Big(G_2 D_F^{\gamma+(1,0)} v - \zeta_1^{-1} G'_2 D_F^{\gamma+(0,1)} v\Big)\Big) \\
&= \sum_{1\le|\gamma|\le|\alpha|+1} \zeta_1^{-(|\alpha|+1)+\gamma_1} G_\gamma D_F^\gamma v.
\end{aligned}
$$

A similar formula can be derived for $D^{(\alpha_1,\alpha_2+1)} v$. Hence, (A.2) holds for all α' with $|\alpha'| = s+1$ and the Lemma is proven. □

With these relations, we can now establish the transformation between weighted V-spaces on the physical domain and their polar counterparts on the parametric domain, which proves (4.18).

Lemma A.3. *Let $v \in V_\beta^s(K)$, $K \in \mathcal{M}^\mu$, $s \in \mathbb{N}$ and $\beta \in \mathbb{R}$. Then, with $Q = F^{-1}(K)$ and $\widehat{v} = v \circ F$, it holds*

$$
\|v\|_{V_\beta^s(K)} \sim \big\|\widehat{v}\big\|_{\widehat{V}^s_{\odot,\beta}(Q)}.
$$

Proof. Consider one term in $\|v\|_{V_\beta^s(K)}$ as defined in Definition 3.10. By relation (3.8) and Lemma A.2, we have

$$
r^{\beta-s+|\alpha|}|D^\alpha v| \sim \zeta_1^{\beta-s+|\alpha|}|D^\alpha v| \le \sum_{|\gamma|\le|\alpha|} \zeta_1^{\beta-s+\gamma_1}|G_\gamma|\,|D_F^\gamma v|.
$$

After squaring and summing over $|\alpha| \le s$ and applying the Cauchy-Schwarz inequality, the boundedness of all G_γ and the Jacobian determinant (3.5), we obtain

$$
\|v\|^2_{V_\beta^s(K)} = \sum_{|\alpha|\le s} \int_K r^{2(\beta-s+|\alpha|)}|D^\alpha v|^2\,dx \le C \sum_{|\gamma|\le s} \int_Q \zeta_1^{2(\beta-s+\gamma_1)}|D_F^\gamma v|^2\,\zeta_1\,d\zeta = C\,\|\widehat{v}\|^2_{\widehat{V}^s_{\odot,\beta}(Q)}.
$$

Vice versa, as demonstrated in Lemma A.1, a single term of $\big\|\widehat{v}\big\|_{\widehat{V}^s_{\odot,\beta}(Q)}$ can be estimated by

$$
\zeta_1^{\beta-s+\alpha_1}|D_F^\alpha v| \le \sum_{|\gamma|\le|\alpha|} \zeta_1^{\beta-s+|\gamma|}|G_\gamma|\,|D^\gamma v|,
$$

which leads, by similar arguments, to

$$\|\widehat{v}\|^2_{\widehat{V}^s_{\odot,\beta}(Q)} \le C \sum_{|\boldsymbol{\alpha}|\le s} \int_K \xi_1^{2(\beta-s+\alpha_1)} |D^{\boldsymbol{\alpha}}_{\boldsymbol{F}} v|^2 \, d\boldsymbol{x} \le C \sum_{|\boldsymbol{\gamma}|\le s} \int_K r^{2(\beta-s+|\boldsymbol{\gamma}|)} |D^{\boldsymbol{\gamma}} v|^2 \, d\boldsymbol{x} = C \, \|v\|^2_{V^s_\beta(K)}.$$

Combining the two inequalities yields the desired equivalence. □

Appendix B. Properties of the modified quasi-interpolant

In this appendix, we establish key properties of the modified quasi-interpolant (2.17), which are applied in the proofs of Lemma 5.6 and Theorem 5.8 and require technical computations.

Lemma B.1. *Let the assumptions of Theorem 5.3 hold. Then, there is a projector*

$$\mathring{\Pi}^{\widehat{\Gamma},\mathring{\partial}_2}_{(p_1,p_2-1),\Xi} : C(\mathring{\Omega}) \to S_{(p_1,p_2-1)}(\Xi),$$

with $\mathring{\Omega}$ as in (5.12), such that

$$\mathring{\partial}_2\left(\mathring{\Pi}^{\widehat{\Gamma}}_{\boldsymbol{p},\Xi}\mathring{v}_0\right) = \mathring{\Pi}^{\widehat{\Gamma},\mathring{\partial}_2}_{(p_1,p_2-1),\Xi}(\mathring{\partial}_2\mathring{v}_0)$$

holds for all $\mathring{v}_0 \in C(\mathring{\Omega})$ with $\mathring{v}_0(0,\cdot) = 0$.

Proof. First, we recall representation (2.18) of the quasi-interpolant $\mathring{\Pi}^{\widehat{\Gamma}}_{\boldsymbol{p},\Xi}$. The modified dual functionals $\mathring{\lambda}^{\widehat{\Gamma}}_{\boldsymbol{i}_\odot,\boldsymbol{p}}$, $\boldsymbol{i}_\odot \in I_\odot$, evaluated for a function $\mathring{v}_0 \in C(\mathring{\Omega})$ with $\mathring{v}_0(0,\cdot) = 0$, vanish, which is a consequence of Eq. (4.7) with $W \equiv 1$ and $c = 0$. Then, with the formula for differentiation of B-splines [34, Section 1.2.4], it follows

$$\begin{aligned}
\mathring{\partial}_2\left(\mathring{\Pi}^{\widehat{\Gamma}}_{\boldsymbol{p},\Xi}\mathring{v}_0\right)(\mathring{\zeta}_1,\mathring{\zeta}_2) &= \mathring{\partial}_2\left(\sum_{\boldsymbol{i}\in\boldsymbol{I}\setminus\boldsymbol{I}_\odot} \mathring{\lambda}_{\boldsymbol{i},\boldsymbol{p}}(\mathring{v}_0)\mathring{B}_{\boldsymbol{i},\boldsymbol{p}}(\mathring{\zeta}_1,\mathring{\zeta}_2)\right) = \sum_{\boldsymbol{i}\in\boldsymbol{I}\setminus\boldsymbol{I}_\odot} \mathring{\lambda}_{\boldsymbol{i},\boldsymbol{p}}(\mathring{v}_0)\,\mathring{\partial}_2\mathring{B}_{\boldsymbol{i},\boldsymbol{p}}(\mathring{\zeta}_1,\mathring{\zeta}_2) \\
&= \sum_{i_1=2}^{n_1}\sum_{i_2=1}^{n_2} (\mathring{\lambda}_{i_1,p_1}\otimes\mathring{\lambda}_{i_2,p_2})(\mathring{v}_0)\,\mathring{B}_{i_1,p_1}(\mathring{\zeta}_1)\,p_2\left(\frac{\mathring{B}_{i_2,p_2-1}(\mathring{\zeta}_2)}{\mathring{\xi}_{i_2+p_2,2}-\mathring{\xi}_{i_2,2}} - \frac{\mathring{B}_{i_2+1,p_2-1}(\mathring{\zeta}_2)}{\mathring{\xi}_{i_2+p_2+1,2}-\mathring{\xi}_{i_2+1,2}}\right) \\
&= p_2\sum_{i_1=2}^{n_1}\sum_{i_2=1}^{n_2} \mathring{\lambda}_{i_1,p_1}\left(\int_{\mathring{\xi}_{i_2,2}}^{\mathring{\xi}_{i_2+p_2+1,2}} \mathring{v}_0(\cdot,t)\,\mathring{D}^{p_2+1}\mathring{\psi}_{i_2}(t)\,\mathrm{d}t\right)\mathring{B}_{i_1,p_1}(\mathring{\zeta}_1)\left(\frac{\mathring{B}_{i_2,p_2-1}(\mathring{\zeta}_2)}{\mathring{\xi}_{i_2+p_2,2}-\mathring{\xi}_{i_2,2}} - \frac{\mathring{B}_{i_2+1,p_2-1}(\mathring{\zeta}_2)}{\mathring{\xi}_{i_2+p_2+1,2}-\mathring{\xi}_{i_2+1,2}}\right) \\
&= p_2\sum_{i_1=2}^{n_1} \mathring{\lambda}_{i_1,p_1}\left(\sum_{i_2=1}^{n_2}\int_{\mathring{\xi}_{i_2,2}}^{\mathring{\xi}_{i_2+p_2+1,2}} \mathring{v}_0(\cdot,t)\,\mathring{D}^{p_2+1}\mathring{\psi}_{i_2}(t)\,\mathrm{d}t\left(\frac{\mathring{B}_{i_2,p_2-1}(\mathring{\zeta}_2)}{\mathring{\xi}_{i_2+p_2,2}-\mathring{\xi}_{i_2,2}} - \frac{\mathring{B}_{i_2+1,p_2-1}(\mathring{\zeta}_2)}{\mathring{\xi}_{i_2+p_2+1,2}-\mathring{\xi}_{i_2+1,2}}\right)\right)\mathring{B}_{i_1,p_1}(\mathring{\zeta}_1).
\end{aligned}$$

By reordering the sum that appears as an argument of the dual functional $\mathring{\lambda}_{i_1,p_1}$, we obtain

$$\begin{aligned}
&\sum_{i_2=1}^{n_2}\int_{\mathring{\xi}_{i_2,2}}^{\mathring{\xi}_{i_2+p_2+1,2}} \mathring{v}_0(\cdot,t)\,\mathring{D}^{p_2+1}\mathring{\psi}_{i_2}(t)\,\mathrm{d}t\left(\frac{\mathring{B}_{i_2,p_2-1}(\mathring{\zeta}_2)}{\mathring{\xi}_{i_2+p_2,2}-\mathring{\xi}_{i_2,2}} - \frac{\mathring{B}_{i_2+1,p_2-1}(\mathring{\zeta}_2)}{\mathring{\xi}_{i_2+p_2+1,2}-\mathring{\xi}_{i_2+1,2}}\right) \\
&= \int_{\mathring{\xi}_{1,2}}^{\mathring{\xi}_{1+p_2+1,2}} \mathring{v}_0(s,t)\,\mathring{D}^{p_2+1}\mathring{\psi}_1(t)\,\mathrm{d}t\,\frac{\mathring{B}_{1,p_2-1}(\mathring{\zeta}_2)}{\mathring{\xi}_{1+p_2,2}-\mathring{\xi}_{1,2}} \\
&\quad + \sum_{i_2=2}^{n_2}\left(\int_{\mathring{\xi}_{i_2,2}}^{\mathring{\xi}_{i_2+p_2+1,2}} \mathring{v}_0(s,t)\,\mathring{D}^{p_2+1}\mathring{\psi}_{i_2}(t)\,\mathrm{d}t - \int_{\mathring{\xi}_{i_2-1,2}}^{\mathring{\xi}_{i_2+p_2,2}} \mathring{v}_0(s,t)\,\mathring{D}^{p_2+1}\mathring{\psi}_{i_2-1}(t)\,\mathrm{d}t\right)\frac{\mathring{B}_{i_2,p_2-1}(\mathring{\zeta}_2)}{\mathring{\xi}_{i_2+p_2,2}-\mathring{\xi}_{i_2,2}} \\
&\quad - \int_{\mathring{\xi}_{n_2,2}}^{\mathring{\xi}_{n_2+p_2+1,2}} \mathring{v}_0(s,t)\,\mathring{D}^{p_2+1}\mathring{\psi}_{n_2}(t)\,\mathrm{d}t\,\frac{\mathring{B}_{n_2+1,p_2-1}(\mathring{\zeta}_2)}{\mathring{\xi}_{n_2+p_2+1,2}-\mathring{\xi}_{n_2+1,2}} \\
&= \sum_{i_2=2}^{n_2}\left(\int_{\mathring{\xi}_{i_2,2}}^{\mathring{\xi}_{i_2+p_2+1,2}} \mathring{v}_0(s,t)\,\mathring{D}^{p_2+1}\mathring{\psi}_{i_2}(t)\,\mathrm{d}t - \int_{\mathring{\xi}_{i_2-1,2}}^{\mathring{\xi}_{i_2+p_2,2}} \mathring{v}_0(s,t)\,\mathring{D}^{p_2+1}\mathring{\psi}_{i_2-1}(t)\,\mathrm{d}t\right)\frac{\mathring{B}_{i_2,p_2-1}(\mathring{\zeta}_2)}{\mathring{\xi}_{i_2+p_2,2}-\mathring{\xi}_{i_2,2}}.
\end{aligned}$$

The first and last term of the reordered sum vanish since Ξ_2 is an open knot vector and fractions with zero denominator are defined to have value zero. Next, we rewrite the term in brackets,

$$\begin{aligned}
&\int_{\mathring{\xi}_{i_2,2}}^{\mathring{\xi}_{i_2+p_2+1,2}} \mathring{v}_0(s,t)\,\mathring{D}^{p_2+1}\mathring{\psi}_{i_2}(t)\,\mathrm{d}t - \int_{\mathring{\xi}_{i_2-1,2}}^{\mathring{\xi}_{i_2+p_2,2}} \mathring{v}_0(s,t)\,\mathring{D}^{p_2+1}\mathring{\psi}_{i_2-1}(t)\,\mathrm{d}t \\
&= \int_{\mathring{\xi}_{i_2,2}}^{\mathring{\xi}_{i_2+p_2+1,2}} \mathring{v}_0(s,t)\,\mathring{D}^{p_2+1}\mathring{\psi}_{i_2}(t)\,\mathrm{d}t - \int_{\mathring{\xi}_{i_2,2}}^{\mathring{\xi}_{i_2+p_2+1,2}} \mathring{v}_0(s,\alpha(t))\,\mathring{D}^{p_2+1}(\mathring{\psi}_{i_2-1}\circ\alpha(t))\left|\alpha'(t)\right|\,\mathrm{d}t,
\end{aligned} \tag{B.1}$$

where we use the transformation $\alpha(t) := t - h_2$ based on the mesh size h_2 in angular direction. With definitions (2.6) and (2.7), we further compute

$$\begin{aligned}
\psi_{i_2-1}(t-h_2) &= G_{i_2-1}(t-h_2)\Phi_{i_2-1}(t-h_2)\\
&= g\left(\frac{2(t-h_2)-\xi_{i_2-1,2}-\xi_{i_2+p_2,2}}{\xi_{i_2+p_2,2}-\xi_{i_2-1,2}}\right)\left(\frac{(t-h_2-\xi_{i_2,2})\cdots(t-h_2-\xi_{i_2+p_2-1,2})}{p_2!}\right)\\
&= g\left(\frac{2t-(\xi_{i_2-1,2}+h_2)-(\xi_{i_2+p_2,2}+h_2)}{\xi_{i_2+p_2+1,2}-h_2-(\xi_{i_2,2}-h_2)}\right)\left(\frac{(t-(\xi_{i_2,2}+h_2))\cdots(t-(\xi_{i_2+p_2-1,2}+h_2))}{p_2!}\right)\\
&= g\left(\frac{2t-\xi_{i_2,2}-\xi_{i_2+p_2+1,2}}{\xi_{i_2+p_2+1,2}-\xi_{i_2,2}}\right)\left(\frac{(t-\xi_{i_2+1,2})\cdots(t-\xi_{i_2+p_2,2}))}{p_2!}\right) = G_{i_2}(t)\Phi_{i_2}(t) = \psi_{i_2}(t).
\end{aligned}$$

It follows that the expression (B.1) can be written in terms of a new dual functional,

$$\mu_{i_2,p_2-1}(\mathring{w}) := \int_{\mathring{\xi}_{i_2,2}}^{\mathring{\xi}_{i_2+p_2+1,2}} \int_{\alpha(t)}^{t} \mathring{w}(z)\,\mathrm{d}z\,\mathring{D}^{p_2+1}\mathring{\psi}_{i_2}(t)\,\mathrm{d}t,$$

with $\mathring{w}(\cdot) = \mathring{\partial}_2\mathring{v}_0(s,\cdot)$. By combining all results, we obtain

$$\begin{aligned}
\mathring{\partial}_2\left(\mathring{\Pi}^{\widehat{\Gamma}}_{\boldsymbol{p},\boldsymbol{\Xi}}\mathring{v}_0\right) &= p_2\sum_{i_1=2}^{n_1}\lambda_{i_1,p_1}\left(\sum_{i_2=2}^{n_2}\mu_{i_2,p_2-1}(\mathring{\partial}_2\mathring{v}_0(s,\cdot))\frac{\mathring{B}_{i_2,p_2-1}(\mathring{\zeta}_2)}{\mathring{\xi}_{i_2+p_2,2}-\mathring{\xi}_{i_2,2}}\right)\mathring{B}_{i_1,p_1}(\mathring{\zeta}_1)\\
&= p_2\sum_{i_1=2}^{n_1}\sum_{i_2=2}^{n_2}\left(\lambda_{i_1,p_1}\otimes\mu_{i_2,p_2-1}\right)(\mathring{\partial}_2\mathring{v}_0)\mathring{B}_{i_1,p_1}(\mathring{\zeta}_1)\frac{\mathring{B}_{i_2,p_2-1}(\mathring{\zeta}_2)}{\mathring{\xi}_{i_2+p_2,2}-\mathring{\xi}_{i_2,2}} = \mathring{\Pi}^{\widehat{\Gamma},\mathring{\partial}_2}_{(p_1,p_2-1),\boldsymbol{\Xi}}(\mathring{\partial}_2\mathring{v}_0),
\end{aligned}$$

where

$$\mathring{\Pi}^{\widehat{\Gamma},\mathring{\partial}_2}_{(p_1,p_2-1),\boldsymbol{\Xi}}(\mathring{w}) := p_2\sum_{i_1=2}^{n_1}\sum_{i_2=2}^{n_2}\left(\lambda_{i_1,p_1}\otimes\mu_{i_2,p_2-1}\right)(\mathring{w})\mathring{B}_{i_1,p_1}(\mathring{\zeta}_1)\frac{\mathring{B}_{i_2,p_2-1}(\mathring{\zeta}_2)}{\mathring{\xi}_{i_2+p_2,2}-\mathring{\xi}_{i_2,2}} \tag{B.2}$$

is the resulting new projector. □

Lemma B.2. *Let the notation of Lemmata 5.6 and B.1 hold. Then, there is a constant $C > 0$ such that*

$$\left\|\mathring{\Pi}^{\widehat{\Gamma},\mathring{\partial}_2}_{(p_1,p_2-1),\boldsymbol{\Xi}}(\mathring{\partial}_2\mathring{v}_0)\right\|_{\widehat{L}^2_{-1/2}(\mathring{\Omega}_C)} \le C\left\|\mathring{\partial}_2\mathring{v}_0\right\|_{\widehat{L}^2_{-1/2}\left(\widetilde{\mathring{\Omega}}_C\right)}$$

for all $\mathring{v}_0 \in C(\mathring{\Omega})$ with $\mathring{v}_0(0,\cdot) = 0$.

Proof. We recall the definitions of the projector (B.2) and the scaling transformation (5.12) and apply the continuous Cauchy-Schwarz inequality to compute

$$\begin{aligned}
\left\|\mathring{\Pi}^{\widehat{\Gamma},\mathring{\partial}_2}_{(p_1,p_2-1),\boldsymbol{\Xi}}(\mathring{\partial}_2\mathring{v}_0)\right\|^2_{\widehat{L}^2_{-1/2}(\mathring{\Omega}_C)} &\le p_2^2\sum_{i_1=2}^{n_1}\sum_{i_2=2}^{n_2}\left|(\lambda_{i_1,p_1}\otimes\mu_{i_2,p_2-1})(\mathring{\partial}_2\mathring{v}_0)\right|^2\int_{\mathring{\Omega}_C}\left|\mathring{\zeta}_1^{-1/2}\,\mathring{B}_{i_1,p_1}(\mathring{\zeta}_1)\frac{\mathring{B}_{i_2,p_2-1}(\mathring{\zeta}_2)}{\mathring{\xi}_{i_2+p_2+1,2}-\mathring{\xi}_{i_2,2}}\right|^2\mathrm{d}\mathring{\zeta}_1\,\mathrm{d}\mathring{\zeta}_2\\
&\le p_2^2\sum_{i_1=2}^{n_1}\sum_{i_2=2}^{n_2}\left|\int_{\mathring{\xi}_{i_1,1}}^{\mathring{\xi}_{i_1+p_1+1,1}}\int_{\mathring{\xi}_{i_2,2}}^{\mathring{\xi}_{i_2+p_2+1,2}}\int_{\alpha(t)}^{t}\mathring{\partial}_2\mathring{v}_0(s,z)\,\mathrm{d}z\,\mathring{D}^{p_2+1}\mathring{\psi}_{i_2}(t)\,\mathrm{d}t\,\mathring{D}^{p_1+1}\mathring{\psi}_{i_1}(s)\,\mathrm{d}s\right|^2 Ch_2^{-2}\\
&\le Ch_2^{-2}\sum_{i_1=2}^{n_1}\sum_{i_2=2}^{n_2}\left|\int_{\mathring{\xi}_{i_1,1}}^{\mathring{\xi}_{i_1+p_1+1,1}}\int_{\mathring{\xi}_{i_2,2}}^{\mathring{\xi}_{i_2+p_2+1,2}}\int_{\mathring{\xi}_{i_2-1,2}}^{\mathring{\xi}_{i_2+p_2+1,2}}\left|\mathring{\partial}_2\mathring{v}_0(s,z)\right|\mathrm{d}z\,\mathring{D}^{p_2+1}\mathring{\psi}_{i_2}(t)\,\mathrm{d}t\,\mathring{D}^{p_1+1}\mathring{\psi}_{i_1}(s)\,\mathrm{d}s\right|^2\\
&= Ch_2^{-2}\left(\int_{\mathring{\xi}_{i_2-1,2}}^{\mathring{\xi}_{i_2+p_2+1,2}}\mathring{D}^{p_2+1}\mathring{\psi}_{i_2}(t)\,\mathrm{d}t\right)^2\sum_{i_1=2}^{n_1}\sum_{i_2=2}^{n_2}\left|\int_{\mathring{\xi}_{i_1,1}}^{\mathring{\xi}_{i_1+p_1+1,1}}\int_{\mathring{\xi}_{i_2-1,2}}^{\mathring{\xi}_{i_2+p_2+1,2}}\left|\mathring{\partial}_2\mathring{v}_0(s,z)\right|\mathrm{d}z\,\mathring{D}^{p_1+1}\mathring{\psi}_{i_1}(s)\,\mathrm{d}s\right|^2\\
&\le C\sum_{i_1=2}^{n_1}\sum_{i_2=2}^{n_2}\left|\int_{\mathring{\xi}_{i_1,1}}^{\mathring{\xi}_{i_1+p_1+1,1}}\int_{\mathring{\xi}_{i_2-1,2}}^{\mathring{\xi}_{i_2+p_2+1,2}}\left|\mathring{\partial}_2\mathring{v}_0(s,z)\mathring{D}^{p_1+1}\mathring{\psi}_{i_1}(s)\right|\mathrm{d}z\,\mathrm{d}s\right|^2.
\end{aligned}$$

Then, we set $E_{(i_1,i_2)} := (\mathring{\xi}_{i_1,1},\mathring{\xi}_{i_1+p_1+1,1})\times(\mathring{\xi}_{i_2-1,2},\mathring{\xi}_{i_2+p_2+1,2}) \subset \widetilde{\mathring{\Omega}}$ and simplify the term above by using the continuous and discrete Cauchy-Schwarz inequality combined with the equivalence of finite-dimensional norms,

$$\begin{aligned}
&C\sum_{i_1=2}^{n_1}\sum_{i_2=2}^{n_2}\left|\int_{\mathring{\xi}_{i_1,1}}^{\mathring{\xi}_{i_1+p_1+1,1}}\int_{\mathring{\xi}_{i_2-1,2}}^{\mathring{\xi}_{i_2+p_2+1,2}}\left|\mathring{\partial}_2\mathring{v}_0(s,z)\mathring{D}^{p_1+1}\mathring{\psi}_{i_1}(s)\right|\mathrm{d}z\,\mathrm{d}s\right|^2\\
&\le C\sum_{i_1=2}^{n_1}\sum_{i_2=2}^{n_2}\left(\int_{E_{(i_1,i_2)}}\left|\mathring{\partial}_2\mathring{v}_0(s,z)\right|^2\mathrm{d}z\,\mathrm{d}s\right)\left(\int_{E_{(i_1,i_2)}}\left|\mathring{D}^{p_1+1}\mathring{\psi}_{i_1}(s)\right|^2\mathrm{d}z\,\mathrm{d}s\right)
\end{aligned}$$

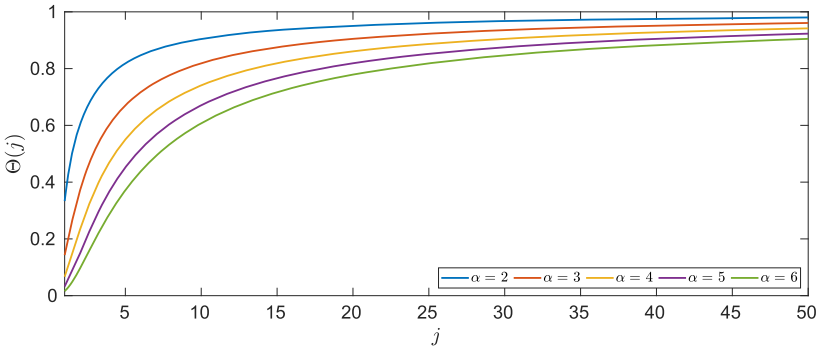

Fig. C.1. Illustration of the function Θ for $\alpha \in \{2, 3, \dots, 6\}$.

$$\leq C\left(\sum_{i_1=2}^{n_1}\sum_{i_2=2}^{n_2}\left(\int_{E_{(i_1,i_2)}}\left|\mathring{\partial}_2\mathring{v}_0(s,z)\right|^2 \mathrm{d}z\,\mathrm{d}s\right)^2\right)^{1/2}\left(\sum_{i_1=2}^{n_1}\sum_{i_2=2}^{n_2}\left(\int_{E_{(i_1,i_2)}}\left|\mathring{D}^{p_1+1}\mathring{\psi}_{i_1}(s)\right|\mathrm{d}z\,\mathrm{d}s\right)^2\right)^{1/2}$$

$$\leq C\left(\sum_{i_1=2}^{n_1}\sum_{i_2=2}^{n_2}\int_{E_{(i_1,i_2)}}\left|\mathring{\partial}_2\mathring{v}_0(s,z)\right|^2 \mathrm{d}z\,\mathrm{d}s\right)\left(\sum_{i_1=2}^{n_1}\sum_{i_2=2}^{n_2}\int_{E_{(i_1,i_2)}}\left|\mathring{D}^{p_1+1}\mathring{\psi}_{i_1}(s)\right|\mathrm{d}z\,\mathrm{d}s\right)$$

$$\leq C\sum_{i_1=2}^{n_1}\sum_{i_2=2}^{n_2}\left\|\mathring{\partial}_2\mathring{v}_0\right\|^2_{L^2\left(E_{(i_1,i_2)}\right)}\sum_{i_1=2}^{n_1}\sum_{i_2=2}^{n_2}h_2h_1 \leq C\left\|\mathring{\partial}_2\mathring{v}_0\right\|^2_{\mathring{\tilde{L}}^2\left(\mathring{\tilde{\Omega}}_C\right)}\cdot 1 \leq C\left\|\mathring{\partial}_2\mathring{v}_0\right\|^2_{\mathring{\tilde{L}}^2_{-1/2}\left(\mathring{\tilde{\Omega}}_C\right)},$$

and the demonstration is complete. □

Appendix C. Proof of local quasi-uniformity of graded meshes

Finally, we show an auxiliary result needed to establish the local quasi-uniformity of the graded meshes, stated in Lemma 3.18.

Lemma C.1. *Let $\alpha \geq 1$. The sequence $(\Theta(j))_{j=1}^{\infty}$ with*

$$\Theta(j) := \frac{j^\alpha - (j-1)^\alpha}{(j+1)^\alpha - j^\alpha}$$

is monotonously increasing and satisfies $\lim_{j\to\infty}\Theta(j) = 1$.

Proof. For $\alpha = 1$, it holds $\Theta(j) = 1$ for all $j \in \mathbb{N}$ and the assertion follows directly. For $\alpha > 1$, we consider the function

$$\Theta : [1,\infty) \to \mathbb{R}, \quad \Theta(x) := \frac{x^\alpha - (x-1)^\alpha}{(x+1)^\alpha - x^\alpha},$$

which is illustrated for $\alpha \in \{2, 3, \dots, 6\}$ in Fig. C.1, where the claimed properties can be anticipated visually. More precisely, let $f : [1,\infty) \to \mathbb{R},\ f(x) := x^\alpha$ and $g : [1,\infty) \to \mathbb{R},\ g(x) := (x+1)^\alpha$. By the generalized mean value theorem, it follows

$$\Theta(j) = \frac{f(j) - f(j-1)}{g(j) - g(j-1)} = \frac{f'(x)}{g'(x)} = \left(\frac{x}{x+1}\right)^{\alpha-1} =: \widetilde{\Theta}(x).$$

for some $x \in (j-1, j)$ and for every $j \in \mathbb{N}$. The derivative of the new function $\widetilde{\Theta}$ is given by

$$\widetilde{\Theta}'(x) = (\alpha-1)\left(\frac{x}{x+1}\right)^{\alpha-2}\frac{1}{(x+1)^2} = (\alpha-1)x^{\alpha-2}(x+1)^{-\alpha},$$

and, since $\alpha > 1$ and $x > j - 1 \geq 0$, it always holds $\widetilde{\Theta}'(x) > 0$. Thus, the function $\widetilde{\Theta}$ and consequently also the sequence $(\Theta(j))_{j=1}^{\infty}$ are monotonously increasing. Moreover, we have

$$\lim_{j\to\infty}\Theta(j) = \lim_{x\to\infty}\widetilde{\Theta}(x) = \lim_{x\to\infty}\left(\frac{x}{x+1}\right)^{\alpha-1} = 1$$

and the proof is concluded. □

References

[1] T.J.R. Hughes, J.A. Cottrell, Y. Bazilevs, Isogeometric analysis: CAD, finite elements, NURBS, exact geometry and mesh refinement, Comput. Methods Appl. Mech. Eng. 194 (39–41) (2005) 4135–4195. https://doi.org/10.1016/j.cma.2004.10.008

[2] A. Buffa, G. Gantner, C. Giannelli, D. Praetorius, R. Vázquez, Mathematical foundations of adaptive isogeometric analysis, Arch. Comput. Methods Eng. 29 (7) (2022) 4479–4555. https://doi.org/10.1007/s11831-022-09752-5

[3] T. Apel, A.-M. Sändig, J.R. Whiteman, Graded mesh refinement and error estimates for finite element solutions of elliptic boundary value problems in non-smooth domains, Math. Methods Appl. Sci. 19 (1) (1996) 63–85. https://doi.org/10.1002/(SICI)1099-1476(19960110)19:1<63::AID-MMA764>3.0.CO;2-S

[4] T. Apel, S. Nicaise, The finite element method with anisotropic mesh grading for elliptic problems in domains with corners and edges, Math. Methods Appl. Sci. 21 (6) (1998) 519–549. https://doi.org/10.1002/(SICI)1099-1476(199804)21:6<519::AID-MMA962>3.0.CO;2-R

[5] I. Babuška, Finite element method for domains with corners, Computing 6 (1970) 264–273. https://doi.org/10.1007/bf02238811

[6] B. Mercier, G. Raugel, Résolution d'un problème aux limites dans un ouvert axisymétrique par éléments finis en r, z et séries de Fourier en θ, RAIRO Anal. Numér. 16 (4) (1982) 405–461.

[7] L.A. Oganesjan, L.A. Rukhovets, Variational-difference schemes for linear second-order elliptic equations in a two-dimensional region with piecewise smooth boundary, Ž. Vyčisl. Mat i Mat. Fiz. 8 (1968) 97–114. In Russian. English translation in USSR Computational Mathematics and Mathematical Physics 8 (1968) 129–152.

[8] L. Beirão da Veiga, D. Cho, G. Sangalli, Anisotropic NURBS approximation in isogeometric analysis, Comput. Methods Appl. Mech. Eng. 209/212 (2012) 1–11. https://doi.org/10.1016/j.cma.2011.10.016

[9] U. Langer, A. Mantzaflaris, S.E. Moore, I. Toulopoulos, Mesh grading in isogeometric analysis, Comput. Math. Appl. 70 (7) (2015) 1685–1700. https://doi.org/10.1016/j.camwa.2015.03.011

[10] T. Apel, P. Zilk, Isogeometric analysis of the Laplace eigenvalue problem on circular sectors: regularity properties and graded meshes, Comput. Math. Appl. 175 (2024) 236–254. https://doi.org/10.1016/j.camwa.2024.09.018

[11] M. Wiesheu, T. Komann, M. Merkel, S. Schöps, S. Ulbrich, I. Cortes Garcia, Combined parameter and shape optimization of electric machines with isogeometric analysis, Optim. Eng. (2024). https://doi.org/10.1007/s11081-024-09925-0

[12] J.A. Cottrell, T.J.R. Hughes, Y. Bazilevs, Isogeometric Analysis. Toward Integration of CAD and FEA, John Wiley & Sons, Ltd., Chichester, 2009. https://doi.org/10.1002/9780470749081

[13] Y. Zhang, Y. Bazilevs, S. Goswami, C.L. Bajaj, T.J.R. Hughes, Patient-specific vascular NURBS modeling for isogeometric analysis of blood flow, Comput. Methods Appl. Mech. Eng. 196 (29-30) (2007) 2943–2959. https://doi.org/10.1016/j.cma.2007.02.009

[14] J. Lu, X. Zhou, Cylindrical element: isogeometric model of continuum rod, Comput. Methods Appl. Mech. Eng. 200 (1–4) (2011) 233–241. https://doi.org/10.1016/j.cma.2010.08.007

[15] S. Zhong, G. Jin, T. Ye, J. Zhang, Y. Xue, M. Chen, Isogeometric vibration analysis of multi-directional functionally gradient circular, elliptical and sector plates with variable thickness, Compos. Struct. 250 (2020) 112470. https://doi.org/10.1016/j.compstruct.2020.112470

[16] Y. Xue, G. Jin, T. Ye, K. Shi, S. Zhong, C. Yang, Isogeometric analysis for geometric modelling and acoustic attenuation performances of reactive mufflers, Comput. Math. Appl. 79 (12) (2020) 3447–3461. https://doi.org/10.1016/j.camwa.2020.02.004

[17] C. Arioli, A. Shamanskiy, S. Klinkel, B. Simeon, Scaled boundary parametrizations in isogeometric analysis, Comput. Methods Appl. Mech. Eng. 349 (2019) 576–594. https://doi.org/10.1016/j.cma.2019.02.022

[18] J. Arf, M. Reichle, S. Klinkel, B. Simeon, Scaled boundary isogeometric analysis with C^1 coupling for Kirchhoff plate theory, Comput. Methods Appl. Mech. Engrg. 415 (2023) Paper No. 116198, 26. https://doi.org/10.1016/j.cma.2023.116198

[19] M. Reichle, J. Arf, B. Simeon, S. Klinkel, Smooth multi-patch scaled boundary isogeometric analysis for Kirchhoff-Love shells, Meccanica 58 (8) (2023) 1693–1716. https://doi.org/10.1007/s11012-023-01692-z

[20] M. Reichle, M. Klassen, J. Li, S. Klinkel, A modified approach for a scaled boundary shell formulation in structural isogeometric analysis, Eng. Anal. Bound. Elem. 159 (2024) 81–94. https://doi.org/10.1016/j.enganabound.2023.11.017

[21] A. Falini, C. Giannelli, T. Kanduč, M.L. Sampoli, A. Sestini, An adaptive IgA-BEM with hierarchical B-splines based on quasi-interpolation quadrature schemes, Internat. J. Numer. Methods Eng. 117 (10) (2019) 1038–1058. https://doi.org/10.1002/nme.5990

[22] M. Feischl, G. Gantner, A. Haberl, D. Praetorius, Adaptive 2D IGA boundary element methods, Eng. Anal. Bound. Elem. 62 (2016) 141–153. https://doi.org/10.1016/j.enganabound.2015.10.003

[23] T. Takacs, B. Jüttler, Existence of stiffness matrix integrals for singularly parameterized domains in isogeometric analysis, Comput. Methods Appl. Mech. Eng. 200 (49–52) (2011) 3568–3582. https://doi.org/10.1016/j.cma.2011.08.023

[24] T. Takacs, B. Jüttler, H^2 regularity properties of singular parameterizations in isogeometric analysis, Graph. Models 74 (6) (2012) 361–372. https://doi.org/10.1016/j.gmod.2012.05.006

[25] D. Toshniwal, H. Speleers, R.R. Hiemstra, T.J.R. Hughes, Multi-degree smooth polar splines: a framework for geometric modeling and isogeometric analysis, Comput. Methods Appl. Mech. Eng. 316 (2017) 1005–1061. https://doi.org/10.1016/j.cma.2016.11.009

[26] H. Speleers, D. Toshniwal, A general class of C^1 smooth rational splines: application to construction of exact ellipses and ellipsoids, Comput.-Aided Des. 132 (2021) Paper No. 102982, 14. https://doi.org/10.1016/j.cad.2020.102982

[27] Y. Bazilevs, L. Beirão da Veiga, J.A. Cottrell, T.J.R. Hughes, G. Sangalli, Isogeometric analysis: approximation, stability and error estimates for h-refined meshes, Math. Models Methods Appl. Sci. 16 (7) (2006) 1031–1090. https://doi.org/10.1142/S0218202506001455

[28] L. Beirão da Veiga, A. Buffa, G. Sangalli, R. Vázquez, Mathematical analysis of variational isogeometric methods, Acta Numer. 23 (2014) 157–287. https://doi.org/10.1017/S096249291400004X

[29] T. Takacs, Approximation properties of isogeometric function spaces on singularly parameterized domains, 2015, arXiv:1507.08095

[30] T. Takacs, Approximation properties over self-similar meshes of curved finite elements and applications to subdivision based isogeometric analysis, Comput. Aided Geom. Des. 116 (2025) 102413. https://doi.org/10.1016/j.cagd.2025.102413

[31] T.J.R. Hughes, G. Sangalli, Mathematics of Isogeometric Analysis: A Conspectus, John Wiley & Sons, Ltd., 2017, pp. 1–40. https://doi.org/10.1002/9781119176817.ecm2100

[32] E.M. Garau, R. Vázquez, Algorithms for the implementation of adaptive isogeometric methods using hierarchical B-splines, Appl. Numer. Math. 123 (2018) 58–87. https://doi.org/10.1016/j.apnum.2017.08.006

[33] L.L. Schumaker, Spline functions: basic theory, Cambridge Mathematical Library, Cambridge University Press, Cambridge, third edition, 2007. https://doi.org/10.1017/CBO9780511618994

[34] T. Lyche, C. Manni, H. Speleers, Foundations of spline theory: B-splines, spline approximation, and hierarchical refinement, in: Splines and PDEs: From Approximation Theory to Numerical Linear Algebra, 2219 of *Lecture Notes in Math.*, Springer, Cham, 2018, pp. 1–76.

[35] L. Piegl, W. Tiller, The NURBS Book, Springer Berlin, Heidelberg, 1995. https://doi.org/10.1007/978-3-642-97385-7

[36] B.-G. Lee, T. Lyche, K. Mørken, Some examples of quasi-interpolants constructed from local spline projectors, in: Mathematical Methods for Curves and Surfaces (Oslo, 2000), Innov. Appl. Math., Vanderbilt Univ. Press, Nashville, TN, 2001, pp. 243–252.

[37] C. de Boor, A Practical Guide to Splines, 27 of *Applied Mathematical Sciences*, Springer-Verlag, New York, revised edition, 2001.

[38] G.E. Farin, NURB Curves and Surfaces: From Projective Geometry to Practical Use, A. K. Peters, Ltd., Wellesley, MA, 1995.

[39] R. Vázquez, A new design for the implementation of isogeometric analysis in Octave and Matlab: GeoPDEs 3.0, Comput. Math. Appl. 72 (3) (2016) 523–554. https://doi.org/10.1016/j.camwa.2016.05.010

[40] J. Lu, Circular element: isogeometric elements of smooth boundary, Comput. Methods Appl. Mech. Eng. 198 (30–32) (2009) 2391–2402. https://doi.org/10.1016/j.cma.2009.02.029

[41] T. Takacs, Construction of smooth isogeometric function spaces on singularly parameterized domains, in: Curves and Surfaces, 9213 of *Lecture Notes in Comput. Sci.*, Springer, Cham, 2015, pp. 433–451. https://doi.org/10.1007/978-3-319-22804-4_30

[42] T. Nguyen, K. Karčiauskas, J. Peters, A comparative study of several classical, discrete differential and isogeometric methods for solving Poisson's equation on the disk, Axioms 3 (2) (2014) 280–299. https://doi.org/10.3390/axioms3020280

[43] T. Jonsson, M.G. Larson, K. Larsson, Graded parametric CutFEM and CutIGA for elliptic boundary value problems in domains with corners, Comput. Methods Appl. Mech. Eng. 354 (2019) 331–350. https://doi.org/10.1016/j.cma.2019.05.024

[44] T. Takacs, D. Toshniwal, Almost-C^1 splines: biquadratic splines on unstructured quadrilateral meshes and their application to fourth order problems, Comput. Methods Appl. Mech. Eng. 403 (2023) Paper No. 115640, 34. https://doi.org/10.1016/j.cma.2022.115640
[45] V.G. Maz'ya, B.A. Plamenevskiĭ, L^p-estimates of solutions of elliptic boundary value problems in domains with ribs, Trudy Moskov. Mat. Obshch. 37 (1978) 49–93, 270.
[46] P. Grisvard, Elliptic Problems in Nonsmooth Domains, 24 of *Monographs and Studies in Mathematics*, Pitman (Advanced Publishing Program), Boston, MA, 1985.
[47] M. Dauge, Elliptic Boundary Value Problems on Corner Domains, 1341 of *Lecture Notes in Mathematics*, Springer-Verlag, Berlin, 1988. https://doi.org/10.1007/BFb0086682
[48] S.A. Nazarov, B.A. Plamenevsky, Elliptic Problems in Domains with Piecewise Smooth Boundaries, 13 of *De Gruyter Expositions in Mathematics*, Walter de Gruyter & Co., Berlin, 1994. https://doi.org/10.1515/9783110848915.525
[49] T. Apel, J.M. Melenk, Interpolation and quasi-interpolation in h- and hp-version finite element spaces, in: Encyclopedia of Computational Mechanics Second Edition (Eds E. Stein, R. Borst and T.J.R. Hughes), John Wiley & Sons, Ltd., Chichester, 2017, pp. 1–33. https://doi.org/10.1002/9781119176817.ecm2002m
[50] T. Apel, Anisotropic Finite Elements: Local Estimates and Applications, Advances in Numerical Mathematics, B. G. Teubner, Stuttgart, 1999.
[51] J. Rossmann, On two classes of weighted Sobolev-Slobodetskiĭ spaces in a dihedral angle, in: Partial Differential Equations, Part 1, 2 (Warsaw, 1990), 27, Part 1, 2 of *Banach Center Publ.*, Polish Acad. Sci. Inst. Math., Warsaw, 1992, pp. 399–424.
[52] T. Apel, A.-M. Sändig, S.I. Solov'ëv, Computation of 3D vertex singularities for linear elasticity: error estimates for a finite element method on graded meshes, Math. Model. Numer. Anal. 36 (6) (2002) 1043–1070 (2003). https://doi.org/10.1051/m2an:2003005
[53] R.A. Adams, J.J.F. Fournier, Sobolev Spaces, 140 of *Pure and Applied Mathematics (Amsterdam)*, Elsevier/Academic Press, Amsterdam, 2nd edition, 2003.
[54] J. Pfefferer, Numerical Analysis for Elliptic Neumann Boundary Control Problems on Polygonal Domains, Dissertation, Universität der Bundeswehr München, Fakultät für Bauingenieurwesen und Umweltwissenschaften, Neubiberg, 2014. https://athene-forschung.unibw.de/node?id=92055.
[55] C. de Falco, A. Reali, R. Vázquez, GeoPDEs: a research tool for isogeometric analysis of PDEs, Adv. Eng. Software 42 (12) (2011) 1020–1034. https://doi.org/10.1016/j.advengsoft.2011.06.010
[56] T. Apel, P. Zilk, Isogeometric analysis of the Laplace eigenvalue problem on circular sectors: regularity properties, graded meshes & variational crimes, 2024, arXiv:2402.16589
[57] C. Bracco, C. Giannelli, M. Kapl, R. Vázquez, Isogeometric analysis with C^1 hierarchical functions on planar two-patch geometries, Comput. Math. Appl. 80 (11) (2020) 2538–2562. https://doi.org/10.1016/j.camwa.2020.03.018
[58] R.S. Lagunero, K. Fellner, T. Apel, V. Kempf, P. Zilk, Lipolysis on Lipid Droplets: mathematical modelling and numerical discretisations, 2025, arXiv:2401.17935
[59] K. Raval, C. Manni, H. Speleers, Tchebycheffian B-splines in isogeometric Galerkin methods, Comput. Methods Appl. Mech. Eng. 403 (2023) Paper No. 115648, 31. https://doi.org/10.1016/j.cma.2022.115648
[60] H. Speleers, Algorithm 1020: computation of multi-degree Tchebycheffian B-splines, ACM Trans. Math. Software 48 (1) (2022) Art. 12, 31. https://doi.org/10.1145/3478686
[61] H. Speleers, On the normalization of trigonometric and hyperbolic B-splines, 2025, arXiv:2508.01817